Iron Sulfide-Coated Sand for Remediation of Arsenic(III)-Contaminated Anoxic Groundwater

by

Young-Soo Han

A dissertation submitted in partial fulfillment
of the requirements for the degree of
Doctor of Philosophy
(Environmental Engineering)
in The University of Michigan
2009

Doctoral Committee:

Associate Professor Avery H. Demond, Co-Chair
Professor Kim F. Hayes, Co-Chair
Associate Professor Udo Becker
Associate Professor Terese M. Olson

Dedication

To my parents and mother-in-law,

my husband, Dong-Hee, and

my lovely sons, Hoyeon and Seoyoen

Acknowledgements

I am heartily thankful to my advisor, Dr. Avery H. Demond, who is my academic mother and a role model. She has encouraged, supported and advised me very much. She always treats me as the best student, even though I did not deserve this merit, being an international student mother, who was always so busy juggling study, kids and language. I appreciate my co-advisor, Dr. Kim F. Hayes, who taught me what a teacher should be like. I learned so much from his advice and his expertise in aquatic chemistry and geochemistry. Drs. Demond and Hayes also have supported my family, both me and Dong-Hee, so our family could continue our lives in the USA. Also, I am thankful for Dr. Hayes's continuous support of my post-doctoral research in Michigan. I would like to thank Dr. Terese M. Olson who advised me about the coating studies and the sorption mechanisms. I appreciate Dr. Udo Becker who advised me with his valuable expertise in surface chemistry and XPS. With his help, I found out how interesting the mechanisms in geoenvironmental chemistry are.

I would like to thank to Tom Yavaraski for help with the laboratory work. Thanks to Kai Sun and Hiping Sun at EMAL for training me on XPS, SEM and XRD, as well as Devon Renock in the department of Geological Science, who shared his precious knowledge on XPS and CASA XPS software. Especially I would like to thank to Dr. Hoon Young Jeong for his advice and many valuable discussions about my experimental results. He also provided the XAS data through collaboration with his work on nanoparticulate FeS and mine on FeS-coated sand. I would also like to thank Dr. Tanya Gallegos, who initiated the FeS coating study and trained me during my first year of laboratory work. Thanks to other colleagues in the SERDP project group, Dr. Sung Pil Hyun, Dr. Jun Hee Lee, Andrew Henderson, and Monica Higgins, as well as Li Wang of Tufts University for the discussions on this work. Thanks especially to Andrew

Henderson for letting me borrow his pump so I could finish my column study and his willingness to share his knowledge in PRB systems and geochemical modeling.

Financial support for this research was provided by funds from the Department of Defense SERDP project CU-1375 and research fellowships from the Rackham Graduate School at the University of Michigan. X-ray absorption spectroscopy was performed by Dr. Hoon Young Jeong at the Stanford Synchrotron Radiation Laboratory, a facility operated by the Department of Energy Office of Basic Energy Sciences. Two years of tuition for my graduate study was supported by the Korea Science and Engineering Foundation.

I would like to give my thanks to my friends in EWRE, Dr. Hoa Trinh, Jeongdae Im, Sukhwan Yoon, and Trinh Duc Tran. I give deep thanks to my friends in faith of Jesus Christ, Hyunju Kim, Juyoung Park, Jinwha Park, and Jeongmin Seo as well as my sisters in my Bible study group. Also, thanks to my best friend, Yunju Lee, who is the only person of whom I can ask difficult favors and truly open my heart.

Finally, I would like to thank to my family. It is difficult to fully express my overwhelming gratitude to them. I cannot find any words which express my deep appreciation for my mother-in-law, Cha Soon Park. Without her devotion to my family during last 5 years, I would not be here. I deeply thank my parents, Sang Jun Han and Kyung Soon Cho; my sister, Youngji; and my brother, Dongjin for their love and prayers, a debt of gratitude that I can only hope to be able to pay back. I also thank my adorable sons, Hoyeon and Seoyeon, who allow me to know the indescribable joy of being their mom. Last and most importantly, I would like to thank my husband, Dr. Dong-Hee Lim, who is a companion of the whole of my life, spiritually and academically. He is always such a good supporter and a guide to me in the love of Jesus Christ. I am greatly thankful to my God who made me and has a wonderful plan for me. I return all my glory to God.

Table of Contents

List of Tables

List of Figures

List of Appendices

List of Abbreviations

AWS: acid-washed sand

BE: binding energy

BET: Brunauer, Emmett and Teller method, generally called BET

BTC: break-through curve

CHEs: 2-(cyclohexylamino) ethanesulfonic acid

CXTFIT: a code for estimating transport parameters from laboratory or field tracer experiments (Toride et al., 1995)

EGME: ethylene glycol monoethyl ether

EXAFS: extended x-ray absorption fine structure

FWHM: full width at half maximum

HFO: hydrous ferric oxide

HR-TEM: high resolution transmission electron microscopy

IC: ion chromatography

ICP-MS: inductively coupled plasma-mass spectrometry

LAXRPD: low angle X-ray powder diffraction

MOM: method of moments

MOPs: 3-(N-morpholino)propanesulfonic acid

NS: natural sand

PCS: photon correlation spectroscopy

PE: pass energy

PHREEQC: a computer program for speciation, batch-reaction, one-dimensional transport, and inverse geochemical calculations (Parkhurst and Appelo, 1999)

PRB: permeable reactive barrier

PZC: point of zero charge

SEM: scanning electron microscopy

SSA: specific surface area

SSA_{ext}: external specific surface area

SSR: solid solution ratio

SSRL: Stanford Synchrotron Radiation Lightsource

TEM: transmission electron microscopy

XANES: x-ray absorption near edge structure

XAS: x-ray absorption spectroscopy

XPS: x-ray photoelectron spectroscopy

XRD: x-ray diffraction

ZVI: zero valent iron

Abstract

This study investigated the feasibility of using reduced iron sulfide (FeS) as a permeable reactive barrier (PRB) material for remediating As(III) contaminated groundwater under anoxic conditions. FeS is more advantageous than more commonly used materials such as zero valent iron (ZVI) or oxyhydroxide-based materials in treating As(III)-contaminated groundwater, under anoxic conditions, as other Fe(III)-based adsorbents display a lower removal capacity and may release immobilized arsenic back into solution by reductive dissolution. To use nano-sized FeS as a PRB material, a method was developed to coat natural sand giving a coating 1.2 to 4.0 mg FeS/g. The removal capacity of the FeS-coated sand was 30%, 70% and 300% at pH 5, 7 and 9, respectively, of the maximum capacity of nanoscale FeS. Although some reduction of uptake capacity was observed at pH 5 and 7, these capacities are still greater than those of aluminum oxide coated sand under anaerobic conditions. At pH 9, FeS-coated sand outperformed nanoscale FeS due to the uptake of As(III) by Fe oxyhydroxide that formed during the coating procedure or preexisted on the sand. These secondary Fe mineral phases on FeS-coated sand were also thought to be responsible for the inhibitory effect of dissolved silicate on As(III) adsorption at pH 9. There was no inhibitory silicate effect in the nanoscale FeS system at pH 5, 7 and 9 and in the FeS-coated sand system at pH 5 and 7 wherein FeS dominantly controlled the As(III) removal process. Spectroscopic methods such as x-ray absorption spectroscopy and x-ray photoelectron spectroscopy were used to evaluate the As(III) uptake mechanisms of FeS-coated sand under acidic (pH 5) and basic (pH 9) conditions. At pH 5, precipitation of orpiment (As_2S_3) or realgar (AsS) was found in nanoscale FeS and FeS-coated sand systems, respectively, while the adsorption of (thio-)arsenite species or the adsorption of arsenite, respectively, was found

at pH 9. Even though the detailed form of minerals or surface-complexed As(III) species was different, the overall extent and pH-dependent removal behavior in batch reactor studies were similar between the nanoparticulate FeS and FeS-coated sand systems. The differences in As(III) removal mechanisms as a function of pH, however, affected the capacity of FeS-coated sand in the column studies compared to that in the batch reactor studies. At pH 5, where precipitation dominates, the column capacity was closely related to the amount of sulfide with the column capacity greater than that of the batch system due to the continuous supply of sulfur from the dissolution of FeS. In contrast, at pH 9, where adsorption dominates, the As(III) removal capacity of the column system was comparable to the batch reactor as long as the sorption non-linearity was considered and the retention time was adequately long. Overall, this dissertation supports FeS as a promising material for use in a PRB to remove As(III) under anoxic conditions by demonstrating that it can be successfully coated onto sand particles appropriately sized for PRB application, with a capacity in packed columns comparable to or exceeding that of nanoscale FeS as long as the retention time is adequate.

CHAPTER I

INTRODUCTION

1.1 Arsenic as a groundwater contaminant

Arsenic (As) is a ubiquitous element found in the natural and built environment, occurring both naturally and anthropogenically. The range of As concentrations found under natural groundwater conditions is large, ranging from less than 0.5 μg/L to more than 5,000 μg/L. High-As ground water areas have been found in Argentina, Chile, Mexico, China, and Hungary, and more recently in West Bengal, Bangladesh, and Vietnam. O'Day et al. (2004) concluded that approximately 90 million people, including 13 million in the United States, face the potential of an adverse impact from As-polluted groundwater.

Arsenic has various oxidation states such as -3, -2, -1, 0, +3 or +5; however, two oxidation states, As(III) (arsenite) and As(V) (arsenate), predominate in surface and near surface environments, depending on pe. Between these two, As(III) is more mobile and more difficult to remove from groundwater under acidic and neutral pH conditions (pH under 9.2) (Smedley and Kinniburgh, 2002). Arsenic also can exist as an aqueous form associated with sulfur. Thioarsenites and thioarsenates species are often found in sulfidic environments and these complicating forms of various thio-arsenic species make it difficult to accurately predict As speciation in reduced conditions (Wood et al., 2002; Wilkin et al., 2003). In general, charged anionic species tend to be more strongly sorbed to mineral surfaces than neutral species. Also, compared to metal cations, which usually form highly insoluble oxide and hydroxide phases, arsenic exhibits higher solubility and mobility as dissolved species in aqueous solution under both oxidizing and reducing conditions, while other oxyanions such as selenium and chromium are immobilized under reducing conditions (Zhu and Tabatabai, 1995). Therefore removal of dissolved arsenic

species from groundwater is more challenging than that of other cationic or anionic contaminants (Smedley and Kinniburge, 2002; Bissen and Frimmel, 2003).

1.2 Arsenic removal using a permeable reactive barrier (PRB)

Permeable Reactive Barriers (PRBs) have been evaluated as an effective and economical technology for the *in-situ* treatment of groundwater for various kinds of contaminants (Puls, 1999; Blowes et al., 2000; Bryant et al., 2003). A PRB consists of a reactive porous medium installed in the subsurface as a treatment zone which can capture single or multiple target contaminants, while the groundwater flows through it by means of the natural head difference in the aquifer. The most commonly used barrier material is granular zero-valent iron. Recently, various other reactive materials have been examined such as iron oxide, aluminum oxide, and zeolite. However, small particulate materials are not suitable for use in PRBs because of their lower permeability when installed in a treatment zone. To eliminate the problems with permeability, efforts have been devoted to coating sand with reactive materials such as $FeOOH/Fe(OH)_3$ (Appelo and Postma, 1999; Thirunavukkarasu et al., 2003; Herbel and Fendorf, 2006), MnO_2 (Appelo and Postma, 1999; Guha et al., 2001), red mud (Genc-Fuhrman and Gencfuhrman, 2005; Jerez and Flury, 2006), and humic acid, ferrihydrite and aluminosilicate (Jerez and Flury, 2006).

There are a number of possible PRB reactive materials aimed at removing arsenic: iron oxide-coated sand, activated alumina, manganese dioxide-coated sand, pressurized granulated iron particles, iron oxide-doped alginate, and zero-valent iron. The list of absorbents for arsenic removal and their total removal capacity is presented in Table 1.1. Among these, iron oxide-coated sand is emerging as an effective reactive material for arsenic removal under oxidizing conditions (Gupta et al., 2005). For example, ferrihydrite-coated quartz (Herbel and Fendorf, 2006), crystalline HFO (Manna et al., 2003), iron-oxide coated cement (Kundu and Gupta, 2006) remove 90.45 mg/g, 33.33 mg/g, and 25 mg/g (pure mineral weight-basis in each case) of As(III), respectively. These materials show much higher As(III) removal capacities than granular reactants such as activated alumina (0.18 mg/g) (Singh and Pant, 2004), Fe-conditioned zeolite (0.59 mg/g) (Onyango et al., 2003), and modified red mud (3.32 mg/L) (Genc-Fuhrman

and Gencfuhrman, 2005). Zerovalent iron (ZVI) or Fe(0), as the most widely used PRB material, is also used to remediate As(III) (Su and Puls, 2001; Bang et al., 2005b). Its removal mechanism relies mainly on the secondary formation of ferric oxide coating as a result of the Fe(0) corrosion.

1.3 Problems in using ferric-oxide based PRB materials under anaerobic conditions

Even though iron oxide has been reported to successively remove As(III) and As(V) from polluted groundwater, the sorbed arsenic could be released back into solution if the redox condition changes (Masscheleyn et al., 1991; McGeehan and Naylor, 1994; Tufano and Fendorf, 2008). This release of the adsorbed arsenic can be attributed to the reductive dissolution of Fe(III) oxyhydroxide solids under anaerobic conditions as Fe(III) is reduced to Fe(II). This shortcoming might be also problematic in ZVI-based PRBs. It is thought that the iron oxyhydroxide corrosion products of ZVI provide the reactive surface for the arsenic uptake (Furukawa et al., 2002; Manning et al., 2002), which, like the pure iron oxyhydroxide sorbents, may eventually release arsenic back into solution over prolonged use under anaerobic conditions (Tufano and Fendorf, 2008).

Despite the concern of releasing As(III) back into solution by the dissolution of oxyhydroxide as a corrosion product, a pilot-scale ZVI-based PRB, emplaced in 2005 for treatment of arsenic in groundwater from a smelter plant in Helena MT, has effectively removed arsenic for several years of operation (Wilkin et al., 2009). Even though anaerobic conditions prevailed, significant bacterial sulfate reduction is occurring at this site with the production of iron sulfides within the ZVI implicated, in part, for the effective arsenic removal to date. This is consistent with other studies that have linked effective arsenic removal in ZVI systems with the production of sulfide (Kober et al., 2005).

1.4 Iron sulfide for use in PRBs

The example of a pilot-scale ZVI in Helena, MT demonstrates the importance of sulfide in As(III) sequestration. The formation of acid volatile sulfide (AVS) under reducing conditions is often observed in natural sediments or reactive zone of permeable

reactive barriers where sulfate-reduction bacteria (SRB) control the geochemical conditions of a system (Herbert et al., 2000; Smyth et al., 2001; Burton et al., 2008a; Burton et al., 2008b). From the ZVI PRB samples collected from the pilot-scale ZVI after one year of reaction in the field, the role of iron sulfide was implicated by X-ray absorption spectroscopy (XAS) techniques employed to characterize sorbed As species. In this case, As(III)-S species sorbed on FeS surface were postulated (Beak and Wilkin, 2009). This example, showing the role of sulfide in As(III) sequestration, is consistent with the fact that no high arsenic concentrations have been reported in sulfide-abundant subsurface sediments (O'Day et al., 2004). The effective sequestration of As(III) by a synthesized nanoparticulate mackinawite (hereafter referred to as nanoscale FeS) was investigated by Gallegos (2007) at pH 5, 7 and 9 under strict anaerobic conditions. The As(III) sorption by FeS displayed typical Langmuir type isotherm curves with the maximum amounts of 2×10^{-3}, 2×10^{-4} and 5×10^{-5} mol As removed/g FeS (150, 15, and 3.75 mg As(III)/g sand) at pH 5, 7 and 9, respectively. These are greater, especially at pH 5, than most of the other powder absorbents that have been tested under aerobic conditions, except for the removal capacity of As(III) by hydrous ferric oxide (HFO) reported by Dixit and Hering (2003). However, owing to the stability of iron sulfides under anoxic conditions against reductive dissolution, nanoscale FeS appears to be more suitable for removing As(III) when anoxic conditions are expected to prevail.

To develop FeS as a PRB material, optimal particle sizing is important. For example, the nano-sized FeS synthesized in the laboratory (e.g., Gallegos et al. (2007) may not suitable for trench and fill PRB applications due to its potential to create a low permeability zone and the possibility of being washed out in a short time. Therefore, to utilize FeS in a PRB, a sand coating with nanoscale material may be desirable (Herbel and Fendorf, 2006; Jerez and Flury, 2006). Alternatively, geochemical conditions may be induced to form iron sulfide coatings through microbial activity. FeS is often found as a coating on natural mineral surfaces and in sulfate-reducing zones of PRB materials (Herbert et al., 2000; Smyth et al., 2001; Burton et al., 2008a; Wilkin et al., 2009). However, a biotic coating of FeS on natural sand was not attempted. Instead, in this study, a process for coating nano-sized FeS on natural sand was developed and its As(III)-uptake characteristics investigated using batch and column reactors. The results of this

study indicate that FeS-coated sand could be used as a reactive material for a PRB for remediating As(III)-contaminated groundwater under anaerobic conditions, particularly at lower values of pH (e.g., pH≈5).

1.5 Objectives of this study

Synthesized mackinawite (FeS), as a nano-sized mineral that often exists in natural reducing environments, has been verified as a suitable reactant to remove As(III) under anoxic conditions (Gallegos, 2007). Although mackinawite has a high As(III) removal capacity, it may not be optimal for direct application in a permeable reactive barrier as a porous medium due to its small particle size. Therefore, the development of synthetic mackinawite as a PRB reactive porous material necessitated the development of a FeS material having a particle of a reasonable size. Here, the coating of a commercially obtained sand was evaluated to that end. While the interaction between As(III) and nano-scale FeS has been studied by other researchers, the potential applicability of FeS in PRBs has not been investigated nor has the effectiveness and reaction characteristics of an FeS-coated sand.

In this study, therefore, the goals were to develop a mackinawite (FeS) coated sand and to evaluate As(III) sequestration by this coated sand using batch and column systems under anoxic conditions under a range of pH conditions. Given these goals, four tasks were undertaken: 1) develop a method for producing FeS coating on a natural sand and characterize the surface properties of the developed FeS-coated sand (Chapter IV), 2) evaluate the As(III) uptake capacity, sorption behavior, and the impact of dissolved silicate on As(III) uptake by FeS-coated sand at pH 5, 7, and 9 (Chapter V), 3) characterize spectroscopically the solid phase reaction products of As(III)-reacted with FeS-coated sand for verifying the As(III) removal mechanisms under different pH conditions (Chapter VI), and 4) compare batch and column reactor studies to assess the impact of hydrodynamics on the uptake of As(III) by FeS-coated sand (Chapter VII).

The working hypotheses are that :

1. FeS can be successfully coated on a natural sand surface and the FeS coating on the sand shows similar characteristics and effectiveness of FeS when it is reacted with As(III),

2. Arsenic(III) can be effectively treated with FeS-coated sand under anoxic conditions over a range of pH values,

3. The capacity of the FeS coating is comparable with nanoscale mackinawite on an FeS normalized basis, both in batch and in column reactors, and

4. The capacity of the FeS-coating may be dependent on the concentration of competing anions such as silicate ion, as As(III) is one of the more weakly bonded by the mineral surface.

1.6 Dissertation organization

This dissertation contains eight chapters. This chapter, Chapter I provides a brief description of the problem and the motivation for this research. Chapter II reviews previous literature describing the characteristics of FeS, the reaction between As(III) and FeS, impact of solution conditions such as pH and dissolved silicate when As(III) reacts with other mineral surfaces, the coating of other nanoscale sorbent materials on sand and comparative studies of batch and column systems. Chapter III describes the methodologies and materials in this work. Chapter IV presents the method of coating FeS onto a natural sand and the characteristics of the coated sand. Chapters V presents batch study results of As(III) removal capacities and impact of solution conditions, in particular pH and dissolved silicate concentration, on As(III) removal by FeS-coated sand. Chapter VI discusses the results of x-ray photoelectron spectroscopy characterization of As(III) solid phase reaction products responsible for As(III) removal at pH 5 and 9. Chapter VII deals with the reactive transport of As(III) in FeS-coated sand systems including the interpretation of column breakthrough curves, the comparison of column and batch results and possible causes of the discrepancies between uptake capacity derived from column and batch results. Finally, Chapter 8 provides a summary of the conclusions and the implications of the research results for the remediation of As(III)-contaminated groundwater by FeS coated sand systems.

Table 1.1 Studies of arsenic sorption by metal oxides.

As species	Adsorbent (particle size)	pH	Sorption capacity (Isotherm model used)	Reference
As(III)	Bauxite (activated alumina)		1.2 mg/g (Langmuir isotherm)	Ghosh and Yuan, 1987
As(III)	Granular ZVI (d=1-1.68 mm)		0.3 mg/g	Lackovic et al., 2000
As(III)	Sulfate ($BaSO_4$) modified iron oxide-coated sand (d_{50} = 0.5 mm)	pH 7.2	0.15 mg/g (Langmuir isotherm)	Vaishya and Gupta, 2002
As(III)	HFO	pH 8	422.7 mg/g Fe	Dixit and Hering, 2003
As(V)		pH 4	327.3 mg/g Fe	
As(III)	Goethite	pH 8	21.8 mg/g Fe	Dixit and Hering, 2003
As(V)		pH 4	21.8 mg/g Fe	
As(III)	Iron-oxide coated sand (IOCS)	pH 7.6	0.041 mg/g IOCS	Thirunavukkarasu et al., 2003
As(V)	(d = 0.6-0.8 mm)		0.042 mg/g IOCS	
As(III)	Crystalline HFO (CHFO)	pH 6	33.33 mg /g CHFO	Manna et al., 2003
As(V)	(d = 0.14-0.29 mm)		25.0 mg/g CHFO (Langmuir isotherm)	
As(III)	Fe-conditioned zeolite (0.668 mm)	pH 7.8	0.588 mg/g (C_0=1.272 mg/L)	Onyango et al., 2003
As(III)	Activated alumina (d = 2.0 ± 0.1 mm)	pH 7.6	0.18 mg/g (Langmuir isotherm)	Singh and Pant, 2004
As(V)	Hardened paste of Portland cement (d = 4.88 – 4.92 mm)	pH 4~5	95% removal (C_0 = 0.2 ppm)	Kundu et al., 2004

Table 1.1 Studies of arsenic sorption by metal oxides (Continued)

As species	Adsorbent (particle size)	pH	Sorption capacity (Isotherm model used)	Reference
As(V)	Modified red mud (Bauxsol) Activated Bauxsol (0-0.5 mm)	pH 4.5 / 7.1 pH 7.1	3.32 mg/L / 1.64 mg/L 2.14 mg/L (Langmuir isotherm)	Genc-Fuhrman and Gencfuhrman, 2005
As(III)	Iron-oxide coated sand Uncoated sand (d_{50} = 0.5 mm)	pH 7.5	0.028 mg/g 0.0056 mg/g (Langmuir isotherm)	Gupta et al., 2005
As(III)	Nanoscale zero-valent iron	pH 7	3.5 mg/g at 25° C (Freundlich isotherm)	Kanel et al., 2005
As(III)	Iron-oxide coated cement (0.212mm)	pH 8	25.0 mg/g (Langmuir isotherm)	Kundu and Gupta, 2006
As(III) As(V)	Ferrihydrite-coated quartz (unblended)	pH 7	90.45 mg/g ferrihydrite 36.25mg/g ferrihydrite	Herbel and Fendorf, 2006
As(III) As(V)	Mn-substituted iron oxyhdroxide ($Mn_{0.13}Fe_{0.87}OOH$)	pH 6-7	4.58 mg/g 5.72 mg/g (Langmuir isotherm)	Lakshmipathiraj et al., 2006

CHAPTER II

BACKGROUND

2.1 Characteristics of FeS

2.1.1 General properties

Mackinawite (iron monosulfide, FeS) is typically considered the first iron sulfide formed from the reaction of Fe and S in low temperature aqueous environments. Berner (1962; 1964) identified it as a tetragonal black iron(II) monosulfide from the precipitation of Fe(II) salt and S(-II) salt. Mackinawite has been called by a variety of terms (e.g., hydrotroilite, kansite, precipitated FeS, amorphous FeS, disordered mackinawite) because of the difficulties in identifying the exact form of nano-particulate minerals that form from the initial precipitation. Another difficulty in identification is its high sensitivity to oxidation. Rickard and Morse (2005) concluded that most of the differently defined materials, including amorphous FeS, were actually mackinawite.

Mackinawite's particle size and surface area, two properties that may impact As(III) uptake, have been studied by many researchers. Wolthers et al. (2003) reported 4 nm as the average primary particle size with 350 m^2/g of specific surface area (SSA). This large surface area suggests the potentially high reactivity of mackinawite. However, the measured surface area and particle size have been found to depend on the mackinawite preparation method and measurement techniques used. For example, the SSA of mackinawite measured using BET (Brunauer, Emmett and Teller method, generally called BET) showed a much smaller SSA, ranging from 0.05 to 80 m^2/g, which might have resulted from the aggregation of mackinawite particles during preparation (Wolthers et al., 2003). More recently, Jeong et al. (2008) intensively studied the particle size and SSA of laboratory-synthesized mackinawite and suggested that conventional transmission electron microscopy (TEM) or BET analysis tends to reflect the degree of

particle aggregation rather than the surface area of the particles when dispersed in aqueous suspensions. In contrast, the SSA determined by high resolution transmission electron microscopy (HR-TEM) (Ohfuji and Rickard, 2006), low angle X-ray powder diffraction (LAXRPD) (Wolthers et al., 2003), the ethylene glycol monoethyl ether (EGME) method and photon correlation spectroscopy (PCS) gave much higher SSA values within reasonable agreement, 276 to 424 m^2/g (Jeong et al., 2008).

2.1.2 Formation of FeS and its transformation

In general, two approaches have been used in the abiotic synthesis of mackinawite at low temperatures: (1) by reaction of metallic iron with a sulfide solution (Lennie et al., 1995), and (2) by reaction of a ferrous iron solution with a sulfide solution (Rickard, 1969). The first approach used iron wire which was dissolved in a buffer solution as the way of synthesizing mackinawite with almost no sulfur vacancy occupancy or surplus Fe occupancy; thus, the stoichiometry approaches FeS. This FeS was proved to be crystalline mackinawite. The mackinawite synthesized by the second approach was stable for up to 4 months without elevated temperature; no formation of greigite or pyrite were observed during the experimental period, under well-controlled conditions intended to eliminate oxygen exposure (Benning et al., 2000).

The iron sulfide phase produced by these two synthesis methods has been stated to be amorphous FeS or disordered mackinawite with nano-scaled particle size. The initially precipitated nano-sized mackinawite transforms to more crystalline mackinawite in several days (Wilkin and Barnes, 1996), but the complete transformation to well-crystalline mackinawite can take up to 2 years (Rickard, 1995). Therefore, freshly generated mackinawite in the natural environment is expected to be nano-sized, and may naturally form as a coating on different mineral surfaces, given the tendency of nano-particulate mackinawite to aggregate (Lee, 2009). For example, in an acid-sulfate soil sediment, more than 300 μmol S/g of nanoparticulate mackinawite was measured as a result of transformation from schwertmannite ($Fe_8O_8(OH)_6SO_4$) (Burton et al., 2008a). The accumulation of disordered (amorphous) mackinawite was also observed in a permeable reactive barrier composed of organic material at concentrations up to 195 μmol S/g (Herbert et al., 2000).

Since the complete formation of well crystallized mackinawite takes a relatively long time under strictly anaerobic conditions, it is generally considered that mackinawite transforms to more oxidized and more stable forms of iron sulfide such as greigite or pyrite over time. Schoonen and Barnes (1991) demonstrated that amorphous FeS progressively transformed to more sulfur-rich FeS phases as follows:

Amorphous FeS → Mackinawite (FeS) → Greigite (Fe_3S_4) → Pyrite/Marcasite (FeS_2)

This transformation sequence may occur in the presence of intermediate sulfur species, such as S(0), polysulfides, polythionates, or thiosulfate (Schoonen and Barnes, 1991) or via iron loss by near-surface oxidation (Wilkin and Barnes, 1996) or in the presence of proper oxidizing agents such as H_2S (Rickard and Morse, 2005). Also the transformation of mackinawite to pyrite is temperature dependent, i.e., a faster transformation is observed with increasing temperature (Benning et al., 2000). In this study, FeS was used under a strictly controlled anoxic atmosphere and at ambient temperature. Thus, it was expected that no transformation of FeS to pyrite through surface oxidation has occurred. However, it was anticipated that some oxidation of mackinawite might occur through contact with water or other oxidants over the time frame of weeks to months. In fact, recent work by Gallegos et al. (2008), indicated that mackinawite may be oxidized to greigite or magnetite from anoxic corrosion by water, depending on the solution pe and pH.

2.1.3 Surface charge

The surface charge characteristics of FeS are important to understanding how it might be coated onto natural sand. To characterize the surface charge of a mineral surface, which is a function of pH, zeta potential is often used. The pH value when the zeta potential becomes zero is called pH_{pzc}. The pH_{pzc} of quartz sand is well known to be near pH 2 and the surface charge becomes more negative when the pH increases above pH_{pzc}. However, there exists a discrepancy among measured values of the pH_{pzc} of FeS. For example, the pH_{pzc} value measured by Wolthers et al. (2003) and Widler and Seward (2002) differed greatly: 7.5 and 2.9, respectively. More recently, Gallegos (2007)

reported the pH_{pzc} of the FeS surface as near pH 5 based on electrokinetic measurements. The near neutral value of pH_{pzc} (7.5) is not consistent with the pH_{pzc} of other metal sulfide such as sphalerite (ZnS), galena (PbS), chalcopyrite ($CuFeS_2$), pyrrhotite (FeS), pyrite (FeS_2), vaesite (NiS_2), cattierite (CoS_2) and hauerite (MnS_2) whose pH_{pzc} values range from 0.6 to 3.3 (Bebie et al., 1998). In their study, the pH_{pzc} value of very crystalline mackinawite aged at high temperature (130˚C) was measured as pH 2.9. This values is not applicable to the mackinawite synthesized in this study because their well-crystalline mackinawite might not represent the surface condition of poorly crystalline FeS, which might have much higher solubility, synthesized at low temperature. Therefore, the value of 5 for pH_{pzc}, which was measured using FeS formed using essentially the same synthesis method as used in this study, might closely represent the pH_{pzc} of the FeS in this study. The major difference in synthesis methods is that the FeS used in this study was prepared using freeze-drying, while the FeS used in Gallegos et al. (2007) was prepared as a thick paste without drying.

2.1.4 Solubility of FeS

The solubility of mackinawite is important in determining the As(III) uptake capacity of FeS when precipitation governs the As(III) removal mechanism. The dissolution of FeS may be determined by the oxidative or reductive condition of the system but is mainly controlled by the pH of the system. Therefore the solubility of FeS is mostly studied associated with the pH of the solution. The solubility of mackinawite (FeS) under acidic conditions can be expressed by:

$$FeS + 2H^+ \rightarrow Fe^{2+} + H_2S_{aq} \quad (2\text{-}1)$$

or

$$FeS + H^+ \rightarrow Fe^{2+} + HS^- \quad (2\text{-}2)$$

Since the S^{2-} ion is insignificant in most aqueous solutions, FeS solubility under acidic (equation (2-1)) and basic (equation (2-2)) conditions is conventionally represented using H_2S_{aq} and HS^- species. The solubility constants are expressed as $\log K_{sp,1} = \log [Fe^{2+}] + \log [H_2S_{aq}] + 2pH$, $K_{sp,2} = \log [Fe^{2+}] + \log [HS^-] + pH$ and [ ] refers to activity, Fe^{2+} is

shorthand for hexaqua Fe(II) and aq refers to the aqueous species. If either $K_{sp,1}$ or $K_{sp,2}$ is known, the other constant can be calculated by using $K_1=[H_2S_{(aq)}]\cdot[HS^-_{(aq)}]^{-1}\cdot[H^+_{(aq)}]^{-1}=10^{+6.98}$ (Wolthers et al., 2005).

The solubility products of FeS have shown some variation depending on the method of synthesizing FeS and the measurement of its dissolution. Davison et al. (1999) reported log $K_{sp,1}$ equal to 3.98±0.12 (3.00±0.12 as $K_{sp,2}$); Benning et al. (2000) reported log $K_{sp,1}$ equal to 3.77 (3.21 as $K_{sp,2}$) at 25°C; Wolthers et al. (2005) reported log $K_{sp,1}$ as 4.87±0.27 and most recently, Rickard (2006) experimentally determined log $K_{sp,1}$ to be 3.5±0.25. These differences in $K_{sp,1}$ are quite significant. According to Rickard and Morse's (2005) estimation, an order of magnitude of difference will cause a 20 times difference in concentration of dissolved Fe at pH 5. This discrepancy in the solubility product of FeS may be caused by the use of a filter with a coarse pore diameter, leading to the overestimation of FeS solubility due to the presence of solid phase FeS particles in the filtrate (Rickard and Morse, 2005). Also other differences in experimental conditions such as the sample preparation method, exposure to oxygen or loss of H_2S gas during the experiments, may also explain the different values of the solubility constants.

These suggested reaction and solubility product values are mostly applicable in acidic solutions because the dissolved iron or sulfur concentrations are measurable in this range. The solubility of FeS in solutions above pH 6 had been considered poorly known, but Rickard (2006) intensively investigated the solubility of FeS for a wide range of pH values (3-10), and reported the pH-independence of dissolution of FeS above pH 6. Therefore, the FeS dissolution reaction may be more important in a system where the pH is 6 or under. This fact suggests that the precipitation process, which may be responsible for the removal of bulk amount of As(III) removal, would be more important in acidic conditions than in basic conditions.

2.1.5 FeS as a divalent metal scavenger

Due to its common occurrence and high reactivity under reducing conditions, mackinawite has been studied as a possible removal material for toxic trace metals. Previous studies have shown that mackinawite effectively immobilizes heavy metals such as Pb(II) and Cd(II) (Coles et al., 2000), Hg(II) (Jeong, 2005), Cd(II), Cr(III), Cu(II),

Ni(II), and Zn(II) (Morse and Arakaki, 1993). Most of these cations can be precipitated as metal sulfides, and the partition coefficient of each metal strongly increases with the decreasing solubility of the precipitated form of metal sulfides. The possible reactions for the incorporation of divalent metals into FeS are given as following (Morse and Luther, 1999):

1) $Fe^{2+} + HS^- \rightarrow FeS + H^+$ (FeS formation)
2) $FeS + Me^{2+} \rightarrow Fe\text{-}S\text{—}\ Me^{2+}$ (Metal adsorption onto FeS)
3) $Fe\text{-}S\text{—}\ Me^{2+} \rightarrow Fe(Me)S + Fe^{2+}$ (Metal inclusion into FeS)
4) $FeS + Me^{2+} \rightarrow MeS + Fe^{2+}$ (Metal exchange reaction)

As listed above, the divalent metal sequestration is mainly related to the direct substitution reaction of FeS rather than an adsorption reaction. FeS is thought to be potentially a major sink for many trace metals during early digenesis in anoxic conditions with the solubility of the metal sulfides controlling the reactions in the process (Morse and Arakaki, 1993). The sequestration of arsenic by FeS is intensively reviewed in the next sections.

2.2 Interaction between FeS and As(III)

2.2.1 Removal of arsenic by metal sulfides

The uptake of divalent cations by iron sulfide has been widely described, but much less is known about the incorporation of anions. Among oxyanions, arsenite has a high pKa (~9.2) so the highest degree of adsorption would be expected at high values of pH, if it follows the trend of adsorption maximum near the pKa value. However, most of the metal-hydr(oxides) show their highest arsenite adsorption at circumneutral pH, indicating less adsorption attributed to electrostatic effects (Dzombak and Morel, 1990; Hiemstra and Van Riemsdijk, 1999). In contrast, arsenic adsorption onto sulfide metals, such as PbS (galena), ZnS (sphalerite), FeS (troilite) and FeS_2 (pyrite), increased with increasing pH (Bostick and Fendorf, 2003; Bostick et al., 2003). This is evidence that this adsorption is on the sulfide mineral surfaces, not the oxidized metal (hydr)oxide surfaces. Thus, an earlier study of anion sorption by metal sulfides, which suggested that the metal

sulfide surface behaves analogously to the metal (hydr)oxide surface (Balsley et al., 1996), appears not to be applicable to arsenic sorption.

The incorporation of arsenic in sulfidic minerals such as PbS, ZnS, HgS or Cu_2S might be much different from that in FeS, because these other metal sulfides have a lower solubility than arsenic sulfide, while FeS has a much higher solubility than arsenic sulfide. This fact was demonstrated by the sulfide addition experiment by Bostick et al. (2003). According to their experimental results, the relative degree of As(III) adsorption to PbS and ZnS at pH 7 was not affected by sulfide addition. In other words, the precipitation of arsenic sulfide did not occur when arsenic was mixed with PbS and ZnS. In contrast, because of the higher solubility of FeS than arsenic sulfide, in an FeS system, the solid phases will be controlled by arsenic sulfide, particularly at low pH where sulfide dissolution is activated. Gallegos et al. (2007) indicated realgar precipitation as the reaction product between FeS and As(III) under low pH conditions, which was corroborated using X-ray adsorption spectroscopy (XAS) and X-ray diffraction (XRD) studies. Their XAS data indicated that the As(III) valence state was reduced and was primarily coordinated as As-S (~2.26Å) and As-As (2.54 Å). This was considered a realgar-like solid. They suggested that at higher pH conditions, arsenic is dispersed onto the solid by direct bonding to an O-atom, indicative of surface complexation uptake, with precipitation limited by the minimal amount of FeS dissolution.

2.2.2 Adsorption of As(III) on FeS

2.2.2.1 Adsorption mechanism of As(III) on FeS

Arsenic sorption by mackinawite has not yet been extensively studied, despite the rising interest in the environmental applicability of mackinawite and concerns over arsenic contamination of groundwater. There have been a few studies of reactivity between arsenic and mackinawite. Using XAS, Farquhar et al. (2002) found that mackinawite formed outer-sphere complexes with both As(III) and As(V) (except in the case of high As(III) concentration of 0.2 mM). Wolthers et al. (2003, 2005) conducted arsenic sorption experiments with disordered mackinawite and similarly reported outer-sphere complexes as a sorption mechanism. Gallegos et al. (2007) reported isotherm data under acid conditions that revealed that As(III) uptake is strongly correlated with a

decrease in total sulfur in solution, suggesting a precipitation reaction prefaced by mackinawite dissolution. In contrast, under alkaline conditions where mackinawite dissolution is minimal, adsorption is the primary As(III) uptake mechanism with a minor contribution from arsenic sulfide precipitation. Gallegos et al. (2007, 2008) revealed that mackinawite and arsenic form inner-sphere complexes as indicated by the independence of ionic strength of the solution, which contrasts with results reported by Farquhar et al. (2002) and Wolthers et al. (2003 and 2005).

An adsorption mechanism can be systemically explained using a surface complexation model. Wolthers et al. (2005) proposed FeS surface species as a two-site model. The two sites were assumed to protonate and deprotonate according to the following surface protonation reactions:

$$\equiv FeSH^0 + H^- \leftrightarrow \equiv FeSH_2^+ \qquad Log\ K_{st1}^{app} = 8.0 \pm 0.1 \qquad (2\text{-}3)$$

$$\equiv FeSH^0 \leftrightarrow \equiv FeS^- + H^+ \qquad Log\ K_{st2}^{app} = -6.5 \pm 0.1 \qquad (2\text{-}4)$$

$$\equiv Fe_3SH^0 + H^- \leftrightarrow \equiv Fe_3SH_2^+ \qquad Log\ K_{wk1}^{app} = 7.85 \pm 0.05 \qquad (2\text{-}5)$$

$$\equiv Fe_3SH^0 \leftrightarrow \equiv Fe_3S^- + H^+ \qquad Log\ K_{wk2}^{app} < -9.5 \qquad (2\text{-}6)$$

where $\equiv FeSH^0$ is the neutral, strongly acidic mono-coordinated surface functional sulfide group that can protonate and deprotonate, $\equiv Fe_3SH^0$ is a neutral, weakly acidic tricoordinated sulfur site that can protonate and deprotonate, and K_{stl}^{app}, K_{st2}^{app}, K_{wk1}^{app}, and K_{wk2}^{app} are the apparent surface acidity constants and are variable model parameters. Wolthers et al. (2005) decided the concentrations of both reactive sites were equal, $[\equiv FeSH^0] = [\equiv Fe_3SH^0]$, and approximately equal to 1.2 mmol g^{-1} FeS. Their model, however, does not includes iron hydroxyl ($\equiv FeOH^0$), which was suggested by Bebie et al. (1998) as one of two main surface species, iron hydroxyl ($\equiv FeOH^0$) and sulfide ($\equiv SH^0$). Also this surface complexation model showed the reversal of surface charge at pH near 7.5 but this value would not be matched with the surface properties of FeS used in Gallegos et al. (2007) and this current study. Despite these limitations, this surface complexation model represents a first description of the surface chemistry of disordered mackinawite.

An XAS investigation of the uptake of As(III) by synthetic FeS reported that the uptake of As(III) at basic values of pH may be primarily attributed to uptake by adsorption as an As(III) oxyanion, demonstrated by the fact that the oxidation state of arsenite remained at a state of +3 after contact with FeS (Gallegos et al., 2007). In contrast to the adsorption of As(III) as oxyanion under the presence of FeS, a different adsorption mechanism was also reported in other metal sulfide systems. Bostick et al. (2003) suggested the formation of the thioarsenite trimer, $As_3S_3(SH)_3$, as the As(III) retention mechanism on PbS and ZnS surface according to the following reaction :

$$6{\equiv}MeSH + 3As(OH)_3 \leftrightarrow 6{\equiv}MeOH + As_3S_3(SH)_3 + 3H_2S \qquad (2\text{-}7)$$

a reaction which supposes no influence of the sulfide addition on As(III) retention, as corroborated by batch adsorption experiments. The formation of thioarsenite trimers, $H_xAs^{III}{}_3S_6{}^{x-3}$ (x=1-3), was also proposed and experimentally proved under sulfidic conditions at saturation with As_2S_3 (Spycher and Reed, 1989; Webster, 1990; Eary, 1992), while monomeric thioarsenites, $H_xAs^{III}S_3{}^{n-3}$, $H_xAs^{III}OS_2{}^{n-3}$, would be more likely under conditions undersaturated with As_2S_3. Moreover, an As-thioanion system would be considerably more complex as it would entail the supposition of at least six thiolated species (Wood et al., 2002; Wilkin et al., 2003). This possible variation of As-S species makes it difficult to accurately predict As speciation in FeS solutions.

2.2.2.2 Sorption isotherm fitting

An adsorption isotherm is determined by measuring the sorbed concentration of contaminants relative to the concentration in solution. In a simple system, the sorbed amount of contaminants is directly proportional to the concentration in solution and the ratio between these two concentrations is called the distribution coefficient (K_d). The adsorption of As(III) by FeS, however, displayed significant non-linearity with the typical shape of a Langmuir isotherm curve (Gallegos, 2007). Therefore, similar characteristics of sorption would be expected in an FeS-coated sand system. The Langmuir isotherm assumes limited sorption sites and can be described by:

$$q_{eq} = \frac{q_m K_l C_{eq}}{1 + K_l C_{eq}} \quad (2\text{-}8)$$

where q_{eq} is the amount of As(III) sorbed by a solid (mg/g), q_m is the total As(III) sorption capacity (mg/g) determined by fitting, K_l is the Langmuir constant (L/mg), and C_{eq} is the As(III) concentration left in solution (mg/L). This equation can be expressed in a linear form as:

$$\frac{C_{eq}}{q_{eq}} = \frac{1}{K_l q_m} + \frac{1}{q_m} C_{eq} \quad (2\text{-}9)$$

Using the obtained experimental results of adsorbent concentration in solution (C_{eq}) and solid (q_{eq}) at equilibrium, the linearized Langmuir isotherm can be plotted as a straight line. If the sorption data is linear, the fitted parameters q_m and K_l can then be obtained from the slope and y-intercept of the line. The parameter q_m represents the total amount of As(III) removed when the surface site is saturated (or the removal capacity is exhausted). The parameter K_l is a Langmuir constant, which represent how fast the removal capacity is exhausted. If K_l *is* small, the solute reaches its total capacity abruptly. If the K_l is high, the solute slowly approaches its total capacity. The Langmuir isotherm is widely used to describe the sorption behavior of arsenic, as presented in Table 1.1. Although Langmuir type sorption usually describes the adsorption behavior, a similar shape may occur even when removal mechanism is controlled by different processes, such as bulk or surface precipitation.

2.2.3 Precipitation of arsenic sulfide

Wilkin and Ford (2006) assessed the competition for solid-phase sulfide between arsenic and iron thermodynamically with the following reaction:

$$3FeS_{(s)} + 2As(OH)_3^0 + 6H^+ = As_2S_{3(s)} + 3Fe^{2+} + 6H_2O \qquad \log K=33.89 \quad (2\text{-}10)$$

The equation and thermodynamic constant indicate that the formation of amorphous orpiment (As_2S_3) is favored over mackinawite as pH decreases, and/or as the concentration of ferrous iron decreases. This expectation was hypothesized based on orpiment as a primary host of arsenite in sulfidic environments; however, some research has reported the occurrence of realgar as the controlling solid instead of orpiment (O'Day et al., 2004).

The precipitation of realgar from the reaction of $FeS_{(s)}$ and As(III) can be thermodynamically calculated using the solubility equations shown in Table 2.1. The obtained values of log K imply that the precipitation of realgar is favorable according to:

$$4.5FeS_{(s)} + 4H_3AsO_{3(aq)} + 8H^+ \leftrightarrow 4AsS_{(s)} + 4.5Fe^{2+} + 0.5SO_4^{2-} + 10H_2O \qquad \log K=49.19 \qquad (2\text{-}11)$$

The formation of both orpiment and realgar is favorable compared to the formation of FeS.

More recently, the evidence of precipitation reactions in As(III) sequestration was provided by spectroscopic studies (Gallegos et al., 2007). In their XAS measurements, X-ray absorption near edge structure (XANES) data of FeS reacted with As(III) at pH 5, which can be taken as an indication of the oxidation state of As in the particular coordination environment, showed X-ray absorption edge location to be higher than that of arsenopyrite ($Fe^{II}As^{-I}S^{-I}$), lower than that of As^{III} and within the range of that of realgar ($As^{II}S^{-II}$). The extended x-ray absorption fine structure (EXAFS) data, which allows bond distances and coordination numbers to be determined for coordination shells within 6 Å of the central atom of interest, also supported the formation of realgar under neutral and acidic values of pH (pH under 7). The precipitation of AsS was also verified by XRD measurements, which showed the presence of a realgar solid. Gallegos and coauthors further supported the hypothesis of the precipitation of realgar using thermodynamic modeling. The reduction of As(III) to As(II) was explained with the counter reaction of FeS oxidation into greigite (Fe_3S_4) or green rust ($Fe_2(OH)_5$) at low and high pH by the following two reactions:

$$3FeS + H_3AsO_3 + 3H^+ = 1/2\ Fe_3S_4 + AsS + 3/2Fe^{2+} + 3H_2O$$

$$\log K=17.85 \qquad (2\text{-}12)$$

$$2FeS + H_2AsO_3^- + 2H_2O = AsS + Fe_2(OH)_5 + HS^-$$

$$\log K=3.33 \qquad (2\text{-}13)$$

Given these equations, the oxidation of FeS may become more favorable as the concentration of As(III) increases.

Table 2.1 Aqueous thermodynamic data of S and As solid species, I=0 M, T=298.15K

Reaction	**logK**	**Reference**
Solubility of solid species		
$FeS_{(s)} + 2H^+ \leftrightarrow Fe^{2+} + H_2S_{(aq)}$	3.5	Rickard, 2006
$As_2O_{3(am)} + 6H_2O \leftrightarrow 3H^+ + 3HS^- + 2H_3AsO_{3(aq)}$	-44.83	Eary, 1992
Orpiment $+ 6H_2O \leftrightarrow 3H^+ + 3HS^- + 2H_3AsO_{3(aq)}$	-46.41	Pokrovski et al., 1996
Realgar $+ 0.5SO_4^{2-} + 10H_2O \leftrightarrow 4H_3AsO_{3(aq)} + 4.5HS^- + 3.5H^+$	-64.90	Pokrovski et al., 1996
Precipitation of arsenic sulfide from FeS		
$3FeS_{(s)} + 2As(OH)_3^0 + 6H^+ \leftrightarrow As_2S_{3(am)} + 3Fe^{2+} + 6H_2O$	33.89	Wilkin and Ford, 2006
$3FeS_{(s)} + 2As(OH)_3^0 + 6H^+ \leftrightarrow$ Orpiment $+ 3Fe^{2+} + 6H_2O$	35.94	Calculated
$4.5\ FeS_{(s)} + 4\ H_3AsO_{3(aq)} + 8\ H^+ \leftrightarrow$ Realgar $+ 4.5\ Fe^{2+} + 0.5\ SO_4^{2-} + 10\ H_2O$	49.19	Calculated
$H_2S_{(aq)} \leftrightarrow HS^- + H^+$	-6.99	Commonly known

2.2.4 Redox reaction of As(III) and FeS

The major elements of interest in this study, iron, sulfur and arsenic, are redox-sensitive. Under oxidizing conditions, the dominant species are Fe(III), SO_4^{2-}, and As(V) while under reducing conditions, Fe(II), S^{2-} (or HS^-), and As(III) are the dominant species. Generally, microbially-mediated reduction and oxidation of arsenic play important roles in the transformation of arsenic in sediments, soil, geothermal water, surface water and water treatment sludge (Meng et al., 2003). However, the biotic control of the sulfide mineral redox system may also play a role.

In the Fe-S-As system, the following redox reactions are considered to occur (Al-Abed et al., 2007):

$H_3AsO_4 + 2H^+ + 2e^- = H_3AsO_3 + 2H_2O$ logK = 18.9 (2-14)

$Fe^{3+} + e^- = Fe^{2+}$ logK = 13.0 (2-15)

$SO_4^{2-} + 9H^+ 8e^- = HS^- + 4H_2O$ logK = 33.7 (2-16)

Controlling the redox potential in an aqueous solution is more difficult than controlling its pH, so fewer studies have reported the effect of pe than have reported the effect of pH. Al-Abed et al. (2007) assessed the effect of redox potential on the mobility of arsenic from a contaminated mineral processing waste containing about 0.47 g/kg of As and 66.2 g/kg of iron. They controlled the redox potential by purging different kinds of compressed gases such as O_2, H_2, N_2, and air through the system, while maintaining a constant pH of 3, 5, 7, 9 or 11. For a given pH, the net change of redox potential did not exceed 200 mV. Their experimental results demonstrated that the amount of As released did not change with varying values of redox potential under the fixed pH conditions. Although Meng et al. (2003) reported a change in soluble As and SO_4^{2-} concentrations over the narrow pe range between -3.0 and -4.0, these could be the effect of pH variation because their reported pH values ranged from pH 6.98-7.76.

The importance of redox on As(III) uptake by FeS was thermodynamically simulated by Gallegos et al. (2008). They found that the redox state of the system depended on FeS concentration and pH such that higher initial FeS concentrations and alkaline values of pH resulted in more negative pe values. Based on a linear relationship between pe and pH, the model predicted the removal of As(III) from solution by precipitation of realgar (AsS) when pe was used as a fitting parameter. The simulation results of the Fe-As-S H_2O pe-pH diagram predicted realgar precipitation under a wide range of pH if the system is much reduced, while orpiment (As_2S_3) precipitation is expected when pe is higher under values of acidic pH. Realgar precipitation seemed to be more prevalent when the FeS concentration in the system is higher, thus resulting in a more reduced condition. This prediction of AsS formation under pH values of 5, 7, and 9 is contradicted by the pe-pH diagram constructed by Meng et al. (2003) where orpiment

was predicted over a much wider range of pH and realgar formation was limited to pH values under 4. Furthermore, for zero valent arsenic, As(0), precipitation was also predicted under low reducing conditions but the occurrence of As(0) is known to be rare in the natural environment.

2.3 Formation of coating on sands

In previous sections, the characteristics of FeS as an arsenic removal agent and the possible As(III) removal processes were reviewed. In this section, the methods of coating various minerals on sand were investigated to develop an optimized method of FeS coating on sand.

2.3.1 Coating conditions

In this study, FeS-coated sand was developed to achieve sulfide-providing porous media which might be effective in the remediation of As(III) in anaerobic environments. Even though powder forms of nanoscale materials such as mackinawite (FeS) may have high reactivities, fine powder materials may not be suitable for used in a permeable reactive barriers because the small particle size may result in low permeability. To eliminate this shortcoming, several methods might be used to enhance the particle size of reactive nanoscale materials: (1) injecting particles into the subsurface for adsorption onto the porous medium (Manna et al., 2003), (2) by forming a coating on larger particles or (3) by directly using a granular materials. Cases of direct injection are reported using various reactive materials such as nano-sized zerovalent iron, bimetallic nanoparticles, and functionalized titanium oxides (Cantrell et al., 1997; Elliott and Zhang, 2001; Schrick et al., 2004; Jia et al., 2007; Saleh et al., 2007). However, the direct injection methods may produce unevenly deposited coatings, which may lead to the plugging of porous spaces (Lee, 2009), and the down gradient contamination of groundwater with nano-sized materials, a recent concern (Biswas and Wu, 2005). Granular mineral materials such as alumina (Singh and Pant, 2004) and crystalline hydrous ferric oxide (Manna et al., 2003; Badruzzaman et al., 2004; Goswami et al., 2006) have proved to be good adsorbents, but their adsorption efficiency is usually not as good as their nano-sized counterparts.

In contrast, coating methods are more widely used (Scheidegger et al., 1993; Coston et al., 1995; Lo and Chen, 1997; Kuan et al., 1998; Thirunavukkarasu et al., 2003; Xu and Axe, 2005; Herbel and Fendorf, 2006). Past efforts have been devoted to coating sand with materials such as FeOOH/$Fe(OH)_3$ (Thirunavukkarasu et al., 2003; Appelo and Postma, 2005; Herbel and Fendorf, 2006), MnO_2 (Guha et al., 2001), red mud (Genc-Fuhrman and Gencfuhrman, 2005) and humic acid, ferrihydrite and aluminosilicate (Jerez and Flury, 2006).

To obtain optimal mineral coatings, conditions have been varied such as temperature, aging time, particle size, and pH (Scheidegger et al., 1993; Coston et al., 1995; Lo et al., 1997; Kuan et al., 1998; Xu and Axe, 2005). The observed effects of temperature on the degree of coating of iron-oxide minerals vary. In some cases, an optimum coating temperature was defined (Stahl and James, 1991; Xu and Axe, 2005), while in other cases, higher amounts of coating were obtained at higher coating temperatures (Edwards and Benjamin, 1989; Bailey et al., 1992; Scheidegger et al., 1993; Lo and Chen, 1997) or no significant temperature dependence was observed (Lo and Chen, 1997). In addition to the effect of temperature on coating amount and stability, Lo et al. (1997) reported that the coating temperature determines the mineral phase of iron-oxide with a higher temperature promoting the crystallization of iron oxide, resulting in amorphous iron-oxide at 60˚C, goethite coating at 150˚C, and hematite coating at greater than 300˚C. Despite the importance of temperature in achieving a good coating, FeS coating should be performed at room temperature. Since FeS is highly sensitive to temperature change, it can be easily transformed to less reactive greigite or pyrite in a short time at a high temperature (Hunger and Benning, 2007).

The effect of substrate particle size on the efficiency of coating is related to the surface area of the substrate. Smaller particles yield greater mass of coating per unit volume due to their greater surface area, as it was reported by Xu and Axe (2005) that when particle diameter decreased from 1.5 to 0.2 mm, the amount of coated iron-oxide mass increased 5-10 times depending on the coating method. This result is not surprising because the surface area is squared when the particle size is doubled. In past coating experiments, aging time has varied from several hours (Gupta et al., 2005; Herbel and Fendorf, 2006) to several days (Lai et al., 1999; Xu and Axe, 2005). Previous studies

suggest that aging time is not a significant control factor when the mineral coating is stable against dissolution. However, regarding FeS coating, aging time might be an important factor because FeS (mackinawite) is easily transformed to the other iron sulfide minerals (Benning et al., 2000).

The effect of pH on coatings was well researched by Scheidegger et al. (1993) who suggested that electrostatic attraction is the primary step in the coating reaction so that in coating of goethite on silica sand, the maximum coating was achieved at a pH near the pH_{PZC} of goethite and an abrupt decrease was observed at values of pH higher than the pH_{PZC} where the surface charge of both silica sand and goethite become negative. The oxide coating showed higher strength when the coating pH is higher than neutral pH, although the reported optimum coating pH varied from 8 to 12 probably depending on the pH_{PZC} values of the coated oxide minerals (Scheidegger et al., 1993; Kuan et al., 1998).

In this study, the pH_{pzc} of mackinawite particle is expected to be near pH 5 as FeS previously synthesized with the same method that will be utilized here gave this value (Gallegos et al., 2007). Therefore, the optimum coating pH is expected to be near 5. However, it should be noted that FeS has a much higher solubility under acidic conditions than that of goethite, demonstrated by the fact that 10% of the suspended particles were lost to the dissolved phase at pH 5 according to aqueous Fe concentrations measured by Gallegos (2007). Given the impact of pH on the electrostatic properties and dissolution, the coating pH is likely to be one of the most important factors in determining the optimum coating conditions.

2.3.2 Characterization of coated sands

In characterizing coated silica sand, several kinds of spectroscopic or other experimental methods are often used such as x-ray powder diffraction (XRD), x-ray photoelectron spectroscopy (XPS), scanning electron microscopy and BET isotherms for surface area measurement (Scheidegger et al., 1993; Xu and Axe, 2005; Jerez and Flury, 2006). XRD is used to identify the mineralogy of a bulk compound mineral, XPS is used to identify the surface elemental composition and to specify oxidation states of an element of interest, and XAS provides information about the oxidation state and bond distances of an element of interest using x-ray absorption near edge spectroscopy

(XANES) analysis and extended x-ray absorption fine structure (EXAFS) analysis. However some of those methods could not be applied to the characterization of FeS-coated sand because of the thin layer of coating and the sensitivity of FeS to heat. The widely used surface area measuring method, BET isotherm, requires heating the sample up to 300°C. The this method could not be used because FeS is easily transformed to greigite or pyrite in short times at high temperatures (Hunger and Benning, 2007). XRD may need a high mineral loading to distinguish the iron phase patterns from the coating from the strong silica or quartz features; in addition, the samples have a greater chance of exposure to oxygen during the measurement. XPS may be a better method to avoid oxygen contact during measurement because the samples are subjected to high vacuum during the experiment, thus, if precautions are taken, oxygen contact can be minimized.

In measuring the amount of coating, acid-extraction methods are often used. Extraction methods for determining the amount of iron sulfide in soils have been summarized by Cornwell and Morse (1987). While 100% recoveries were reported for amorphous FeS-S and mackinawite-S using hot or cold 6N HCl extractions, incomplete recoveries were noted for greigite unless a reducing agent was added. In general, dried FeS was found to be less extractable in HCl than wet FeS, which Rickard and Morse (2005) explained as resulting from less available pore space and a stronger static charge for dried FeS. Incomplete extraction of metal sulfides by single strong acid extractions has been reported previously (Huertadiaz and Morse, 1990; Cooper and Morse, 1998) with larger particle aggregates and resistant sulfide phases being implicated in lower acid extraction efficiencies. To overcome the limitations of single acid extractions, Cooper and Morse (1998) showed that combining sequential HCl and HNO_3 produced a more effective digestion for those iron fractions that were not completely extracted in a single step. Also, a single extraction with a mixture of 3:1 of concentrated HCl and HNO_3 solution (e.g., aqua regia reagent, International Organization for Standardization, ISO/CD 11466), has been shown to be effective for extracting metals from natural soils and has been used in such applications (Ramos, 2006; Tume et al., 2006).

2.4 Competition between arsenic and silicate

A mineral coating formed on sands is associated with dissolved silicate (This term will refer to monomeric silicate ions such as $H_4SiO_4^0$, $H_3SiO_4^{-1}$, etc.) because the silicate from the sand dissolves readily when in contact with groundwater. Therefore in the study of coated sand materials, the impact of the presence of dissolved silicate should be evaluated since silicate as an oxyanion may have competitive sorption properties to arsenite. Silicate concentration in natural groundwater ranges from 0.054 - 0.380 mM (1.5 - 10.65 ppm Si) with levels as high as 0.814 mM (22.82 ppm) (Elgawhary and Lindsay, 1972). In natural waters at pH values less than 9.5, silicate is present primarily as silicic acid, $H_4SiO_4^0$, and remains in a monomeric form unless the dissolved Si concentration and pH are considerably higher (Hiemstra et al., 2007). The pH dependence of dissolved silicate in equilibrium with $SiO_{2(s)}$ is well known and is expected to be relatively constant below 9 but progressively increases above 9.5 as the predominant speciation in solution changes from $H_4SiO_4^0$ to $H_3SiO_4^{-1}$ (Stumm and Morgan, 1981). Despite the well-known pH-dependent equilibrium solubility, some studies reported lower concentrations of dissolved silicate at pH near 7 to 9 than the other pH values. For example, Beckwith and Reeve (1964) found the least amount of aqueous silicate at pH about 7 to 9, with considerably higher quantities below pH 4. Hiemstra et al. 2007 also found that dissolved silicate was lowest near pH 9 but increased at lower pH in systems in which silica was mixed with goethite. These results may also be related to the slower dissolution kinetics of silica at moderate pH conditions. In the study by Elgawhary and Lindsay 1972, amorphous silica dissolution in a 0.02 M $CaCl_2$ solution, required a relatively long time of 10 days to reach a constant concentration at pH 5 and 7, in contrast to the typical batch reactor contact times of As uptake studies of one or two days.

The silicate ion is known to form inner-sphere complexes with Fe(III) solids by exchanging ligands with surface hydroxyl groups, making adsorption strongly pH-dependent (Pokrovski et al., 2003). As such, when silicate adsorbs to ferric iron solids, it may affect its surface properties. For example, when goethite was equilibrated in solutions containing silicate, the pH_{pzc} of the surface shifted to a higher value with increasing silicate concentration (Garman et al., 2004; Hiemstra et al., 2007). These

surface charging effects may impact adsorption of other anions and cations (Anderson and Benjamin, 1985).

The inhibitory effect of dissolved silicate on anion adsorption to Fe(III)-oxide surfaces has been previously attributed to the competition for surfaces sites for anions such as phosphate, chromate, arsenate, and arsenite (Swedlund and Webster, 1999; Mayer and Jarrell, 2000; Su and Puls, 2001; Waltham and Eick, 2002; Garman et al., 2004; Luxton et al., 2008). The effect of silicate on arsenic adsorption/desorption has been also studied mostly in relation to iron oxyhydroxides sorbents. Since the adsorption of silicate on a Fe-oxide surface is expected to be greatest near the pH of the pK_1 of silicic acid (e.g., pH = 9.5) the competitive effect on anion sorption is typically greatest near this pH (Hiemstra et al., 2007). Arsenite has a similar pK_1 of 9.2 with its maximum sorption also near its pK_1, so the competition of silicate with arsenite on iron oxide surfaces is generally expected to be much stronger than the competition with any other anion such as sulfate, chloride and fluoride (Gu et al., 2005). Moreover, the inhibitory effect of silicate in As(III) removal was tested using ZVI columns where the column containing a concentration of 20 mg/L of silicate showed a much earlier breakthrough than the system containing no silicate (Su and Puls, 2003).

Previous studies of the competitive interaction between silicate and arsenite sorption on Fe(III)-oxide indicate that silicate reduces both the adsorption rate and the total arsenic adsorbed (Swedlund and Webster, 1999; Waltham and Eick, 2002; Roberts et al., 2004). Swedlund and Webster (1999) examined the interaction between silicate and ferrihydrite and successfully described the inhibitory effect of silicate on arsenic adsorption with the diffuse layer model. Waltham and Eick (2002) investigated the effect of silicate on the adsorption kinetics and capacity and reported that the rate and total quantity of arsenite adsorption decreased in the presence of silicate at all pH values and concentrations of silicate. The loss amount of adsorption capacity was 40% with 1.0 mM silicate at all pH values. Roberts et al. (2004) also experimentally simulated the case of the Bangladesh groundwater, which contained high concentrations of silicate and phosphate. Given the inhibitory effect of silicate and phosphate on arsenic adsorption, they verified the advantage of using Fe(II) instead of Fe(III) as a sorbent for As(III). The use of Fe(II) for the oxidation of As(III) to As(V) and the formation of iron(III)

hydroxide gave much higher arsenic removal in the presence of high silicate and phosphate compared to the case of Fe(III). This is consistent with the more favorable sorption of As(V) compared to As(III) to iron oxyhydroxide solids. More recently, Luxton and co-workers, who investigated the effect of silicate on the uptake of arsenite by goethite, speculated that silicate blocked potential adsorption sites and/or displaced adsorbed arsenite, thereby reducing the total adsorbed arsenite (Luxton et al., 2008).

2.5 As(III) uptake of FeS-coated sand in batch and column systems

2.5.1 Interpretation of column breakthrough curves (BTCs)

Breakthrough curves (BTCs) are extensively used to characterize the physical and/or chemical processes of solute transport in porous media. The shape of BTCs have been found to be affected by the flow rate, concentration of injected solute, and length of column in both the point-of-breakthrough and steepness of BTCs (Singh and Pant, 2006). The steep slope of a BTC is characteristic of a system that exhibit high film-transfer coefficients, high internal-diffusion coefficients or Langmuir adsorption shaped isotherms. Under equilibrium conditions, non-sorbing solute transport will generate a breakthrough curve with an effluent concentration $C = 0.5\ C_0$ at 1 pore volume with symmetric sorption/desorption curves. In sorbing-solute transport associated with the ideal (i.e., linear) adsorption, the adsorption front of a breakthrough curve is usually retarded by some amount with continuously increasing effluent concentration until $C = C_0$ and 100% of sorbed solute is recovered in desorption. However, in real and complex systems, asymmetric BTCs have been reported in numerous cases. The mechanisms that can create an asymmetric BTC were reviewed by Limousin et al. (2007) such as 1) non-linear sorption isotherm, 2) the presence of immobile water, 3) slow adsorption or desorption kinetics, 4) preferential flowpaths, 5) colloidal transport, or 6) low Peclet number (a low ratio between advection and dispersion) (Limousin et al., 2007).

If complete BTCs exhibit long tails, this suggests that chemical non-equilibrium processes are occurring in the transport reaction. The non-equilibrium processes can also be identified using a flow interruption test, based on an increase in effluent concentration upon restarting the flow (Pang et al., 2002). Some BTCs display incomplete breakthrough curves with an effluent concentration plateau before the column capacity is exhausted. If

the solute transport is coupled with biodegradation or transformation, a plateau of C/C_0 <1 would be observed (Angley et al., 1992; Brusseau et al., 1999). However, a plateau of C/C_0 <1 was reported in some cases where abiotic mechanisms govern the solute transport and retention reactions (Kretzschmar et al., 1997; Pang and Close, 1999; Prima et al., 2002; Kim et al., 2006; Jia et al., 2007). From the reported examples of incomplete BTCs, the causes of plateaus at $C<C_0$ were explained as colloid deposition (Kretzschmar et al., 1997), non-equilibrium sorption and hydrolysis of atrazine (Pang and Close, 1999; Prima et al., 2002), kinetics of irreversible sorption of benzene (Kim et al., 2006) and rate limiting sorption/desorption of contaminants (Pang and Close, 1999; Jia et al., 2007).

The column uptake of a contaminant when precipitation controls the reaction is less frequently reported in the literature than the case of adsorption as the controlling reaction. Mercury removal using ZVI was simulated and it was found that the precipitation of HgS, which resulted in a plateau shape of BTC, was attributable to the removal of mercury under anaerobic conditions (Weisener et al., 2005). In U(VI) transport in soil columns, an incomplete BTC for over thousand pore volumes was observed and the amount of total uptake were calculated to exceed those amounts estimated from batch adsorption isotherms. This incomplete BTC and higher capacity in column reactors were explained by several fundamental differences between column and batch systems including the possible precipitation of $UO_2(OH)_{(s)}$ in column, over the extended contact time (Barnett et al., 2000).

2.5.2 Retention time-dependent BTC behavior

In many cases, uptake of solutes from water flowing through column reactors packed with porous media require more equilibrium time than well-mixed batch reactors comprised of the same particles. Generally, sorption related non-equilibrium is regarded as one of the most common causes of the asymmetric or non-ideal shape of the breakthrough curve (Darland and Inskeep, 1997; Limousin et al., 2007). The nature of the long tailing and slow desorption is also evidence of non-equilibrated sorption reactions. To determine whether a solute is equilibrated with the porous medium, one can compare two BTCs of a reactive solute under two different flow rates or retention times. If BTCs with same injected conditions except flow rate do not superimpose, then

a rate-limited uptake mechanisms is involved (Limousin et al., 2007). An example of this is provided from the study of ^{85}Sr adsorption in a column packed with sand (Singh and Pant, 2006). In this study, the BTC shape changed when the column length, flow rate and the concentration of injected solute were varied demonstrating that ^{85}Sr uptake by sand was rate limited and not at equilibrium within the column.

Kinetic limitations caused by porous media inaccessibility may also be responsible for non-equilibrium uptake and dependence of capacity on flow rate and column length. In a study of goethite particle transport and deposition within a packed sand column, Jia et al (Jia et al., 2007) found that the amount of goethite deposited depended on the flow rate. This kind of kinetic limited deposition has been explained by a particle deposition efficiency that is proportional to the travel distance or travel time of the particles through the porous media (He et al., 2009). The reason for a lower deposition capacity in the shorter column has been explained as resulting from preferential flow through zones of higher permeability that result in more of the deposition sites being bypassed and a more rapid breakthrough (Pang and Close, 1999). Similarly, more bypassing and lower attachment capacity would be expected at higher flow rates observed by Jia et al. (2007).

2.5.3 Batch and column systems

In studying a new adsorbent for PRB application, column experiments are indispensible to evaluate the applicability of the absorbent to the field, because the test with porous medium almost always represents the field conditions better due to analogous advection, dispersion and reaction conditions with natural porous media. Despite these advantages, there are also disadvantages of column systems. The rate of reaction in a column system might be controlled by diffusion through an immobile thin film and the thickness of this film depends strongly on the advective flow rate. Therefore, selecting the flow rate is important. In addition, to eliminate the occurrence of preferential flow paths, a larger column size is recommended but larger means a longer breakthrough time. Besides, a column system is usually more complex because chemical transport includes both physical and chemical processes simultaneously. So while a

column system may better represent conditions in the field, the experiments can be more problematic in terms of determining the controlling processes involved.

In laboratory studies, because of the simplicity and rapidity, batch adsorption tests are more often used to derive the distribution coefficient (K_d), the ratio of solute concentrations between aqueous phase and solid phase which may be used to model transport of solute. In column reactor, K_d is defined as an important component in determining a retardation factor ($R = 1 + \frac{\rho K_d}{\theta}$). Here, R is a retardation factor (unitless), ρ and θ are a bulk density (g/cm^3) and a porosity (unitless) of a porous medium. The retardation factor is commonly obtained using a graphical method, method of moment, or from a parameter estimation approach based on the advection-diffusion equation (Maraqa, 2000). Many studies demonstrate the effectiveness of the retardation based approaches by reporting congruent values between batch and column-derived K_d (Macintyre et al., 1991; Carroll et al., 2006).

However, many incongruent results are also reported. Because the batch experimental conditions are different from these encountered in column experiments differences are often reported as resulting mainly from the following reasons: 1) the solid solution ratio (SSR) is much lower in batch experiment (normally under 100-500g/L for granular reactant and much lower for nanoscale reactant particles) than that of column experiment of which SSR is usually 3000-5000g/L (Maraqa, 2000), 2) equilibrium is generally assumed and readily achieved in batch system but not in column system, and 3) some unexpected side effects such as particle detachment, abrasion, crushing or desorption may occur in batch systems due to the asserted vigorous mixing (Mihaljevic et al., 2004).

In many studies, the distribution coefficient determined with batch tests do not agree with distribution coefficients (K_d) determined in column systems. More commonly, the values in the flow system are lower than those in the batch system (Dufresne and Hendershot, 1986; Rainwater et al., 1987; Maraqa et al., 1998; Pang and Close, 1999). This effect was found more pronounced for compounds with characteristics of large partitioning. For example, in batch and column study of ^{85}Sr adsorption, the batch obtained capacity was one order of magnitude higher than that in column experiment

(Szenknect et al., 2005). They conducted various laboratory methods to find the reason for this discrepancy from the loss of fine particles during the initial conditioning of the sand column or the production of fines during the equilibrium period in the batch system, consequently changing reactivity by generating extra surface of reactive sites.

The reverse trend, however, has also been reported (Miller et al., 1989; Seo et al., 2008). Seo et al. (2008) reported higher sorption capacities of various heavy-metal ions by a natural sediment in the column experiments. They speculated the reason for the higher capacity in column system to be due to the co-precipitation of metal sulfide enhancing the metal retention compared to the batch system where the heavy metals were only retained by an adsorption mechanism. Similarly, three different soils used for U(VI) adsorption yielded about twice as much of total U(VI) uptake in a column experiment compared to the amount obtained from batch adsorption isotherms (Barnett et al., 2000). The authors provided several possible explanations for this discrepancy such as a longer contact time in column experiments which may have allowed for migration of U(VI) into microspores of solid phase, the gradual injection of U(VI) in column experiment which could have led to a different and more efficient arrangement of U(VI) on the sediment surfaces, and the presence of higher concentration of competitive dissolving solutes in the batch reactor which may have inhibited U(VI) adsorption. Additionally, the precipitation of $UO_2(OH)$ was also speculated to be the reason of additional uptake observed in column reactor.

The discrepancies between batch and column techniques may be prominent when the sorption behavior is non-linear as a function of contaminant concentration. In non-linear sorption, the solute distribution coefficient is a function of an equilibrium solute concentration. If non-linearly sorption is modeled with a linear model, the R value may be overestimated compared to using a more appropriate non-linear sorption model (Rousseau, 1995). To achieve similar solute uptake behavior in both batch and column systems, the influent concentration injected in column needs to be similar to the maximum equilibrium concentration in batch (Maraqa, 2000). Otherwise, the batch-derived R value may easily under or overestimate the column-derived R. Past analysis of the nonlinearly sorptive behavior has revealed that application of the Langmuir and Freundlich isotherms systematically underestimate and overestimate, respectively,

column-derived R values, even when local equilibrium conditions are met in columns (Wise, 1993). In the case of dissolved organic carbon transport, good agreement was obtained between batch and column results in sandy soil system wherein simple and linear adsorption was characterized, while batch experiment apparently underestimated the retardation factor for a more clayey soil with non-linear adsorption characteristics (Li and Shuman, 1997).

Moreover, sorption non-equilibrium may also cause inconsistencies in determining R values in batch and column systems. When local equilibrium in a column reactor is not achieved, higher removal capacity in batch system is often reported in the literature (Bilkert and Rao, 1985). In contrast, if the batch sorption is slow and the system is assumed to be equilibrated but is not, then the batch estimated R will be smaller than the actual R (Macintyre et al., 1991). When long tailing occurs in the breakthrough curve (BTC) due to non-equilibrium sorption/desorption, curve fitting methods will underestimate the R in the column (Luo et al., 2006). In such cases, the method of moment (MOM) is appropriate to use because this leads to an R value that is independent of kinetic limitations.

2.5.4 Solid/solution ratio effect

The "solid/solution ratio (SSR) effect" or "solution effect" is the most fundamental difference between batch and column systems. Generally, in porous column systems, the solid/solution ratio (as mass(g) solid/volume (L) solution) is 3000-5000 g/L which is much higher than most batch systems which range from 100-500 g/L for larger granular material and to as low as 0.1 g/L for nanoscale materials. Theoretically, adsorption isotherm treatment of sorption data implicitly assume that the distribution of solute between solid and solution phase is SSR-independent. However, in many cases, the SSR effect positively or negatively affects the value of the distribution coefficient. Or these, it is more typical for the solute sorption to decrease with SSR. The reason why a higher SSR results in the inhibition of the adsorption process is not clearly known but the trend of lower removals with higher SSR is often reported in the literature (Bajracharya et al., 1996; Porro et al., 2000; Phillippi et al., 2007; Wang et al., 2009). Generally, this trend is more prominent when the sorption characteristics are non-ideal

(non-linear and/or non-equilibrium) or in multi-component solute systems. For example, in the study of Grolimund et al. (1995), the intensive prewashing of soil to remove pre-adsorbed competitive ions eliminated the SSR effect. Wang et al.(2009 showed that experimentally derived K_d values from batch reactors decreased with increasing SSR and reached a steady-state SSR value when the SSR exceeded 250 g/L (0.25) (Wang et al., 2009). This SSR of 0.25 has also been suggested as a good value for conducting batch reactor experiments to avoid batch-column discrepancies by Porro et al. (2000). The SSR effect is often explained in terms of the difference between solute and sorbent concentration (Hemming et al., 1997). In low SSR systems, the concentration of surface sites is limited so even the less favorable sorption sites would be utilized, while in high SSR systems, the there is an excess of surface sites for the solute so only the most favorable sites would be utilized. A mechanistic explanation of SSR effect has recently been provided for U(VI) sorption on goethite-coated sand in the presence of the co-solute phosphate. In that system, the adsorption of U(VI)-phosphate as a ternary surface complex enhanced the U(VI) adsorption at low SSR, but at high SSR, the competition between U(VI) and the excess phosphate in solution decreased adsorption (Cheng et al., 2006). Their surface complexation model supported well this mechanistic explanation of the basis for the SSR-dependent U(VI) sorption.

2.5.5 Comparison of batch and column derived solute removal capacities

2.5.5.1 Using total uptake capacity

In batch systems, the uptake capacity is generally obtained from isotherm data, especially when the data can be modeled with the Langmuir isotherm, which is characterized by a leveling-off and maximum uptake value with increasing solute concentration. In column experiments, uptake capacities can be calculated from the data in a variety of ways. For example, the capacity (or total amount retained) can be calculated by integrating the areas above the observed BTCs during adsorption phase (Barnett et al., 2000). Sometimes the column breakthrough point is used to determine a contaminant removal capacity of a column. The breakthrough point can be selected as the point where the detectable concentration begin, the point at which C/C_0 achieves a specific number, such as $C/C_0 = 0.1$ (Wibulswas, 2004), or the point where the effluent

concentration exceeds the maximum contaminant level. Based on the experimental results reported by Wibulswas (2004), the column capacity determined by estimating the adsorbed amount of solute up to the BTC point at $C/C_0 = 0.1$ for three different clay columns led to capacity values that were 78%, 19% and 18% of the batch capacity values determined by Langmuir isotherm analysis. In contrast, in a study of the total retained amount of heavy metals (As, Cd, Cr, Cu, Hg, Pb and Zn) by a natural sediment (Seo et al., 2008), a higher maximum adsorption capacity was found in the column experiments compared to the capacity obtained from batch reactor analysis. The authors suggested the reason for this difference was the precipitation of metal sulfide in the columns, a mechanism which did not occur in the batch reactors.

2.5.5.2 Using the distribution coefficient

The column and batch results of an adsorbent are often compared using a distribution coefficient (K_d). In batch reactor, K_d is defined as the ratio of adsorbate concentrations between aqueous phase and solid phase and in column reactor, K_d is defined as an important component of a retardation factor ($R = 1 + \frac{\rho K_d}{\theta}$). Here, R is the retardation factor (unitless), ρ and θ are the bulk density (g/cm^3) and porosity (unitless), respectively, of a porous medium.

Finding R in a batch results

The Langmuir isotherm, which is derived by assuming a limited number of equivalent sorption sites, is described by the equation (Appelo and Postma, 2005):

$$q_e = \frac{q_m C_{eq}}{K_l + C_{eq}} \qquad (2\text{-}17)$$

where C_{eq} (μg/g) is the equilibrium concentration of solute in solid, K_l (μg/L) is the Langmuir constant related to the binding energy of the sorption system and q_m (μg/g solid) is the adsorption capacity. In the Langmuir isotherm model, if the solute

concentration is small, if $C_{eq} << K_l$, the sorbed concentration increases linearly, but if the solute concentration is large, if $C_{eq} >> K_l$, the surface becomes saturated and the adsorption levels off to q_m.

When the equilibrium concentration of a solute is low enough, the curve is essentially linear and the distribution coefficient, K_d can be estimated simply as

$$K_d = q / C_{eq} = q_m / K_l \qquad (2\text{-}18)$$

When the surface approaches saturation, the distribution coefficient becomes a function of equilibrium solute concentration, C_{eq}, and can be expressed by the following equation:

$$K_d = \frac{q_m K_l}{(1 + K_l C_{eq})^2} \qquad (2\text{-}19)$$

Using the fitted Langmuir isotherm, the determined q_m and K_l predicts K_d for the varying equilibrium concentrations of As(III) in solution. Therefore, in Langmuir type sorption, a retardation factor $R = 1 + \frac{\rho}{\theta} K_d$ can be expressed using equation (2-19) as following ,

$$R = 1 + \frac{\rho}{\theta} \frac{q_m K_l}{(1 + K_l C_{eq})^2} \qquad (2\text{-}20)$$

Finding R in a column results

The transport of solute in a porous media is generally characterized by the system response to an injected solute which is typically presented by breakthrough curve (BTC). The most commonly used techniques of BTC analysis are based on moment analysis or advective-dispersion-reactive transport model analysis. In general, the method of moment (MOM) is more computationally efficient, and sometimes more stable alternative to analytical fitting of measured data (Luo et al., 2006). When applying an advective-dispersion reactive transport model, the formulation must be based on physical

and chemical nature of the system, and adequately describe the complexity of the system through an appropriate number of model parameters (Brooks and Wise, 2005). In the case of the employing the advection-dispersion equation, in ability to fit the BTC come from the inappropriate assumptions in analytical equation such as local equilibrium or homogeneity of the porous medium and the inability of the model to represent the complexity of the system. Shortcomings of the transport model analysis mainly result from the inability of the least square fitting methods to match the shapes when too few parameters or when too many parameters are fitted at a time they lose physical chemical meaning.

In contrast, MOM can provide robust and comparable parameters independent of the physical chemical characteristic of the system. One of the main drawbacks of MOM, is that MOM implicitly assumes reversible sorption, and that 100% mass recovery will be obtained. In column experiments where long tailing results and incomplete mass desorption occurs over the time frame of the measurements, inaccuracies in the model parameters can result. Even so, MOM has been shown to be useful in cases of irreversible sorption, with the analysis showing good agreement with retardation values estimated using analytical solutions (Limousin et al., 2007).

The MOM can be described by the following equations, where the solute breakthrough curve (BTC) may be viewed as a probability distribution function. The nth absolute moments and normalized absolute moments for a pulse input may be defined as

$$\mu_n = \int_0^\infty t^n C(L,t)dt \qquad (2\text{-}21)$$

$$\mu_n^* = \frac{\mu_n}{\mu_0} \qquad (2\text{-}22)$$

where C(L,t) is the flux-averaged concentration at the exit boundary (x=L) at time t. The zeroth moment of a BTC is a measure of the solute mass recovered from the system; the first moment is a measure of the travel time and the second moment is a measure of the mixing and /or the travel time distribution of the system. For a pulse input of solute of

duration t_0, the analytical expressions for the moments of the BTC is (Leij and Dane, 1991)

$$\mu_1^* = \frac{\mu_1}{\mu_0} = \frac{RL}{v} + \frac{t_0^2}{2} \qquad (2\text{-}23)$$

Here, R can be back-calculated using the used experimental conditions L, v and t_0.

CHAPTER III

MATERIALS AND METHODS

In this chapter, general experimental materials and methods used throughout the dissertation are discussed. Specific experimental methods used in each chapter are discussed separately in Chapters 4 to 8. A summary of the experimental systems and conditions for which results are presented in this dissertation are shown in Tables 3.2 -3.5.

3.1 Reagents

All experiments and sample preparations were performed in an anaerobic glove box with a 5% hydrogen/95% nitrogen atmosphere to provide an oxygen-free environment unless noted otherwise. All chemicals used were reagent grade. Deionized and deoxidized water was prepared by bubbling of Milli-Q water (the purified water of a Millipore Milli-Q system, Billerica, MA) with 99.99% nitrogen gas after boiling to remove oxygen and other gases from water. The deoxygenized Milli-Q water was used for making all reagents and the prepared reagents were stored in the glove box for future use.

3.2 Preparing natural sand and acid-washed sand for coating

Wedron 510 silica sand (Wedron Silica Co., Wedron, IL) was used in this study. The sand was reported by the manufacturer to be comprised of rounded grains with a chemical composition of 99.65% SiO_2, 0.065% Al_2O_3 and 0.018% Fe_2O_3. To prepare the sand for coating, it was sieved to obtain the size fraction that passed through a #70 sieve but were retained on a #100 sieve to obtain a geometric mean grain size of 0.15-0.22 mm. It was then washed several times with Milli-Q water, and then soaked in Milli-Q water

overnight with mild shaking. Following the soaking, the sand was rinsed with Milli-Q water until the rinse water was clear and then dried at ambient temperature (around 25 ˚C). The natural iron oxide coating existing on the sand was retained using this washing procedure as evidenced by the sand's retention of its slight orange tint. The amount of Fe-oxide on the Wedron sand was measured by an acid extraction as described below and found to be 0.12 mg ± 0.017 Fe/g sand (2.2×10^{-6} mol Fe/g). This value is within the range of reported natural Fe-coatings of 0.074 - 4.96 mg Fe/g soil sand (Coston et al., 1995).

To assess the importance of the iron-oxide coating on the FeS coating of the Wedron sand, an acid-washed sand (AWS) was prepared using a three-step procedure. First, the sand was soaked in 1 N sodium dithionite for 24 hours to remove any existing metal oxides. Then the sand was soaked in 12N HCl for 24 hours to remove any organic impurities. Finally, the sand was soaked in 15% H_2O_2 for another 24 hours to oxidize any remaining residual impurities. Between each of the chemical washes, the sand was rinsed with Milli-Q water 20-30 times to completely remove the chemical residual. The acid-washed sand contained less than 2.0×10^{-8} mol Fe/g sand, which is about 1% of the amount Fe that existed on the sand (2.2×10^{-6} mol Fe/g sand) prior to the acid washing. In identifying the Fe content of the natural sand and the acid-washed sand, the acid-extraction method which is described in Chapter 4 was used.

3.3 Synthesizing mackinawite (FeS)

FeS was synthesized inside an anaerobic chamber maintained at a 5%H_2/95%N_2 atmosphere by mixing 2.0 L of a 0.57 M $FeCl_2$ (Fisher Chemical) with 1.2 L of 1.1 M Na_2S solution (Butler and Hayes, 1998). The mixture was mechanically stirred for 3 days with a magnetic stirrer and then centrifuged (Du Pont Instruments, Sorvall RC-5B, Hoffman Estates, IL) at 10,000 rpm for 15 minutes to separate the solid from liquid. After decanting the supernatant liquid, the solid was rinsed with Milli-Q water multiple times until the electrical conductivity (Thermo Scientific Orion 5-star, Waltham, MA) of the rinsing solution was below 1 mS/cm (typically within 5 rinses). After freeze-drying, the FeS solids were sealed in glass vials capped with Teflon-coated butyl rubber septa and stored inside the anaerobic chamber until used. The detailed physical properties of

mackinawite prepared in this fashion including specific surface area and particle size have been recently reported by Jeong et al. (2008). The value of specific surface area and particle size depends on the methods used in the measurements, but the values are generally reflecting a high surface area and a small particle size of nano particulate FeS.

3.4 PHREEQC modeling

The geochemical modeling software package PHREEQC (Parkhurst and Appelo, 1999) was used to simulate the FeS coating and the reaction between FeS and As(III) at pH 5. The PHREEQC model allows the basic mixing chemistry and secondary mineral formation as well as surface complexation reaction provided proper chemical constants. In this study, the surface chemical parameters of FeS or FeS-coated sand associated arsenic were not found in literature, so only the basic mixing chemistry, dissolution of minerals and secondary mineral formations were considered as a possibly occurring reaction. Although the applied major reaction process was limited to the precipitation without considering adsorption, this approach may be a reasonable to apply because the modeled two systems, FeS coating and As(III) uptake of 5g/L FeS at pH 5, are known to be essentially controlled by precipitation process. The chemical composition in each system is summarized in Table 3.1. All simulations assumed equilibrium chemistry and the “minteq.v4” database provided from the package were used in all calculations unless otherwise noted.

Ta**ble 3.1** PHREEQC modeling inputs

Solution parameter (all units mol/kgw unless otherwise stated)	**FeS coating batch**	**5g/L FeS reacted with As(III)**
pH	Determined by reactions	5
Temperature (°C)	25	25
FeS	0.022	0.0568
Goethite	0.001	-
Quartz	5.43	-
HCl	0.00036	Added by reactions to fix pH
Na	-	0.1
Cl	-	0.1
As	-	0.0133

3.5 Measuring pe

E_h was measured as a function of solids concentration in the absence of arsenic for FeS-coated sand mixtures to verify the assumption of SSR-dependent-redox condition in FeS-coated sand batches. In FeS-coated sand system, each amount of FeS-coated sand was weighed and mixed with 10 mL pH buffered solution. After equilibration for 2 days, the pH and E_h (redox potential, indicative of pe) were measured in these suspensions. E_h was measured using an ORP (oxidation-reduction potential) combination electrode (Cole-Parmer) while E_h probe was moved up and down in vertical direction to maximize stirring in the small tube volume. Once the readings stabilized, the potentials were recorded. The measured potentials (in mV) were corrected for the standard hydrogen electrode (SHE) and temperature, and then converted to pe by using the equation 3.1 below (Stumm and Morgan, 1996):

$$pe = \frac{F}{2.3RT} E_h \qquad (3.1)$$

where R=gas constant (8.314 J mol^{-1} K^{-1}), T=temperature in K, F=Faraday constant (96,485 ˚C mol^{-1}) and E_h= the corrected E_h value for the standard hydrogen electrode (mV).

Table 3.2 Summary of sand coating experimental conditions

	pH of 2g/L FeS	**Aging time**	**Sand**	**Rinse method**	**2g/L FeS volume added to 50 g sand**
Surface modification	5.8	3 hrs to 3 days	Acid-washed Wedron sand, Wedron sand	No rinse after 3-day-mixing, Short-term (6 times rinse), or Long-term (1 day additional rinse)	32.5 mL
pH-dependent sand coating	4.4 to 6.3	3 days	Wedron sand	No rinse after 3-day-mixing	32.5 mL
Sand coating with varying FeS solution volume	5.5	3 days	Wedron sand	No rinse after 3-day-mixing	32.5, 65, 130 mL

Table 3.3 Summary of batch experimental conditions

	[As(III)]	SSR	pH	Buffer use	Measured element
Sorption Isotherm test	1.3×10^{-6} M to 6.7×10^{-4} M	500g/L	5	0.1N Acetic acid	As, Fe
	1.3×10^{-6} M to 2.6×10^{-4} M	500g/L	7	0.1N MOPs	As, Fe
	1.3×10^{-6} M to 2.6×10^{-4} M	500g/L	9	0.1N CHEs	As, Fe
pH-edge	Zero or 1.3×10^{-5} M	500g/L	5,7 and 9	Titrated	As, Fe, Si, pH
SSR-dependent sorption isotherm	1.3×10^{-6} M to 6.7×10^{-4} M	100g/L, 200g/L, and 500g/L	5	0.1N Acetic acid	As, Fe
	1.3×10^{-6} M to 2.6×10^{-4} M	100g/L, 200g/L, and 500g/L	7	0.1N MOPs	As, Fe
	1.3×10^{-6} M to 2.6×10^{-4} M	100g/L, 200g/L, and 500g/L	9	0.1N CHEs	As, Fe
SSR-dependent pe	-	100g/L, to 5000g/L	5	0.1N Acetic acid	Redox potential
Sorption isotherm with or without 0.35 M silicate	1.3×10^{-6} M to 6.7×10^{-4} M	500g/L	5	0.1N Acetic acid	As, Fe
	1.3×10^{-6} M to 2.6×10^{-4} M	500g/L	7	0.1N MOPs	As, Fe
	1.3×10^{-6} M to 2.6×10^{-4} M	500g/L	9	0.1N CHEs	As, Fe

Table 3.4 Summary of column experimental conditions

	[As(III)]	Sand mass	pH	Buffer use	Measured element
Long column	1.3×10^{-5} M	Around 475g/15cm column	5	0.1N Acetic acid	As, Fe
	1.3×10^{-5} M	Around 475g/15cm column	7	0.1N MOPs	As, Fe
	1.3×10^{-5} M	Around 475g/15cm column	9	0.1N CHEs	As, Fe
Short column	1.3×10^{-5} M	Around 150g/4.8cm column	5	0.1N Acetic acid	As, Fe, Redox potential
	1.3×10^{-5} M	Around 150g/4.8cm column	7	0.1N MOPs	As, Fe
	1.3×10^{-5} M	Around 150g/4.8cm column	9	0.1N CHEs	As, Fe

***** Detailed experimental conditions of column experiments are listed in Table 8.1.

Table 3.5 Summary of sample conditions for the spectroscopic studies

	[As(III)]	Solid	pH	Buffer use	Comment
XAS	1.3×10^{-2} M	5g/L FeS	5	Titrated	Wet paste (Room temp.)
	1.3×10^{-2} M	5g/L FeS	9	Titrated	Wet paste (Room temp.)
	1.3×10^{-3} M	500g/L FeS-coated sand	5	Titrated	Wet paste (Room temp.)
	1.3×10^{-3} M	500g/L FeS-coated sand	9	Titrated	Wet paste(Cryosat)
XPS	1.3×10^{-2} M	5g/L FeS	5	Titrated	Freeze-dried Pass energy 20 eV 2 days aged
	1.3×10^{-2} M	5g/L FeS	9	Titrated	Freeze-dried (Pass energy 20 eV) 2, 25, 50 days aged
	1.3×10^{-3} M	500g/L FeS-coated sand	5	Titrated	Freeze-dried (Pass energy 160 eV) 2 days aged
	1.3×10^{-3} M	500g/L FeS-coated sand	9	Titrated	Freeze-dried (Pass energy 160 eV) 2 days aged
XRD	1.3×10^{-2} M	5g/L FeS	5	Titrated	Freeze-dried 2 days aged
	1.3×10^{-2} M	5g/L FeS	9	Titrated	Freeze-dried 2, 25, 50 days aged
SEM	-	1.2, 2.4 and 4 mg FeS/g FeS-coated sand	pH 5.5 2g/L FeS	Titrated	3-day-aged

CHAPTER IV

FeS COATING

4.1 Introduction

Mackinawite (FeS) has been shown to be an effective sequestration agent for removing arsenic from water under anaerobic conditions. Under such conditions, more commonly applied sorbents such as ferric iron oxide phases may not perform effectively due to reductive dissolution of iron and the release of sorbed contaminants back into the water. Nanosized FeS, however, may not be suitable for trench and fill PRB applications due to its potential to create low permeability zones and short circuiting around a PRB. To eliminate the possibility of permeability reduction by nanoscale particles, a method of coating FeS on a natural sand surface was needed. In past work, in order to obtain optimal mineral coatings of reactive material on host substrates, conditions such as temperature, aging time, pH and particle size have been varied (Scheidegger et al., 1993; Coston et al., 1995; Lo et al., 1997; Kuan et al., 1998; Xu and Axe, 2005). Given that FeS is highly sensitive to oxygen and temperature change, the coating procedure must be performed under anoxic conditions and ambient temperature. Sensitivity of the metastable mackinawite to aging transformation must also be considered (Morse and Arakaki, 1993).

In this chapter, an optimal coating procedure of mackinawite on a natural silica sand was developed. An acid-extraction method was also optimized to quantify the amount of iron sulfide coated on the sand. Scanning electron microscopy and X-ray photoelectron (XPS) spectroscopy were used to characterize the morphology and chemical properties resulting from the sand coating. A comparison of the results of XPS for nanoscale FeS and FeS-coated sand may provide useful information about the oxidation state of iron.

4.2 Methods

4.2.1 Measuring the amount of iron coating on sand by acid-extraction methods

In order to measure the amount of Fe on the sand before and after coating with FeS, several acid extraction procedures were evaluated (Table 4.1). All acid extractions were performed by mixing 3g of the sand with the acid extractants in 15mL polypropylene centrifuge tubes and allowing the mixture to sit without further agitation for a specified amount of time (Table 4.1). Each method in Table 4.1 was run either in duplicate or triplicate. Subsequently, the extracting solution and solid were separated and the solid rinsed with Mill-Q water. The extracting and rinsing solutions were combined for Fe analysis. The total amount of Fe in the combined solutions was measured with an inductively coupled plasma mass spectrometry (ICP-MS, Perkin Elmer, Waltham, MA).

4.2.2 Coating procedure

Three coating steps were performed to determine the optimal coating conditions: (1) first the acid-washed sand was compared to the non acid-washed sand to see which surface preparation was best for the FeS coating. Then, using that surface preparation, the coating was optimized as a function of (2) pH, and (3) the volume ratio of dry sand to a 2g/L FeS suspension.

To compare effectiveness of the surface preparation, 32.5 mL of a 2 g/L FeS solution and 32.5 mL (~50g) of either the non-acid or acid-washed sand were combined in a 50 mL batch reactor tube and continuously mixed using an end-over-end rotator for three days. The aging time of three days was determined as the point in time when the supernatant solution of FeS and sand mixture became clear. This indicated that all the FeS particles were either attached on the sand surface or had self-aggregated into larger particles and settled out. After 3 days of aging, the pH of the FeS/sand mixture was measured, the mixture centrifuged, and the supernatant discarded. The pH of the solution after aging was found to be about 5.8. The separated solid was then subjected to either short term, long term or no rinsing as discussed below and then dried. Drying was done inside a glove box with no oxygen contact. The completely dried FeS-coated sand was

then stored in the glove box until needed. The best coating was obtained for the non acid-washed, natural Wedron sand.

Prior to drying but after discarding the supernatant, the solids were subjected to either a short term (six consecutive Milli-Q water rinses within one hour), a long term (an additional one day contact with Milli-Q water following the short term procedure) or no water rinsing. In all cases, the amount of Fe remaining on the solid was determined after drying the solids by the optimized acid extraction procedure described below. Subsequently, the non-acid washed natural Wedron sand with no rinsing was used for coating optimization as a function of pH and volume mixture ratios.

The optimum coating pH was determined by contacting the 2 g/L FeS suspension in 1:1 volume mixture with the natural Wedron sand over the pH range of 4.5 – 6.5. The pH of the solution was adjusted within this range by titrating with 0.8N HCl. Following a three-day aging, the solid was then separated from the solution by decanting the supernatant and drying without rinsing. The amount of Fe remaining on the solid was then determined by the optimized acid extraction procedure and the optimum pH was determined as the value where the maximum amount of FeS on the sand was obtained.

The impact of varying the volume ratio (from 1:1 – 1:4) of the FeS suspension to sand was tested at the optimum coating pH of 5.5. For this set of experiments, the volume ratio was varied by changing the volume of the 2 g/L FeS suspension at pH 5.5 mixed with 50 g of Wedron sand. A small amount of 0.08N HCl was added as needed to maintain a clear supernatant. After 3 days, the solids were separated from the solution, dried, and analyzed for the amount of Fe coating by the optimized acid extraction method .

4.2.3 Microscopic and spectroscopic characterization of sand coatings

Scanning electron microscopy (SEM) (Philips XL30FEG, Philips, Eindhoven, The Netherlands) was utilized to study the surface morphology of FeS coated sand. The samples were prepared in the anaerobic chamber and transferred using air-tight containers to minimize contact of the sample surface to oxygen. X-ray photoelectron spectroscopy (XPS) using a Kratos Axis Ultra X-ray photoelectron spectrometer (Kratos Analytical Ltd., Manchester, England) was used to examine the chemical composition

and oxidation state of Fe, S, O, Si and C on the surface of the FeS-coated sand. The Al-K_α line (1486.6 eV) was used as the radiation source. Survey and narrow XPS spectra scans were obtained with analyzer pass energies of 160 and 20 eV, respectively. Energies were corrected for charging effects using the reference peak of adventitious carbon C *ls* with a binding energy of 284.6 eV. Raw spectra were smoothed and then fit using a Shirley base-line and a Gaussian-Lorentzian peak shape.

XPS spectra of mackinawite were fit using the binding energies and FWHM (full width at half maximum) values reported in the literature for the four primary iron species for iron sulfides: Fe(II)-S, Fe(II)-O, Fe(III)-S, and Fe(III)-O (Pratt et al., 1998; Thomas et al., 1998; Mullet et al., 2004). In the Fe $2p_{3/2}$ spectra, Fe(II)-S and Fe(II)-O were modeled as single peaks at 706.8±0.1 and 707.7±0.1 eV representing a low-spin configuration of Fe(II) while the presence of Fe(III)-S was fit using the multiplet peaks located at 708.5, 709.5, 710.6 and 711.6 eV and the peak area ratios of 1, 0.68, 0.24 and 0.11, respectively (Herbert et al., 1998; Mullet et al., 2002; Mullet et al., 2004). These multiplet peaks are expected for high spin Fe(III) (Gupta and Sen, 1974). The Fe(III)-O contribution was also fit with four components located at 711.0 eV, 712.0 eV, 713.1 eV and 714.1 eV, using the same peak area ratio reported by others (Herbert et al., 1998; Mullet et al., 2004). The S *2p* spectra of mackinawite were modeled as a doublet ($2p_{1/2}$ and $2p_{3/2}$), separated by a spin-orbit splitting of 1.2 eV. The peak area of $2p_{1/2}$ was constrained to be half that of the $2p_{3/2}$. The O *1s* spectral contributions from FeS were fit with three components at 529.5, 531.0, and 532.2 eV for lattice-oxide oxygen, hydroxide oxygen, and adsorbed water oxygen, respectively (Mullet et al., 2002; Mullet et al., 2004), while the O *1s* from the silicate sands were modeled with contributions at 533, 532 and 531 eV, representing $>SiOH^{2+}$, $>SiOH^{0}$, and $>SiO^{-}$ surface groups, respectively (Duval et al., 2002). Since the Si *2p* spectra of the sands did not show any shift from one sample to another, they were fit using one primary peak at 102.7 eV. For quantitative results, to estimate the standard deviation of each of the component's contribution to the overall XPS spectrum in the fitting procedure, Monte-Carlo analysis (CasaXPS, Casa Software Ltd., UK) was applied. The program applies artificial noise to a spectrum and calculates an error matrix to give the variance of each fit based on the fitting constraints used.

4.3 Results and discussion

4.3.1 Identifying the amount of FeS coating by acid-extraction methods

In this study, several acid extraction procedures were tested (Table 4.1). These included a series of one-day extractions at three different concentrations of HCl (1, 6, and 12 N) and concentrated HNO_3. Of the single acid extractions, the best results were obtained using 6N and 12N HCl digestion over a period of a day, although only about 70% of the total FeS coated on the sand was extracted. The incomplete dissolution using these single acid extractions was thought to be due to one or a combination of the following reasons: the dried FeS-coated sand had aggregated causing the inaccessibility of some of the FeS; some of the mackinawite fine particles self-aggregated into larger particles that did not completely dissolve, FeS particles formed strong bonds with iron oxides on the natural sand surface that were not readily extracted, or the FeS partially oxidized during the coating process, producing iron sulfur and oxide phases that were more resistant to acid extraction. Such incomplete extraction of metal sulfides by single strong acid extractions has been reported previously (Huertadiaz and Morse, 1990; Cooper and Morse, 1998) with larger particle aggregates and resistant sulfide phases being implicated in lower acid extraction efficiencies. To overcome the limitations of single acid extractions, sequential HCl and HNO_3 digestion and a single extraction with a 3:1 mixture of concentrated HCl and HNO_3 solution (e.g., aqua regia reagent, International Organization for Standardization, ISO/CD 11466) were used, which resulted in complete extraction (See Table 4.1). These higher extraction efficiencies obtained in case of using HCl and HNO_3 at a same time have also been reported in the literature (Cooper and Morse, 1998; Ramos, 2006; Tume et al., 2006).

Table 4.1 Efficiency of acid extraction methods

Acid	Description of method	Exposure time	% extracted range	Average ± error %
1 N HCl	Soaking solid in 1N HCl	1 day	42.9-62.2%	56.3 ± 4.7%
6 N HCl	Soaking solid in 6N HCl	1 day	68.4-78.5%	73.4 ± 2.11%
12 N HCl	Soaking solid in 12N HCl	1 day	69.2-82.4%	78.2 ± 2.05%
HNO_3	Soaking solid in concentrated HNO_3	1 day	63.8-87.3%	67.6 ± 3.80%
12N HCl + HNO_3 sequential extraction	Soaking in HCl for 15 minutes and decanting HCl in separate jar for Fe analysis, repeat same with concentrated HNO_3	30 min	99.0-101.0%	100 ± 0.5%
Modified aqua regia	Soaking solid in 3 HCl + 1 HNO_3	1 hour	81.5-86.5%	84.0 ± 2.50%
		1 day	99.2-100.0%	99.6 ± 0.38%

* % extracted is calculated based on assuming that modified aqua regia extracts 100%.

4.3.2 Effect of surface modification (acid-washed sand vs. natural sand)

As shown in Figure 4.1, the water-rinsed natural Wedron sand resulted in a considerably more effective iron sulfide coating compared to the acid-washed sand. This is attributed to the presence of a naturally-existing coating of iron oxide that was evidenced by the slightly orange tint of the natural sand compared to the white color that resulted after acid extraction. The amount of iron oxide on the natural Wedron sand surface measured by the acid extraction was 2.2×10^{-6} mol Fe/g sand. Figure 4.1 also shows that no rinsing following the FeS coating process resulted in a coating that was more resistant to particle detachment than short term rinsing, which, in turn, was better than long term rinsing prior to drying.

During the coating procedure, some attachment of FeS began within minutes (as evidenced by the initial settling of black sand in the bottom of the reaction vessel), but the majority of nanoscale FeS particles still existed as a stable suspension in a solution phase. As the solutions aged over three days, the FeS suspension became progressively clearer and finally became completely clear, with most of the FeS particles settled from the solution either attached on the sand surface or self-aggregated. Some of the self-aggregated FeS particles easily detached from the sand support when the sand was subsequently washed with Milli-Q water. The loss of coating by rinsing was especially prominent in the acid-washed sand coating, with only 2-3% of the coating retained regardless of the rinsing procedure. In contrast, the non acid-washed Wedron sand retained about 65%, 90% or 100%, of coating for the short-term rinsing (six-times consecutive rinses accomplished within one hour), the long-term rinsing (one additional rinse with 1 day contact), or no rinsing, respectively. These results demonstrate that non acid-washed sand is a better support than the acid-washed sand and no rinsing after the coating step gives the most stable and greatest coating amount.

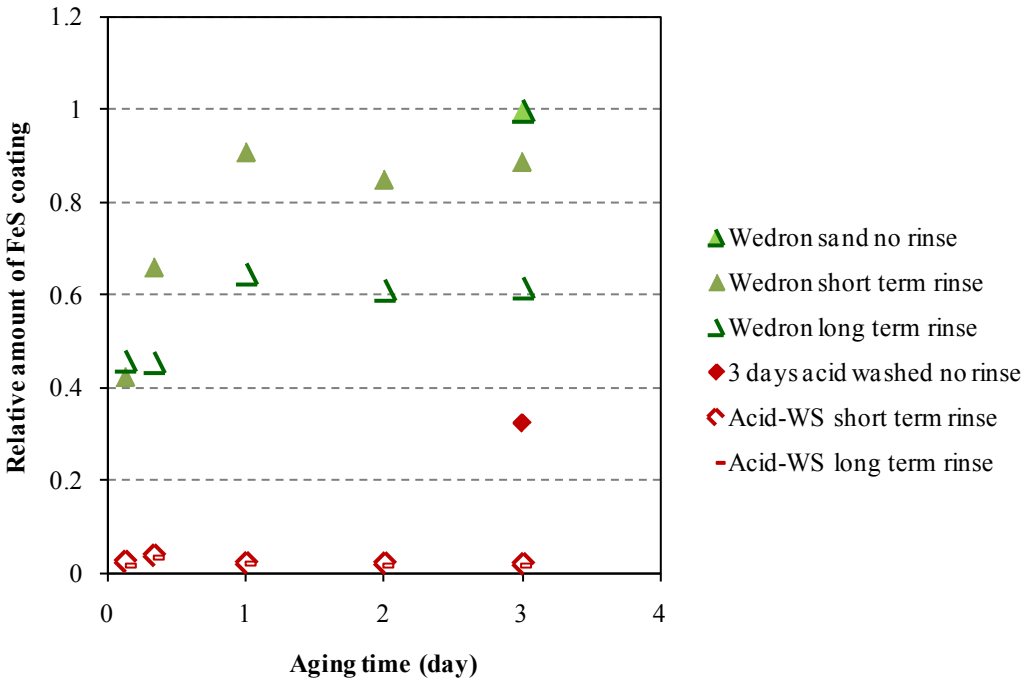

Figure 4.1 Relative mass of coating on surface-modified sand (acid-washed sand: AWS) and unmodified sand (natural sand: NS) as a function of aging time. The amount of FeS coating on natural sand without pre-rinse was assumed as 1.

4.3.3 Optimal pH of coating

Figure 4.2 shows that the optimum pH for coating was in the range of 5 to 5.5. In this pH range, mackinawite particles self-aggregate in solution, as evidenced from the degree of particle settling. FeS suspensions naturally drift toward pH values near 10 over time, unless the solutions are titrated with acid. At pH values above 9, the FeS particles tend to be highly dispersed, stable with respect to settling, and do not deposit on Wedron sand, as evidenced by the black-color of the supernatant of the FeS/sand mixture at the higher pH, compared to the clearness of the supernatant at pH 5 to 5.5. Between pH values of 5 to 5.5, visibly black coatings formed on the natural sand, but the amount of FeS coverage varied, with the sand coated at pH 5.5 yielding almost twice as much FeS compared to the sand coated at pH 5 (Figure 4.2). Even though the initial pH value of the FeS solutions was between pH 5 to 5.5, it should be noted that the final equilibrium pH after mixing with the natural Wedron sand increased to between 6.8 and 7.5. This pH increase was not observed when coating the acid-washed sand. A logical explanation for

this result is that the natural ferric oxide coating on the natural sand undergoes a redox reaction with FeS with protons being consumed during this process.

This optimum coating pH value is thought to be related to the pH_{pzc} (i.e., the pH of the point of zero charge) and solubility of FeS as well as the pH_{pzc} of the sand. At the pH_{pzc} of FeS, the particles have zero charge, resulting in the maximum self-aggregation. For FeS, the pH_{pzc} value is near pH 5 (Gallegos, 2007), so the maximum coating may be expected to occur near pH 5. However, the solubility of FeS is also an important consideration in determining the optimum coating pH. Below pH 6, the solubility of FeS begins to increase dramatically and at pH 5 about 10% of the FeS particles in a 0.65 g FeS/L suspension were dissolved in the aqueous phase (Gallegos, 2007). As shown in Figure 4.2, a small change in pH near pH 5.5 can cause a significant difference in the amount of coating which is attributed to the high solubility of FeS at this pH. Thus, the optimum pH of the FeS solution for coating was determined to be pH 5.5, which is near the pH_{PZC} but where FeS solubility is not too high. The FeS-coated sand so produced yielded an average coating amount of $1.43\times10^{-5} \pm 5 \times10^{-7}$ mol FeS/g sand. Based on the calculated standard error of less than 5%, this method produces a reasonably reproducible amount of coating.

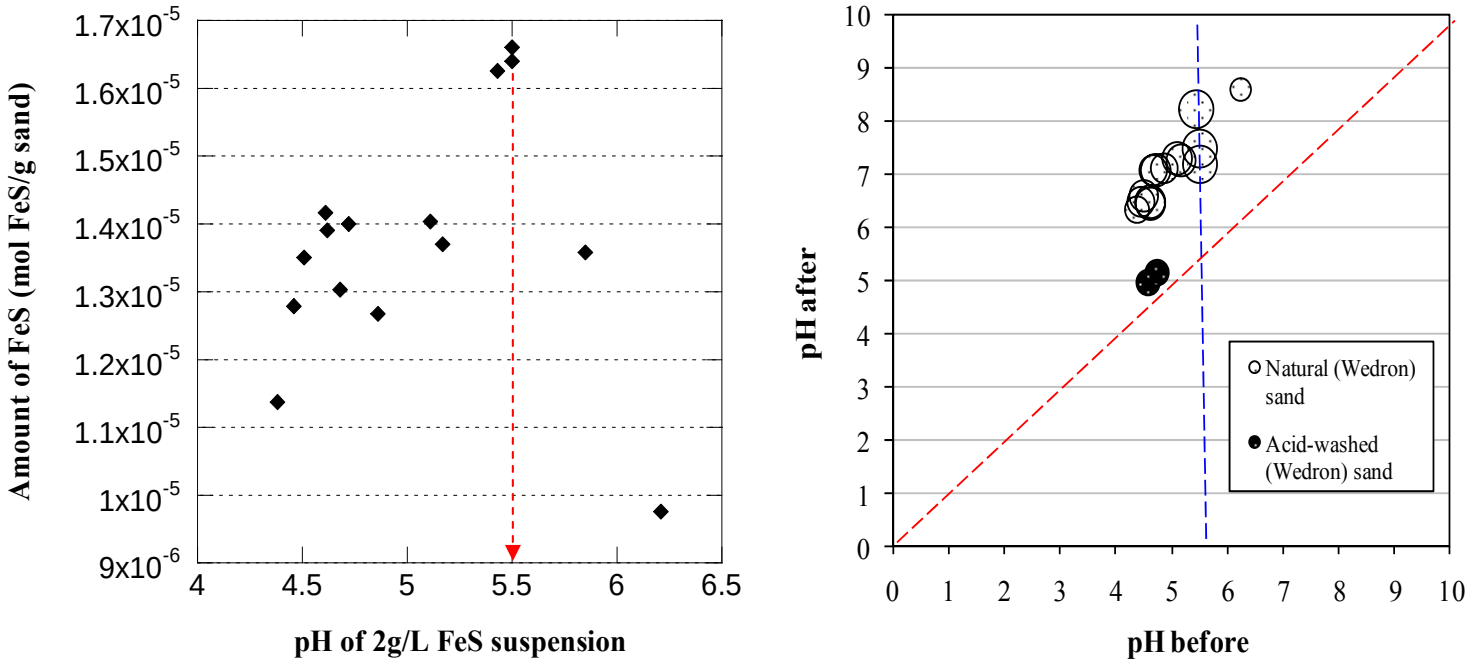

Figure 4.2 Effect of FeS suspension pH (pH before mixing with sand) on FeS coating amount with the optimum coating found at a pH value of 5.5 (left) and the solution pH of FeS suspension before and after mixing with sand (right).

4.3.4 Effect of concentration of FeS solid on coating amount

In the two previous subsections (4.3.2 and 4.3.3), the optimum FeS coating conditions were determined as a function of sand preparation conditions (e.g., using non acid-washed sand, no rinsing after coating, at pH 5.5). Using theses optimum coating results, the impact of mixture volume conditions were evaluated. For these experiments, the ratio of the volume of sand and 2 g/L FeS suspension was adjusted from 1:1 to 1:4. The amount of FeS coating was found to increase by adding a greater total mass of FeS solid (Figure 4.3). Applying more volume of 2 g/L FeS, which was adjusted as pH value at 5.5, from 1:1 volume ration to 1:2 or 1:4 to the same mass of sand resulted in unclear supernatant. This implicated that adding more acid may enhance the self-aggregation of FeS particles to the coated FeS layer on sand surface. So pH of the sand and FeS mixture was further titrated using HCl and the better FeS loading was obtained. The immediate pH reading after titration at maximum coating pH for the 1:2 and 1:4 volume ratios was pH 4.7 and 4.5. This result indicated that the optimum pH of FeS suspension may be strongly related to the total mass of FeS particles existing in the batch presumably because the presence of larger amount of FeS resulted in the stronger tendency of increasing pH towards pH value near 10, consequently needed more acid to maintain the equilibrium pH of suspension close to the pH_{PZC} of FeS. The maximum coating was found to be 1.2, 2.5 and 4.0 mg Fe/g sand for the 1:1, 1:2, and 1:4 ratio experiments, respectively. This indicates that the coating amount could be enhanced by a factor of 3 by increasing the total amount of FeS ratio by a factor of 4. However, it also indicates that there is a point of diminishing returns in that not all of the FeS in the suspension coats the surface at the highest ratio, with the coating efficiency diminishing from 100% for the 1:1 and 1:2 ratio conditions to only 80%. From the standpoint of an optimum use of materials, this would indicate that a coating condition of a 1:2 volume ratio would give the most efficient use of material while maximizing the coating amount.

4.3.5 Microscopic and spectroscopic sand characterization

To characterize the morphology and surface chemical composition of the FeS-coated sand, scanning electron microscopy (SEM) and x-ray photoelectron spectroscopy (XPS) were used. Given the sensitivity of FeS to transformations by oxidation or heat and the thin layer of coated-FeS on the sand, characterization was limited to surface-

sensitive methods in which exposure to heat or oxygen can be minimized. Because the highest amount of FeS coating obtained was just 0.4% of the mass of silica sand, and aggregated nanoscale FeS particles on the silica surface give only weak diffraction peaks, x-ray diffraction was ineffective for investigation of the coating on the sand surface. Also the widely used BET surface area measuring method, in which samples are heated up to 300°C, could not be applied with confidence given that FeS is easily transformed to greigite or pyrite in a short time at a high temperature (Hunger and Benning, 2007).

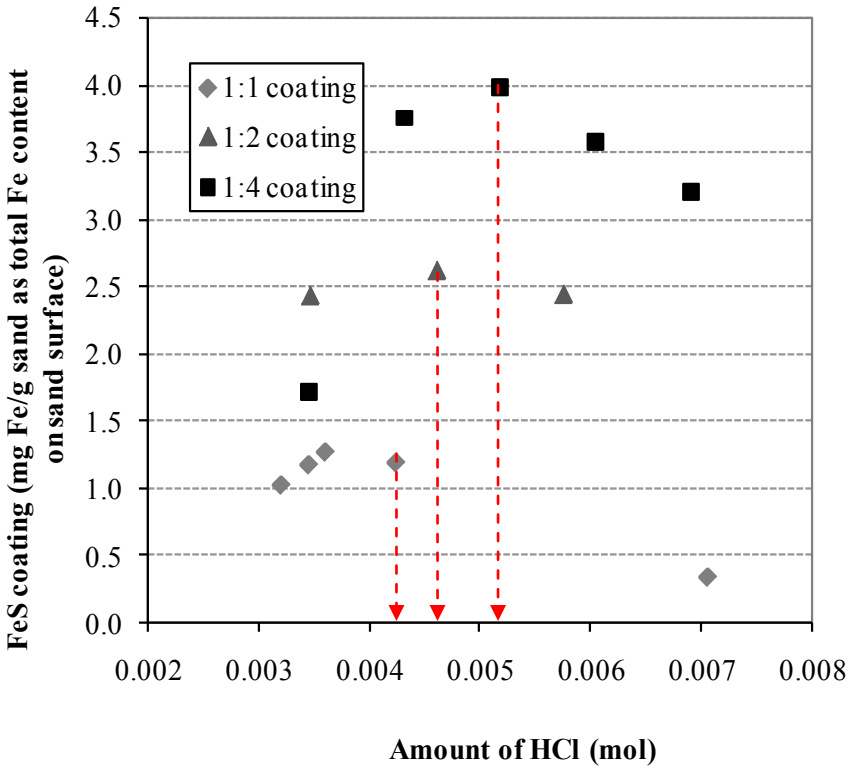

Figure 4.3 Effect of the volume ratio and amount of added acid on coating amount. The ratio represents the unit volume of sand relative to varying volumes of a 2g/L FeS suspension. The 1:1 ratio represents 32.5 mL of sand (~50 g) to 32.5 mL of the 2g/L FeS suspension.

4.3.5.1 Scanning electron microscopy

SEM images of FeS-coated sand illustrate patchwise coating and aggregated nanoparticles of FeS covering the sand surface (Figure 4.4). The indentations on the silica surface appear to be effective locations for the build-up of FeS aggregates. An

increasingly thick layer of FeS coating is visible as the coating amount increases from 1.2 to 4.0 mg FeS/g of coated sand (Figure 4.4b-d). This result demonstrates that self-aggregation among FeS particles is the primary mechanism leading to enhanced amounts of coating as the total amount of FeS in contact with the sand is increased.

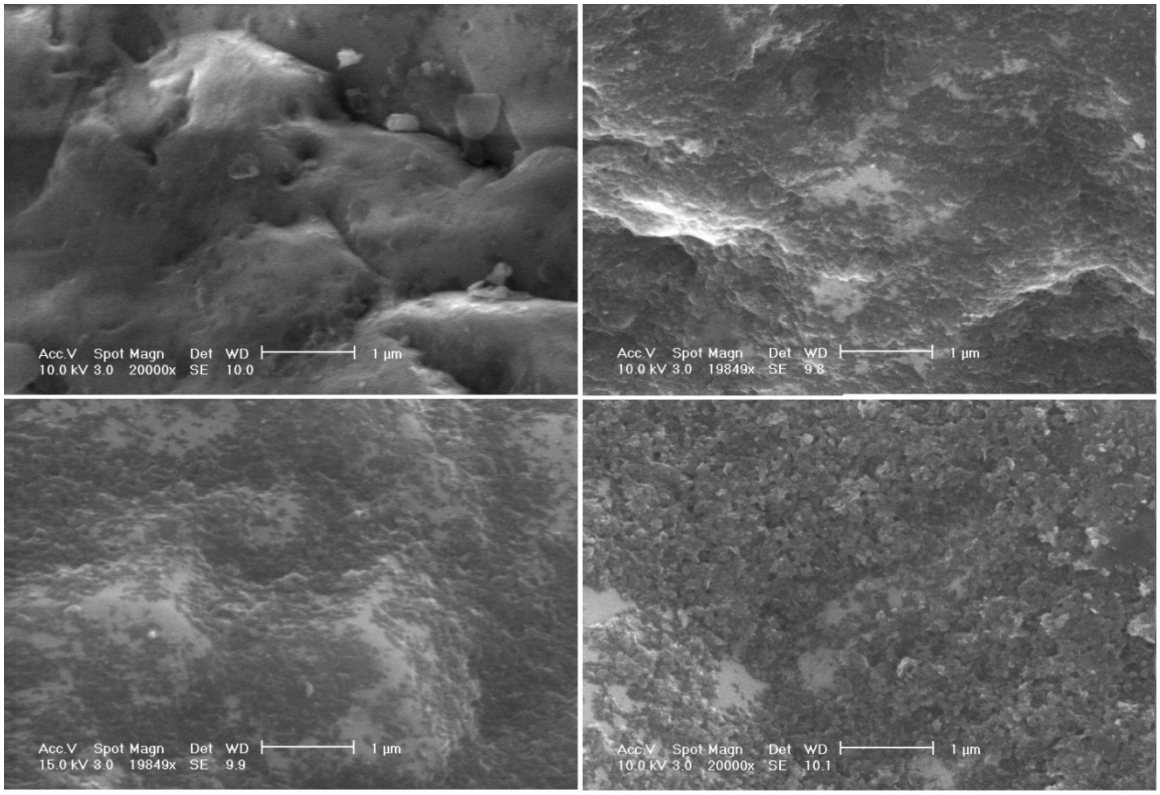

Figure 4.4 SEM images of (a) natural Wedron silica sand and (b) FeS-coated sand with 1.2 mg FeS/g-coated sand (1:1 coating), (c) 2.4 mg FeS/g-coated sand (1:2 coating) and (d) 4 mg FeS/g-coated sand (1:4 coating). FeS deposits as patches on the sand with some areas of the surface appearing uncoated and exposed.

4.3.5.2 XPS

To characterize the surface of the coated sands, XPS spectra were obtained for FeS, FeS-coated sand, Wedron sand and acid-washed Wedron sand. The XPS survey scans of the FeS and FeS-coated sand (4 mg FeS/g sand) indicated the presence of O, C, Na, S, and Fe and the presence of O, C, S, Na, Fe and Si, respectively. The natural Wedron sand without acid washing showed the presence of O, C, Na, Al, Ca, Fe and Si, while the acid-washed Wedron sand survey scan consisted of only O, C and Si.

The narrow scan region spectra for Fe $2p_{3/2}$ is shown in Figure 4.5. The binding energies, peak full width at half maxima (FWHM), and the percentage of fitted species are listed in Table 4.2. The Fe(III)-O species is the sole contributor of Fe 2*p* spectrum in Wedron sand sample but represents only 8.7% of the spectrum of FeS sample (Figure 4.5). Relative to the FeS only sample, coating Wedron sand with FeS increases the Fe(III)-O surface species contribution to 10.1%. At the same time, the Fe(II)-O and Fe(II)-S species contributions in the FeS spectrum which are 13.2% and 33.4%, respectively, change to 25.6% and 26.4%, respectively in the FeS-coated spectrum. These results suggest that upon coating, a partial oxidation of the Fe(II) of FeS occurs via a redox surface reaction. The presence of significant contributions of Fe(III)-S in both the FeS (44.7%) and FeS-coated sand (37.8%) suggest that the partial surface oxidation of FeS resulted during the synthesizing of FeS. In the coating procedure, the FeS suspension was acidified to pH 5.5 with HCl. Acid addition may cause the oxidation of mackinawite to greigite (Fe_3S_4, e.g., $Fe^{II}Fe^{III}{}_2S_4$). The transformation of mackinawite to greigite was previously observed at pH 5 based on XRD evidence (Gallegos et al., 2007). The formation of greigite can be explained as resulting from the following oxidation reaction:

$$4FeS + 2H^+ = H_2(g) + Fe_3S_4 + Fe^{2+} \qquad (4\text{-}1)$$

It is also possible that oxidation of FeS by water could result in the formation of mixed iron oxides such as magnetite via anoxic corrosion as follows:

$$3FeS + 4H_2O = Fe_3O_4 + H_2(g) + 3H_2S \qquad (4\text{-}2)$$

However, given that the reaction of FeS suspensions with natural sand led to an increase in pH but not when FeS was reacted with acid-washed sand (see discussion above), and that the contribution of the Fe(III)-S species remained unchanged during this reaction, a redox reaction such as the following may have occurred:

$$FeS + 2FeOOH = Fe_3O_4 + H_2S \qquad (4\text{-}3)$$

At pH values less than 7, the loss of H_2S gas to the head space in the coating vial or an unexpected loss due to the failure of achieving a completely closed system in each batch would lead to an increase in pH while producing magnetite. The occurrence of the reaction given in equation (4-3) would also explain the appearance of an increase of Fe(III)-O in Fe-coated sand relative to FeS upon FeS reaction with the natural sand and the decrease in the Fe(III)-O of the natural sand.

For further support of the above interpretation, thermodynamic calculations simulating the coating experiments were performed with the PHREEQC equilibrium modeling program (Parkhurst and Appelo, 1999). The details of the simulated coating batch condition are presented in Appendix A1. The results of the modeling predicted that the majority of the FeS remains as mackinawite when reacted with iron oxides, but that some greigite and magnetite may form as a result of FeS oxidation at the equilibrium pH value of 7. Although mixing 2g/L FeS with Wedron sand initially produced a pH value of 5.5, this pH increased to near 7 after three days of mixing with Wedron sand. Therefore, the coating system was simulated at the equilibrium pH value of 7. This is consistent with the interpretation of the Fe 2*p* XPS data that the FeS-coated sand consists of at least three different surface iron phases, with the predominant form being mackinawite and with smaller amounts of iron oxidation products such as greigite and magnetite.

Additional spectral features collected by XPS further confirm the nature of the surface coating. The O 1*s* spectra of each sample support the notion that the FeS-coated sand surface has both coated and uncoated portions on the surface (Figure 4.5). As shown in Figure 4.6, the main peak of O 1*s* of FeS-coated sand has the same position as the acid-washed and unwashed Wedron sand. However, the O 1*s* spectra also show a broadening caused by the OH^- component that is consistent with the presence of OH^- from the hydroxylation of FeS.

Figure 4.7 shows the S 2*p* spectra of FeS and FeS-coated sand. Each surface species in the S *2p* spectrum is fitted with a doublet representing the spin-orbit splitting of the S $2p_{1/2}$ and S $2p_{3/2}$ peaks. The S *2p* spectra of nano particulate FeS mainly consists of S^{2-} species, which is typical of sulfur in mackinawite. The minor spectra were located

at 162.5 and 164.4 eV and are due to sulfur species in higher formal oxidation states such as S_2^{2-} and S_n^{2-} or elemental sulfur, respectively. The presence of these di- or polysulfide in mackinawite is also reported in the literature (Herbert et al., 1998; Mullet et al., 2002). In FeS-coated sand, S *2p* spectra showed higher contribution of spectrums at the binding energy values of the di- and polysulfide. In the coating procedure, nanoparticulate FeS is subjected to a change in pH from higher than 9 or 10 to 5.5 by adding acid. This pH change may stimulate an oxidation of FeS to other forms of iron sulfide such as greigite (Fe_3S_4). Greigite surface properties are not yet intensively studied using XPS, so the presence of greigite can be only guessed from the broaden peak shape in the S *2p* spectra. The S *2p* spectra of FeS-coated sand does not definitely display a spectrum higher than 165 eV, evidence supporting the hypothesis that the formation of sulfate did not occur during the coating procedure.

Table 4.2 Binding energies (BE), peak full width at half maximums (FWHM) and peak areas for Fe $2p_{3/2}$, and O *1s* X-ray photoelectron spectra of FeS (mackinawite), FeS-coated sand, Wedron sand and acid-washed Wedron sand

Sample	Fe			S			O		
	BE/eV	I/%	Species	BE/eV	I/%	Species	BE/eV	I/%	Species
Nanoparticulate FeS	706.0	33.4	Fe(II)-S	160.9	87.1	S^{2-}	259.5	9.5	O^2
	706.6	13.2	Fe(II)-O	162.5	11.0	S_2^{2-}	531.0	84.2	OH^-
	707.5	44.7	Fe(III)-S	164.3	2.0	S_n^{2-}	532.5	6.3	H_2O
	711.1	8.7	Fe(III)-O						
FeS-coated sand	706.8	26.4	Fe(II)-S	160.9	68.2	S^{2-}	529.7	9.5	O^2
	708	25.6	Fe(II)-O	161.9	25.0	S_2^{2-}	531.3	20.2	OH^-, $SiOH^0$
	709.4	37.8	Fe(III)-S	164.0	6.8	S_n^{2-}			
	711.5	10.1	Fe(III)-O				532.1	70.3	H_2O, >SiO-
Wedron-sand	711.5	100.0	Fe(III)-O	-	-	-	529.7	1.9	O^2
							531.3	15.7	OH^-, $SiOH^0$
							532.1	82.5	H_2O, >SiO-
Acid-washed Wedron sand	-	-	-	-	-	-	532.1	100	H_2O, >SiO-

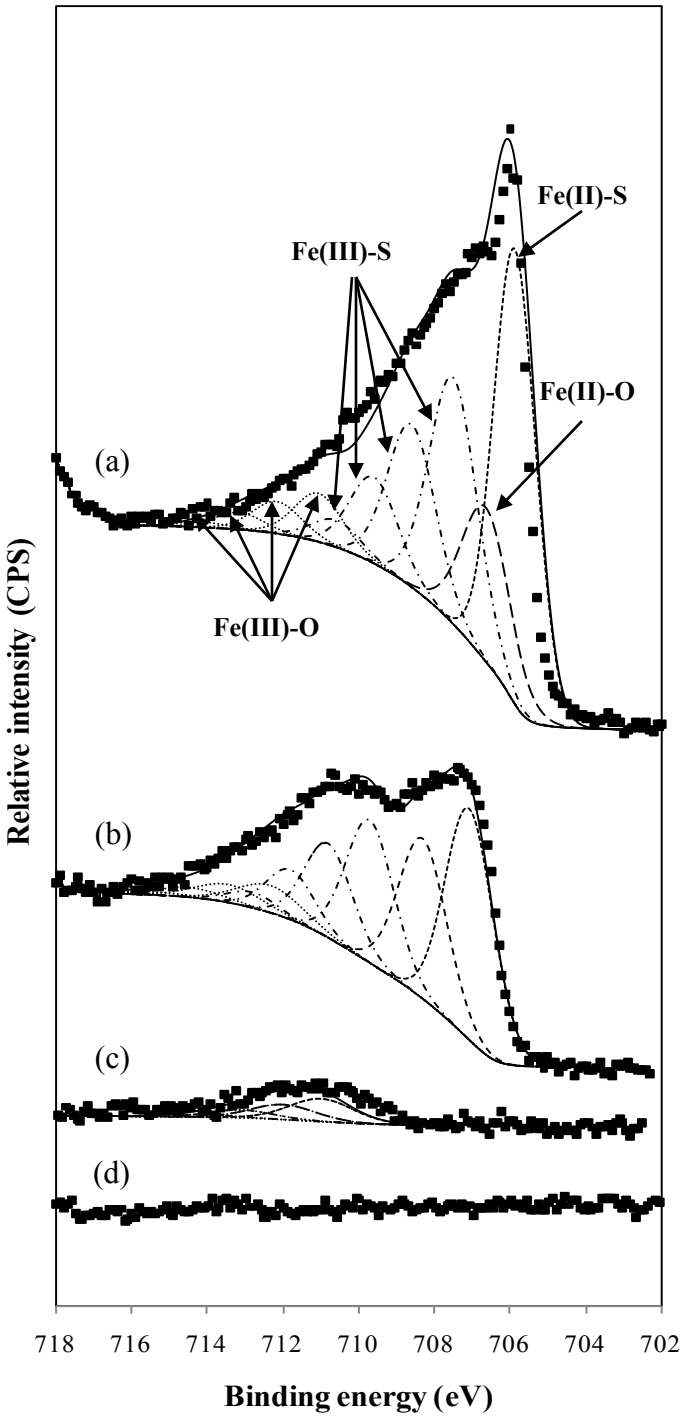

Figure 4.5 Narrow region scans of Fe 2*p* spectra of (a)FeS (mackinawite), (b)FeS-coated sand, (c)Wedron sand and (d)acid-washed Wedron sand surfaces. FeS-coated spectra show characteristics of both FeS and Wedron sand, suggesting that portions of the natural sand remain exposed after the coating process. (CPS: counts per second)

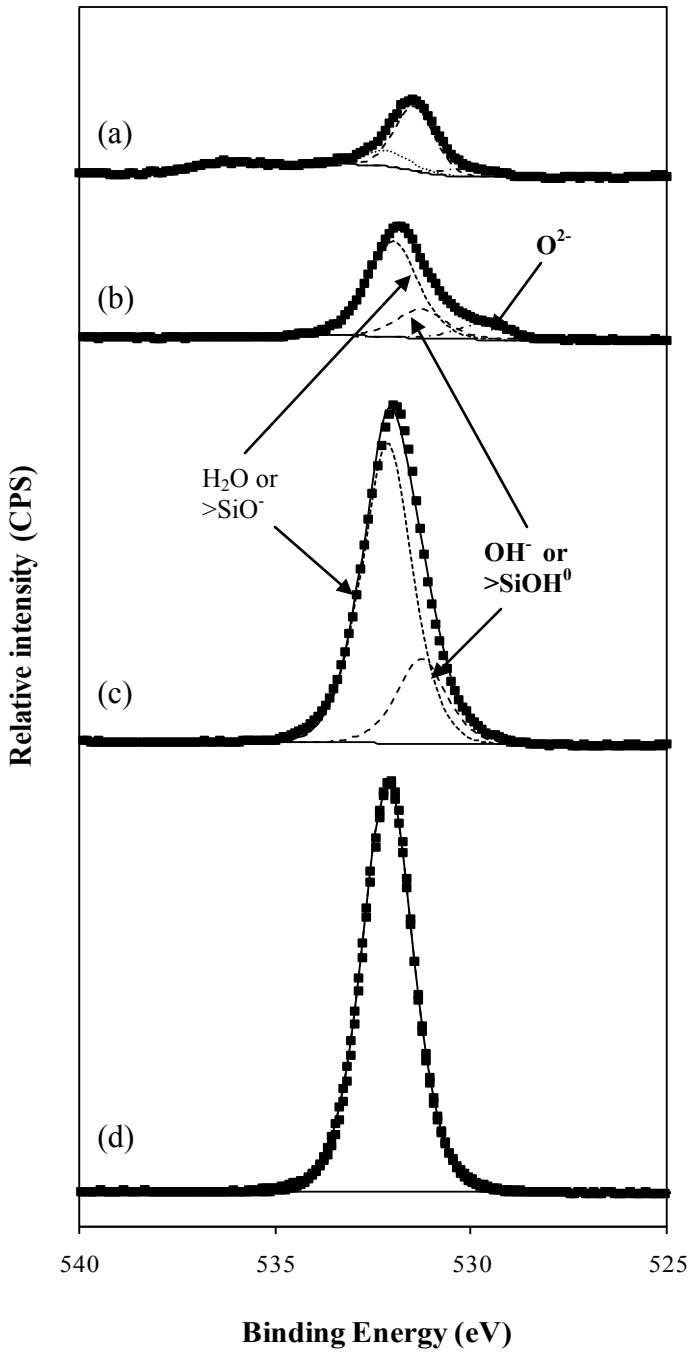

Figure 4.6 Narrow region scans of O *1s* spectra of (a)FeS (mackinawite), (b)FeS-coated sand, (c)Wedron sand and (d)acid-washed Wedron sand surfaces. FeS-coated spectra show characteristics of both FeS and Wedron sand, suggesting that portions of the natural sand remain exposed after the coating process.

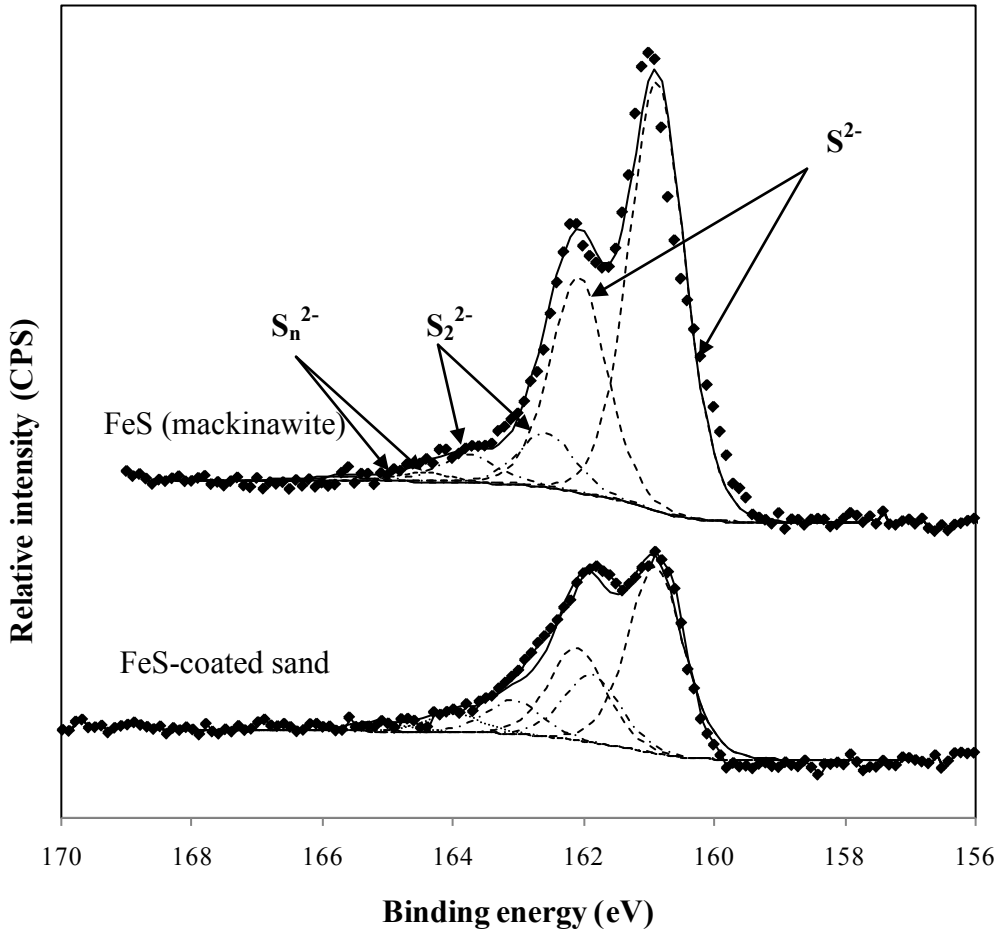

Figure 4.7 Narrow region scans of S *2p* spectra of FeS (mackinawite) and FeS-coated sand. FeS-coated spectra show characteristics of both mainly FeS but some changes may have occurred during the coating process.

4.4 Summary and conclusions

A procedure for coating FeS on a natural sand was developed and has been described. Optimal and reproducible coatings of FeS of sand result from using a coating pH of 5.5 and no rinsing following solid-liquid separation after a three day contact period between the FeS and the sand. The most effective coating from the standpoint of FeS material use was derived from a 1:2 sand (mL) to FeS (mL) suspension ratio but it is possible to load more FeS on the sand surface by increasing the volume. Surface characterization by SEM and XPS show the FeS-coated sand has a patchwise coating that is predominantly comprised of FeS self-aggregates along with a small fraction of oxidized magnetite or greigite phases. Even though several different iron surface mineral phases were identified, the FeS-coated sand is primarily comprised of FeS, the desired phase for PRB application.

CHAPTER V

BATCH STUDIES OF As(III) UPTAKE OF FeS-COATED SAND: IMPACT OF pH AND DISSOLVED SILICATE

5.1 Introduction

Solution conditions may be important in determining the properties of FeS and its sequestration capacity for a contaminant. Uptake by FeS has shown sensitivity to a variety of conditions such as oxygen and pH (Gallegos et al., 2007, 2008), FeS concentration (Gallegos et al., 2008), or composition of co-existing ions. In this chapter, the impact of solution conditions such as pH and the presence of dissolved silicate were investigated on the sorption of As(III) by FeS coated sand. The impact of solid concentration (solid/solution ratio effect) is covered in Chapter 7.

The effective sequestration of As(III) by synthesized nano-sized FeS was observed by Gallegos (2007) at pH 5, 7, and 9 under anoxic conditions. In that study, As(III) sorption isotherms displayed typical Langmuir shape with the maximum amounts sorbed, determined from the isotherm plateau, of 2×10^{-3}, 2×10^{-4}, and 5×10^{-5} mol As removed/g FeS at pH 5, 7 and 9, respectively. The decreasing As(III) removal capacity with increasing pH in Gallegos et al. (2007), is related to the solubility changes of FeS with pH. The solubility of FeS is pH-dependent below pH 6 and pH-independent above pH (Davison et al., 1999; Rickard, 2006). At pH values below 6, the increasing amount of dissolved sulfide promotes the precipitation of arsenic sulfide under acidic pH, while surface-limited adsorption of As(III) species becoming progressively important with increasing pH and lower sulfide solubility. Sorption capacity of FeS-coated sand as a function of pH has been determined in this chapter and compared to the values from Gallegos et al. (2008) for nanoparticulate FeS.

In this work, pH edge behavior was analyzed for As(III) uptake by FeS coated sand.. A concentration of 100 g FeS-coated sand /L (for a total of 0.124 mg/L FeS) was selected for comparison with the 0.1 mg/L nanoscale FeS studies of Gallegos et al. (2008), since the pH edge was most distinctive at this condition.

As reported in the previous chapter, the FeS-coated sand carries appreciable amounts of FeS on sand surface (maximum 4 mg FeS/g sand with 1:4 ratio of sand(mL) to 2g/L FeS(mL)). It is hypothesized that if FeS-coated sand behaves similarly to nanoscale FeS at this condition, then the coated material should retain the primary pH-dependent sorption capacity and edge characteristics of nanoscale FeS.

The potential for an inhibitory effect of silicate on arsenic sorption is also presented in this chapter. Previous studies with goethite and ferrihydrite as adsorbents have shown that dissolved silicate can impact adsorption of arsenic on Fe(III) oxyhydroxide solids (Swedlund and Webster, 1999; Waltham and Eick, 2002; Roberts et al., 2004; Luxton et al., 2008). Since the silicate ion itself forms inner-sphere complexes by exchanging ligands with surface groups, and this process is pH-dependent (Pokrovski et al., 2003), the presence of silicate can potentially decrease the number of sorption sites for arsenic sorption. Dissolved silicate has also been observed to change the pH_{pzc} of the goethite (α-FeOOH), which may enhance the negative surface charge thereby causing reduced arsenic adsorption (Garman et al., 2004; Hiemstra et al., 2007). Given the general relationship between maximum sorption onto metal oxide solids and pK^1 values of oxyacids (Hiemstra et al., 2007), and that silicic acid and arsenious acid have similar pK_1 values near pH 9, a competitive effect between those two anions was considered a possibility in this study of arsenic by FeS-coated sands from which silicate is expected to dissolve. Therefore, in this chapter, the amount of dissolved silicate of FeS-coated sand system under varying pH values were measured and the impact of silicate presence on As(III) removal was investigated.

5.2 Methods

5.2.1 As(III) sorption isotherm on FeS-coated sand at pH 5, 7 and 9

Sorption isotherm tests were performed on FeS-coated sand at pH 5, 7, and 9, to investigate the As(III) uptake capacity of FeS-coated sand at each pH. The pH was buffered with 0.1 N acetate (pH 5), 0.1 N 3-(N-Morpholino)propanesulfonic acids (MOPS) (pH 7), and 0.1 N 2-(cyclohexylamino) ethanesulfonic acids (CHES) (pH 9), The As(III) removal capacity of FeS-coated sand was compared to suspensions of nanoparticulate FeS on a per gram of FeS weight basis. To obtain the sorption isotherms, test tubes with 5 g of FeS-coated sand and 10 ml of buffer solutions were spiked with As(III) stock solution to achieve a concentration range of 1.3×10^{-6} M to 6.7×10^{-4} M initial As(III) concentrations for pH 5, and 1.3×10^{-6} M to 2.6×10^{-4} M for pH 7 and 9. The reaction tubes were then mixed on an end-over-end rotator for 2 days. After 2 days, the supernatant in tubes was filtered through a 0.1 μm nylon filter, diluted, acidified with HNO_3 and then analyzed for arsenic by ICP-MS (Perkin Elmer). All the experimental steps except the supernatant acidifying step for ICP-MS analysis were performed in the anaerobic chamber.

Traditionally, in isotherm tests, a solid material reacts under continuous shaking or stirring in a reaction vessel; however, this mixing method might not represent field conditions because it could break particles, increase particle surface area, or disturb the adsorption/desorption and precipitation/dissolution characteristics (Pang and Close, 1999). Therefore, according to Pang and Close, some studies have used static methods without continuous mixing. However, these methods require relatively long reaction times to reach equilibrium. Studies with high agitation speeds, such as 200 rpm or 400 rpm, demonstrated that it may be difficult to control uptake or boundary layer resistance and the high rpm might cause the particle abrasion (Onyango et al., 2003). Therefore, for all batch experiments, a mixing speed of 10 rpm was selected to give complete but not overly agitated mixing.

5.2.2 pH-dependent As(III) sorption using FeS-coated sand and Wedron sand

The As(III)-sorption tests were performed over the range of pH of 2-12. One gram of FeS-coated sand, 9.9 mL 0.1N NaCl solution and 0.1 mL of 1.3×10^{-3} M $NaAsO_2$

stock solution was placed in 15mL polypropylene tubes to achieve an As(III) concentration of 1.3×10^{-5} M As(III). Various amounts of 0.08N HCl and 0.1N NaOH solutions were added to each tube and mixed with an end-over-end rotator. The change of ionic strength that occurred in adjusting pH was assumed negligible (the maximum addition of ionic strength was less than 0.01 M). After two days of mixing, half of the supernatant was filtered with a 0.1 μm nylon filter and acidified for the analysis of As(III) and Fe_{diss} using an ICP-MS. The other half of the supernatant was used to measure the pH. The same tests were also performed using FeS-uncoated natural sand (Wedron sand) to compare the amount of As(III) uptake.

5.2.3 Silicate effect

FeS-coated sand, a silica-based material, when placed in water will dissolve according to its aqueous solubility properties, resulting in an amount of dissolved silicate which has been reported as an competitive anion for arsenite sorption on Fe(III)-oxide based materials (Swedlund and Webster, 1999; Waltham and Eick, 2002; Roberts et al., 2004). Therefore, dissolved silicate concentrations were measured in the presence and absence of arsenic under various pH conditions in systems comprised of 100g FeS-coated sand/L solution. To prepare the solutions, one gram of FeS-coated sand was added to a 15 mL polypropylene tube along with 9.9 mL of a 0.1M NaCl solution. For the As(III) containing systems, 0.1 mL of a 1.33×10^{-3} M $NaAsO_2$ stock solution was added to each tube to achieve an As(III) concentration of 1.33×10^{-5} M (1 ppm as As(III)). The pH was adjusted same as described in Section 5.2.2. After two days of mixing, half of the supernatant was filtered with a 0.1 μm nylon filter and acidified for the analysis of Si using the ICP-MS and the other half of the supernatant was used for measuring pH.

After determining that the FeS-coated sand system released appreciable amounts of silicate in the aqueous system over the experimental range of pH values (pH 2-12) (Figure 5.6), pure FeS was tested as a control experiment for simulating a silicate-free condition. The 2g/L FeS stock suspension was prepared from mackinawite solid synthesized in the laboratory and was added to each tube to achieve a concentration of 0.5g/L FeS. FeS suspension samples with and without silicate were spiked with the arsenic stock solution. The final solution thus contained 0.5g/L FeS, 0.1N buffer, and the

desired amount of arsenite (0.133 mM or 0.0133 mM) with and without silicate at 0.35 mM. The prepared sample tubes were mixed with an end-over-end rotator for two days and the equilibrated samples were filtered through a 0.1 μm nylon-syringe filter and acidified with HNO_3 for ICP-MS analysis.

To investigate the effect of silicate on the uptake of As(III) by FeS-coated sand, test tubes with 5 g of FeS-coated sand and 10 mL of buffer solutions (0.1N acetic acid at pH 5, 0.1N MOPs at pH 7, and 0.1N CHEs at pH 9) with and without 0.35 mM dissolved silicate were mixed using an end-over-end rotator for 1 day to condition its surface with buffer solution in the absence and presence of silicate. An aliquot of As(III) stock solution was then added to achieve the desired initial concentrations of 1 ppm to 50 ppm As(III) for pH 5, and of 1 ppm to 20 ppm for pH 7 and 9. The prepared reaction tubes were then mixed with an end-over-end rotator for another two days. Then, the supernatant in the tubes was filtered through a 0.1 μm nylon filter, diluted, and then acidified with HNO_3 and analyzed for arsenic with ICP-MS.

5.3 Results and discussion

5.3.1 As(III) uptake capacity of FeS-coated sand

As(III) removal capacities of synthesized FeS reported from Gallegos (2007) (Figure 5.1) were on the order of 140, 15, and 3 mg As(III)/g FeS (2×10^{-3}, 2×10^{-4} and 5×10^{-5} mol As removed/g FeS) at pH 5, 7 and 9, respectively, while FeS-coated sand removed on the order of 42, 10, and 10 mg As/g FeS (5×10^{-4}, 1.5×10^{-4} and 1.5×10^{-4} mol As/g FeS) at pH 5, 7 and 9, respectively (Figure 5.2). Using the plateau values (q_m) of the isotherms as the arsenic uptake capacity, the FeS-coated sand removed around 30%, 70% and 300% of the maximum capacity of FeS at pH 5, 7 and 9, respectively. A loss of capacity of a coating compared to its removal as a nanoparticulate material has been commonly reported in the literature for other materials. At pH 5, the bulk precipitation of realgar (AsS) from a reaction between dissolved sulfide and aqueous As(III) has been previously proposed as the primary mechanism for the high uptake with nanoparticulate FeS (Gallegos et al., 2007, 2008):

$$3FeS + H_3AsO_3 + 3H^+ = 1/2\ Fe_3S_4 + AsS + 3/2\ Fe^{2+} + 3\ H_2O \qquad (5\text{-}1)$$

However, at pH 5, using FeS-coated sand, the normalized amount of arsenic removed per g of FeS was 30% less after the coating process. This may be attributed to the change in the iron mineral composition shown in the XPS results (e.g., oxidation of FeS to greigite, as discussed previously in Chapter 4), or the possible reduction in accessibility of self-aggregated FeS particles on the sand surface. Similar to this, hydrous ferric oxide (HFO) can remove 422.7 mg/g of As(III) at pH 8 (Dixit and Hering, 2003), but ferrihydrite-coated quartz removes 90.45 mg/g (ferrihydrite weight-basis) of As(III) (Herbel and Fendorf, 2006), which is about 20% of the removal capacity of the pure mineral. This effect was also pointed out by Herbel and Fendorf (2006) for a ferrihydrite-coated sand, which also did not remove as much as the pure ferrihydrite normalized by the mass of the iron mineral oxide.

As the pH is increased, the contribution of bulk precipitation of arsenic sulfide to the As(III) removal decreases as the FeS solubility abruptly decreases above pH 6. Instead, a surface sorption mechanism is thought to become increasingly more important as the pH increases above 6 (Gallegos et al., 2007). At pH 7, the FeS-coated sand has about 70% of the capacity as nanoparticulate FeS, perhaps resulting from less accessible FeS surface functional groups on the aggregated FeS nanoparticles on the coated sand. Interestingly, at pH 9, the FeS-coated sand shows approximately three times more removal than nanoparticulate FeS. This result may be attributed to the presence of other oxidized iron mineral phases such as the naturally existing metal (Fe and/or Al) oxide of the uncoated sand surface or the presence of a secondary mineral phase resulting from mackinawite oxidation. The XPS results from Chapter 4 support the notion that some FeS is converted to a Fe(II)/Fe(III) oxide such as magnetite upon the coating of the sand. Recent work has shown that As(III) uptake is enhanced in the presence of magnetite, although this enhancement may only be temporary if prolonged exposure to reducing conditions prevails (Tufano and Fendorf, 2008) in the absence of sulfide.

The As(III) removal capacities calculated using the Langmuir isotherm model applied to the data for FeS-coated sand (Table 5.1), were 41.6, 10.7 and 12.7 mg As/g FeS (0.052, 0.013, and 0.016 mg As/g FeS-coated sand) at pH 5, 7 and 9, respectively. These are comparable to various other absorbents that have been prepared for As(III)

removal in PRB applications. The list of other absorbents for As(III) removal and their total removal capacity were presented in Table 1.1. For example, the adsorption capacity was 0.15 mg/g for a sulfate ($BaSO_4$) modified iron oxide-coated sand (Vaishya and Gupta, 2004), and 0.041 mg/g (Thirunavukkarasu et al., 2003) and 0.028 mg/g (Gupta et al., 2005) for iron-oxide coated sands. For granular ZVI pretreated with acid, a capacity of 0.3 mg/g was obtained for As(III) (Lackovic et al., 2000) while for a iron-oxide coated cement (d_{50} = 212μm) an even higher value of 0.67 mg/g (Kundu and Gupta, 2006) was found. The higher capacity for ZVI may result from the pitting/fracturing from acid pretreatment, while in the case of the porous cement it may be due to accessible internal surface. These examples report the As(III) removal capacities under aerobic conditions wherein the mobility of As(III) effectively decreased in the presence of ferric oxyhydroxides. Under anaerobic conditions, As(III) is generally more difficult to remove from the aquatic environments due to its higher mobility when reduced iron solids prevail (Smedley and Kinniburge, 2002; Bissen and Frimmel, 2003).

Arsenic removal capacities have been reported in a number of ZVI column and batch experiments. Lackovic et al. (2000) reported 1.15 mg As removal/g ZVI and Su and Puls (2001) reported 1.77 mg As/g ZVI from column and batch experiments, respectively. Lien and Wilkin (2005) reported a higher arsenic removal capacity of 7.5 mg As/g ZVI. These values are all smaller than the As(III) removal capacity obtained in this dissertation. Given that ferric-oxide based adsorbents lose their high capacity for As(III) removal under anaerobic conditions, FeS-coated sand appears to be competitive on a capacity basis. Furthermore, both oxide-coated ZVI or ferric oxide-coated materials may ultimately release arsenic by reductive dissolution under anoxic conditions (Tufano and Fendorf, 2008). Therefore, FeS-coated sands may provide an attractive alternative for arsenic removal in PRB applications in which long-term reducing conditions prevail.

Table 5.1 Fitted Langmuir isotherm model parameters of FeS-coated sand

	q_m	K_l	R^2
pH	**(mg As(III)/g FeS)**	**(L/mg As(III))**	**-**
5	52.0	1.39	0.99
7	13.4	0.78	0.95
9	15.8	1.08	0.96

* Langmuir isotherm model: $q_{eq} = \frac{q_m K_l C_{eq}}{1 + K_l C_{eq}}$ here, q_{eq}: the amount of As(III) sorbed by solid (mg/g), q_m: total As(III) sorption capacity (mg/g) determined by fitting, K_l: the Langmuir constant (L/mg) determined by fitting, C_{eq}: the As(III) concentration left in solution(mg/L)

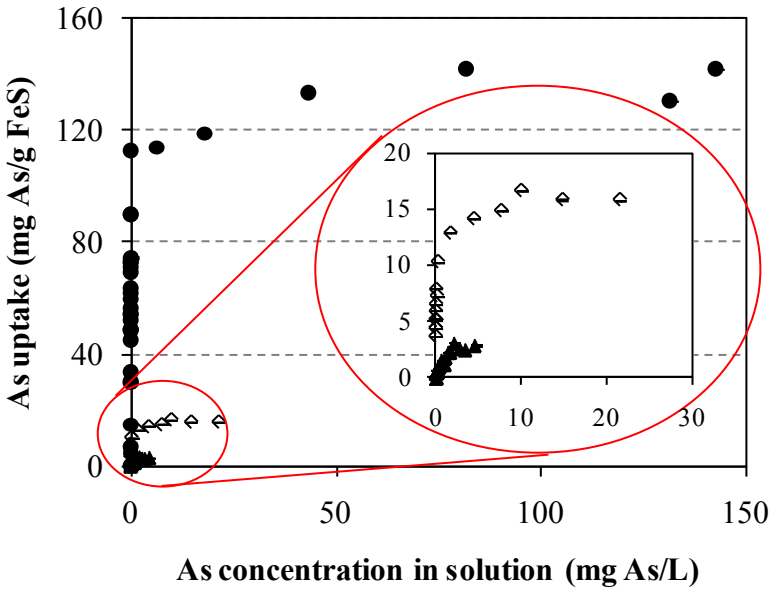

Figure 5.1 Sorption isotherm results at pH 5, 7 and 9 plotted as the amount removed versus the solution concentration of As after two days equlibration time with FeS (this figure was adapted from Han et al.(2009), the original source is Gallegos (2007))

(● 5, ◇ pH 7, and ▲ pH 9).

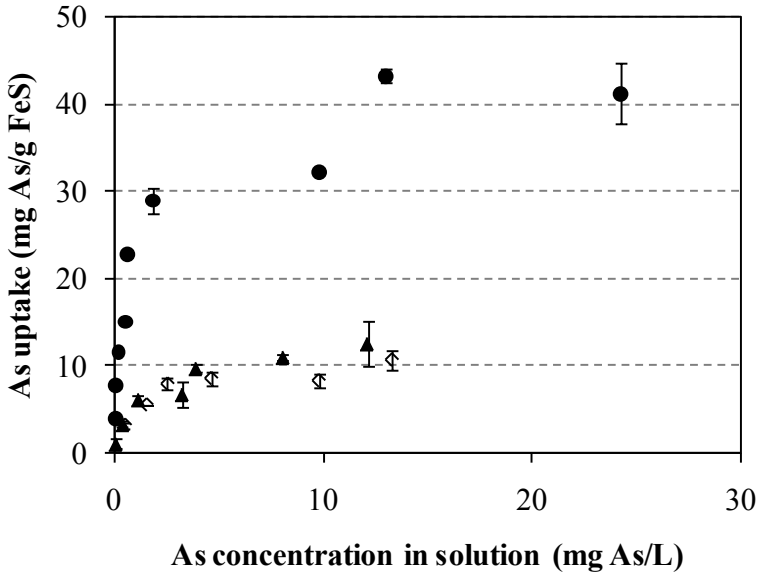

Figure 5.2 Sorption isotherm results at pH 5, 7 and 9 plotted as the amount removed versus the solution concentration of As after two days equilibration time with FeS-coated sand (● 5, ◇ pH 7, and ▲pH 9).

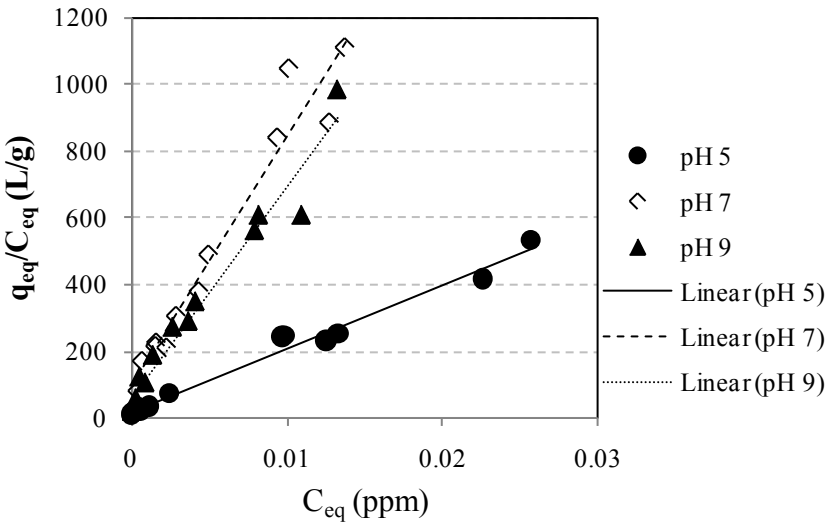

Figure 5.3 Sorption isotherm results fitted with linearized Langmuir isotherm.

5.3.2 Impact of pH

The influence of pH on 1.3×10^{-5} M (1 mg/L) As(III) removal efficiencies were studied over the pH range from 2 to 12, and it was demonstrated that the removal trends and efficiencies resemble those using nanoparticulate FeS. In the As(III) sorption experiments using 0.1 g mackinawite /L reported by Gallegos et al. (2008), FeS removed 100% of As(III) initially present in the aqueous phase at pH values under 6, the lowest removal near pH 8 (less than 10%), 30% at pH 9.2, and less than 30% at pH values near 9.2. A similar trend was observed using FeS-coated sand system as shown in Figure 5.4.

This pH-dependence of As(III) removal can be divided into three zones depending on which solid species controls the As(III) removal (Figure 5.4). In Zone I, As(III) uptake may be attributed to the bulk precipitation of an arsenic sulfide either $AsS_{(s)}$ or $As_2S_{3(s)}$ (Gallegos et al. 2007; 2008). The precipitation in this region is thought to result from the presence of high concentrations of dissolved sulfide at lower pH. As shown in Figure 5.5, the equilibrium solubility of Fe from FeS-coated sand increases significantly below pH 7. Assuming congruent dissolution (i.e., sulfide dissolved in equivalent molar concentration to Fe), this can be taken as an indication of the significantly increased concentration of aqueous H_2S, the principal dissolved sulfide species, in this region. The trend of increasing FeS solubility shown in Figure 5.5 is

similar to that shown earlier for nanoparticulate FeS dissolution by Gallegos et al. (2007). Interestingly, the value of dissolved Fe levels off below pH 4 at a total dissolved Fe concentration that is only approximately 70% of the total iron coated on the sand (1.0×10^{-3} M vs. 1.4×10^{-3}M). This suggests that a fraction of the FeS-coated material (~ 30%) is in a non acid extractable form. While acid-volatile sulfides like freshly prepared nanoscale FeS (as mackinawite) typically dissolve with less stringent acid extraction conditions, iron sulfide oxidation products are not so easily removed and typically require more extensive acid treatments (Huertadiaz and Morse, 1990; Rueda et al., 1992; Cooper and Morse, 1998; van Oorschot and Dekkers, 2001). This is consistent with the XPS results of Chapter 4 that indicated a portion of the original nanoscale FeS is oxidized during the coating procedure.

In Zone II (from pH 7-11 in Figure 5.4), As(III) removal shows a local maximum near pH 9, which is the near pK_{A1} of 9.2 for arsenite. This suggests a ligand exchange sorption reaction with: (1) the FeS surface, which is consistent of both >SOH and >FeOH or (2) the surface sites of the solid phase oxidation products of FeS such as magnetite (Gallegos et al. 2008). In both Zones I and II, the FeS-coated surface appears to regulate As(III) removal according to the shape of pH-dependent sorption envelopes of the FeS-coating sand and the natural iron coating of the Wedron sand.

In contrast, in Zone III, the removal of As(III) is approaching a minimum amount and seems to correspond well to that of the uncoated Wedron sand, indicating that the natural Fe coating may be contributing to the amount of As(III) removed at pH greater than 11. Generally as the pH decreases beyond 10, the capacity for FeS to remove As(III) from solution appears to be quite limited, as previously noted by Gallegos et al. (2008).

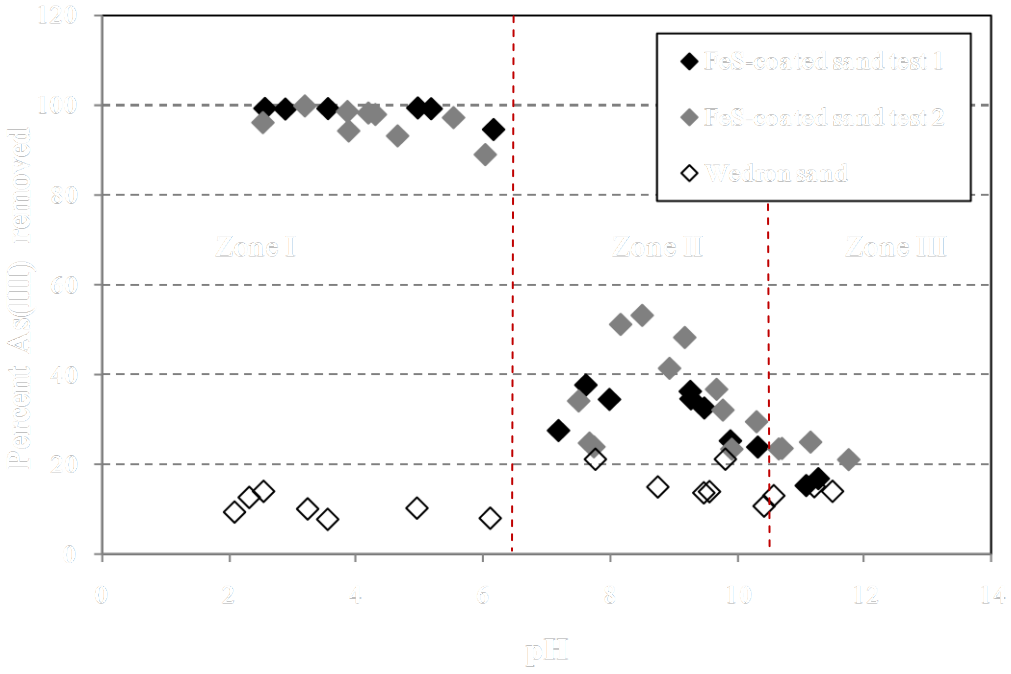

Figure 5.4 Percent removed of 1.33×10^{-5} M (1 mg/L) As(III) as a function of pH for 100 g FeS-coated sand (0.124 g FeS) and uncoated 100g Wedron sand/L in 0.1M NaCl aqueous solutions.

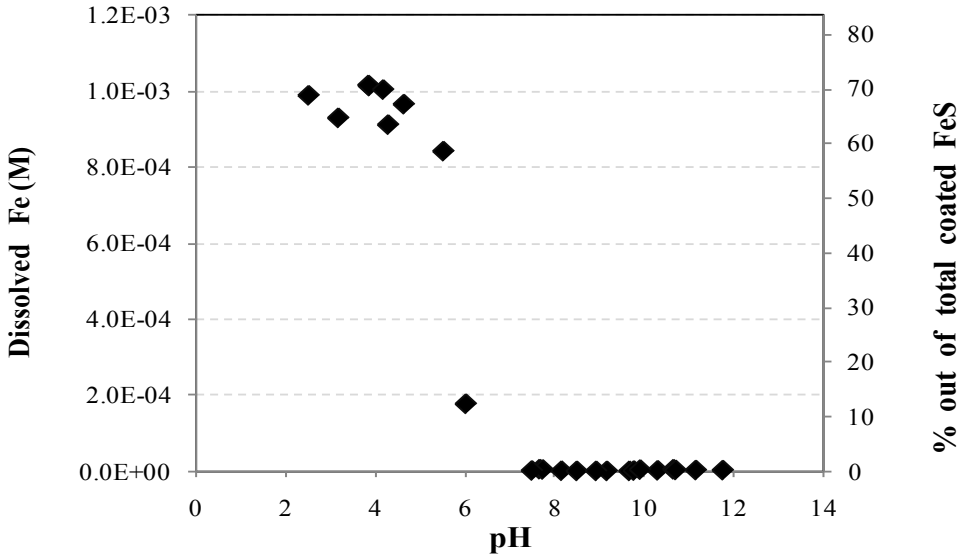

Figure 5.5 Dissolved Fe concentration as a function of pH for 100 g FeS-coated sand/L in 0.01 M NaCl. Also shown is the percentage of total iron lost from the sand.

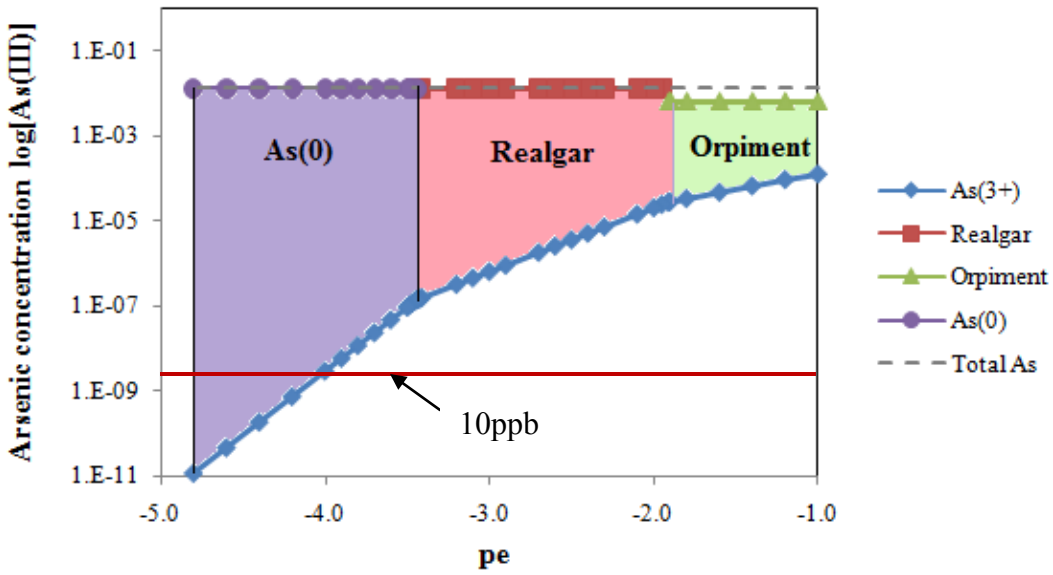

Figure 5.6 Result of PHREEQC simulation of 5g/L FeS reacted with 1.3×10^{-2} M As(III) at pH 5.

In the case of As(III) uptake at pH 5, precipitation is considered to be a primary removal mechanism by FeS-coated sand (see Chapter 6 which provides spectroscopic evidence for this). Thermodynamic predictions of the dissolved arsenic concentration using the PHREEQC program (Parkhurst and Appelo, 1999) without consideration of surface complexation is shown in Figure 5.6 with varying pe and fixed pH. At pe values deriving the precipitation of amorphous As_2S_3 or realgar, it was predicted that the concentrations of dissolved arsenic substantially exceed 10 ppb (1.3×10^{-7}M), the maximum contamination level of arsenic (see Appendix 2). However, this much of high concentration of were not observed in the batch systems tested here. The measured concentrations of arsenic at low pH were typically below the detection limit of the ICP-MS (less than the ppb level). This observation supports the hypothesis that some surface complexation reactions may be operative in arsenic removal at pH 5. Similar results were reported by Jeong et al. (2009) who proposed that As(III) sequestration of unoxidized mackinawite occurs by forming As(0), AsS, and surface precipitates as thioarsenites at pH 4.9. In contrast to these results, the thermodynamic modeling results by Gallegos (2007) explained the arsenic concentration well below 10 ppb with only precipitation process. This difference in results may be caused by the selection of

database. In this study, the higher arsenic concentrations were predicted at pe values higher than -4 as it shown in Figure 5.6. Even though, the thermodynamic modeling results support the findings obtained from the spectroscopic work, they should be treated with caution, as the thermodynamic modeling makes many simplifying assumptions such as precipitation-only reactions with the results dependent on the database.

As(III) removal by the uncoated Wedron sand is relatively low and does not seem to be strongly affected by pH (Figure 5.4). A similar shape of the sorption envelope was reported for As(III) sorption onto magnetite (Dixit and Hering, 2003; Su and Puls, 2008). This As(III) sorption behavior further supports the hypothesis that magnetite is present on Wedron sand corroborating other evidence such as the spectroscopic results and the thermodynamic predictions reported in the characterization of FeS-coated sand in Chapter 4. Thus, the removal of As(III) by FeS-coated sand is by the FeS coating and its surface oxidation products, rather than the original Fe(III) oxide coating of the natural sand.

5.3.3 Impact of dissolved silicate on As(III) uptake by FeS and FeS-coated sand

The amount of silicate dissolved at pH 5, 7 and 9 in 0.1M NaCl solution after a two-day equilibration period with FeS-coated sand was measured and is displayed in Figure 5.7. The results show that dissolved silicate reaches a minimum value between pH 7 to 9, but progressively increases below pH 7 and above pH 9. The presence of 1 ppm of As(III) seems to have little effect on the concentration of dissolved silicate throughout the pH range investigated, presumably because the added As(III) concentration is relatively low compared to the dissolved silicate concentration and that the concentration is controlled by dissolution from the sand. The dissolved silicate concentration in equilibrium with $SiO_{2(s)}$ is expected to be relatively constant below 9 but progressively increase above 9.5 as the predominant speciation in solution changes from $H_4SiO_4^0$ to $H_3SiO_4^{-1}$ (Stumm and Morgan, 1981). The solubility of crystalline forms of SiO_2(s) is around 3 ppm while that of amorphous silica can be an order of magnitude higher. As shown in Figure 5.7, dissolved silicate concentrations are below 3 ppm over most of the pH range except at very low and very high pH conditions. Under these more extreme pH values, the concentration of silicate may reach its equilibrium value faster

than under the moderate pH conditions. The lower silicate concentration near mid pH was also reported in the other studies suggesting a kinetic dissolution limitation (Beckwith and Reeve, 1964; Hiemstra et al., 2007). In the study by Elgawhary and Lindsay (1972), amorphous silica dissolution in 0.02 M $CaCl_2$ required around 10 days to reach a constant concentration at pH 5 and 7 which suggests that shorter time frame experiments could lead to lower dissolved silicate concentrations.

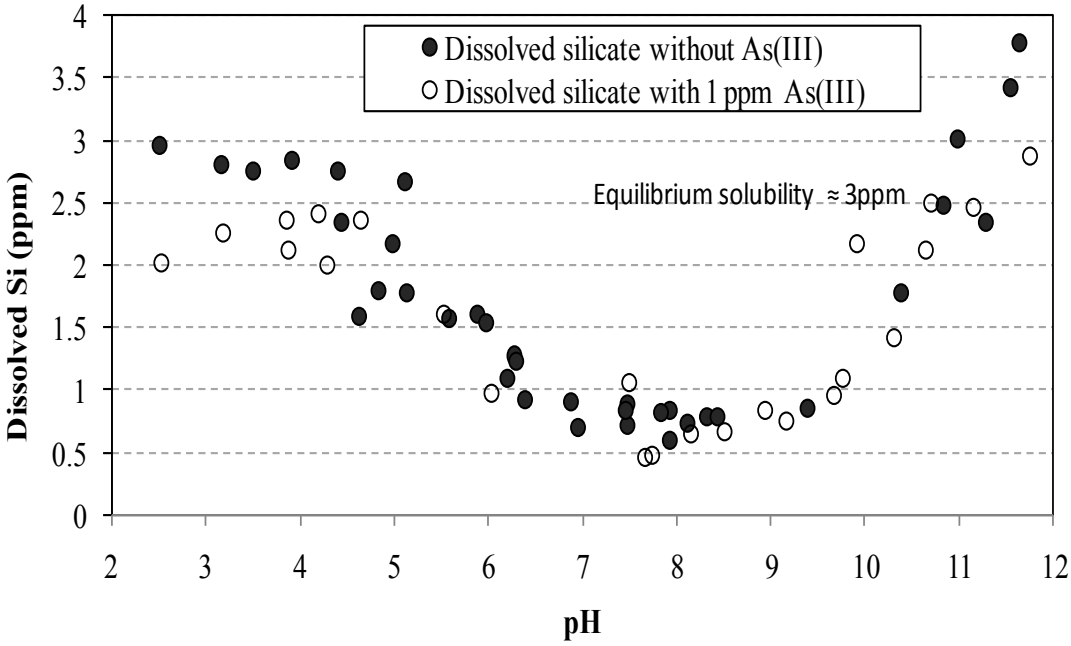

Figure 5.7 Dissolved silica concentration as a function of pH in 100 g FeS-coated sand/L of water.

The effect of the dissolved silicate on As(III) uptake by nanoscale FeS was tested over a range of pH conditions at two different initial As(III) concentrations but, in general, it was found to have little impact over the range of conditions tested (Figure 5.8). For example, at pH 7, in the absence of dissolved silicate, a 0.5 g FeS suspension removed 0.112 mM and 0.012 mM of As(III) out of initial As(III) concentrations of 0.133 mM and 0.0133 mM, respectively. When 0.35 mM silicate was present, As(III) uptake was measured to be 0.110 mM and 0.012 mM As(III), respectively, indicating no impact. At pH 9, As(III) removal also was not affected by the presence of dissolved silicate, even though the As(III) removal efficiency was less than at pH 7. At pH 5, where the highest As(III) uptake was observed, again no significant impact of dissolved silicate was observed. Since the precipitation of arsenic sulfide has is the main mechanism of As uptake at pH 5 (e.g., see Chapter 6), this was not surprising. However, the fact that no impact was also observed at pH 5 and 7, where As(III) adsorption and/or precipitation may occur, indicates that As(III) adsorption by nanoscale FeS is not inhibited by dissolved silicate, regardless of the uptake mechanism. This suggests a potential advantage of FeS-based PRB materials over ferric oxyhydroxide sorbents emplaced in groundwater environments where silica sand and dissolved silicate are expected to typically be present.

Similar to the nanoparticulate FeS system, the dissolved silicate did not have much effect on As(III)-uptake at pH 5 and pH 7 in the FeS-coated sand system (Figure 5.9). However, at pH 9, the addition of 0.35 mM dissolved silicate resulted in less arsenic uptake compared to that in the silicate free system. Under basic pH conditions, As(III) uptake by FeS-coated sand is attributed to both the FeS coating and the iron-oxide-containing natural sand surface as mentioned previously in Chapter 4. Hence, the decrease in As(III) uptake compared to the FeS system at pH 9 is thought to result from the competition between arsenite and the silicate ion to the iron oxide on the natural Wedron sand at pH 9. Since the adsorption of silicate on Fe-oxide surface is expected to be greatest near the pH of the pK_1 of silicic acid (e.g., pH of 9.5) the competitive effect on anion sorption is typically greatest near this pH. Because arsenite sorbs more weakly than arsenate to Fe-oxide surfaces (Garman et al., 2004), desorption by competition with silicate will be more significant when the primary removal mechanism of arsenite is

adsorption to such surfaces (Waltham and Eick, 2002; Luxton et al., 2008). However, when a system is comprised primarily by sorption to FeS, this impact will be minimized, regardless of the pH. At pH 5 and 7, the dissolved silicate had little impact in these FeS-coated sand systems, presumably because, as shown by Gallegos et al. (2007); the primary removal mechanism of As(III) is the precipitation of $AsS_{(s)}$ at pH 5 and either precipitation or adsorption by FeS at pH 7 rather than the sorption to iron oxyhydroxide surface phases that are present on the Wedron sand or oxidized patches of FeS.

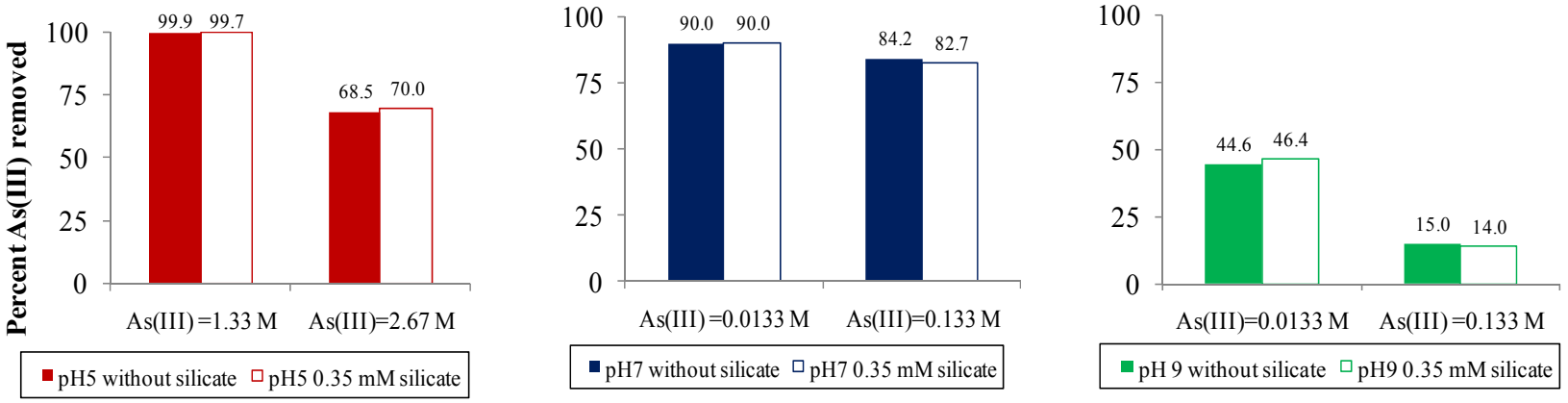

Figure 5.8 Effect of dissolved silicate on As(III) uptake by nanoscale FeS at pH 5, 7 and 9.

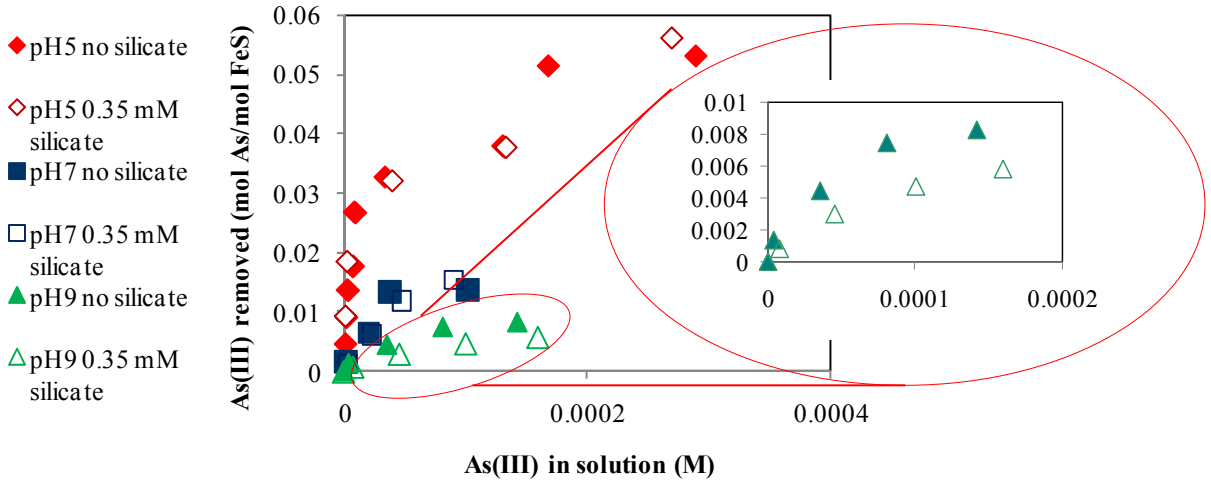

Figure 5.9 Effect of dissolved silicate on As(III) uptake by FeS-coated sand at pH 5, 7 and 9. The circled area is enlarged for better viewing.

5.4 Summary and conclusions

FeS has been previously shown to be an effective sorbent for As(III) (Farquhar et al., 2002; Gallegos et al., 2008). In the case of As(III), the sorption capacity is highest at pH 5 (~$2x10^{-3}$ mol As/g FeS) and decreases over the pH range of 5 to 9. The high uptake capacity for As(III) appears to be due to the precipitation of $AsS_{(s)}$ and appears to be limited only by the availability of sulfide from FeS. At higher pH, the capacity drops off as the mechanism of removal switches from precipitation to a surface area-limited removal process. With FeS-coated sand, As(III) removal is 30%, 70%, and 300% of the maximum capacity of nanoparticulate FeS at pH 5, 7 and 9, respectively. The As(III) uptake capacity by FeS-coated sand is comparable to other iron or aluminum oxide coated sand used for arsenic removal under oxic conditions and is greater under anoxic conditions with a maximum uptake capacity at pH 5 that decreases with pH. Under anoxic conditions, FeS-coated sand is expected to outperform other iron and aluminum oxides for As(III), given that these other sorbents are expected to release arsenic when reducing conditions prevail for long time periods (Tufano and Fendorf, 2008), whereas FeS-based materials may not release sorbed contaminants back into solution by reductive dissolution.

In this chapter, the impact of solution chemistry was evaluated with FeS-coated sand and the results were compared with the behavior of nanoscale FeS under similar solution conditions. pH plays an important role in determining the As(III) uptake mechanism in FeS-coated sand systems. For a similar amount of FeS (~0.1 mg FeS/L), FeS-coated sand exhibits similar pH-dependence to nanoparticulate FeS for removal of As(III) at an initial As(III) concentration of 1.33 $x10^{-5}$ M (1 ppm). This suggests that the primary removal mechanisms of FeS-coated sand over the range of pH values investigated are similar to that of FeS. Some differences occurred at pH values higher than 11 where FeS does not work as a As(III) scavenger but FeS-coated sand still shows some affinity for As(III) attributed to the iron hydroxide coating of the natural sand. From an application perspective, the performance of FeS-coated sand can be determined by the amount of FeS per unit volume that can be delivered regardless of whether FeS is delivered in nanoscale form or coated onto sand grain, even though there is some loss of capacity in the coated sand system.

No impact of the presence of dissolved silicate on As(III) removal was observed at pH 5, 7 and 9 for nanoscale FeS and at pH 5 and 7 for FeS-coated sand. However, a slight lowering (11%) of As(III) uptake was noted at pH 9 in the FeS-coated sand system. This reduction is attributed to the inhibition by silicate of As(III) adsorption to the iron oxyhydroxide phases originally present on the natural sand or the iron oxyhydroxide phases that may have formed from the oxidation of FeS during the coating procedure or subsequently. Although the impact at pH 9 is relatively small, this may not be advisable simply because of the reduced removals. A continuous supply of dissolved silicate in groundwater flowing through the PRB might eventually cause the release of As(III) back into solution similar to that seen in ZVI PRB (Tufano and Fendorf, 2008).

CHAPTER VI

SPECTROSCOPIC INVESTIGATION OF THE ASSOCIATION OF As(III) WITH FeS-COATED SAND

6.1 Introduction

In aquifer sediments, the association of arsenic with sulfide is mainly assumed to take the following forms: as a minor constituent in sulfide minerals, as a sorption complex on sulfide minerals, and/or as precipitated arsenic sulfide minerals (O'Day et al., 2004; Wilkin and Ford, 2006). O'Day et al (2004) observed realgar(AsS)-like arsenic sulfide in their x-ray absorption near-edge structure (XANES) and extended x-ray absorption fine structure (EXAFS) spectra, emphasizing the role of arsenic sulfide in controlling arsenic in natural sediments, rather than the more frequently documented theory of a coprecipitation of arsenic with pyrite or arsenopyrite (Savage et al., 2000). Laboratory studies have also documented the role of sulfide minerals in arsenic removal using various iron sulfides such as troilite, pyrite and mackinawite (Moore et al., 1988; Farquhar et al., 2002; Bostick and Fendorf, 2003; Wolthers et al., 2005). As(III) sorption on troilite and pyrite surfaces was characterized as FeAsS-like surface precipitation (Bostick and Fendorf, 2003). Farquhar et al. (2002) demonstrated that mackinawite is more efficient than other iron-oxide phases or pyrite in removing As(III), by forming outer sphere surface complexes through adsorption along with poorly crystalline arsenic sulfide by precipitation. Disordered mackinawite removed 0.012 mol As(III) per mol FeS at neutral pH and its removal was postulated as an outer sphere surface complex on the surface of mackinawite (Wolthers et al., 2005). In another study, synthesized mackinawite showed a As(III) removal capacity of 0.16 mol As(III)/mol FeS at pH 5 and 0.018 mol As(III)/mol FeS at pH 7 (Gallegos, 2007). The prominently high As(III) removal observed at pH 5 was suggested as the immobilization of As(III) by precipitated

realgar (AsS), evidenced by X-ray absorption spectroscopy (XAS) and X-ray diffraction (XRD) (Gallegos et al, 2007).

FeS-coated sand shows appreciable amounts of As(III) removal at pH 5, 7 and 9 under anaerobic conditions (Chapter 5). Even though the association of As(III) with mackinawite has been intensively studied by several research groups, FeS-coated sand may have different reaction mechanisms. For example, the XPS results shown in Figure 4.5 indicates that the surface of the FeS-coated sand is also comprised of iron-oxides from the natural sand surface or partially oxidized mackinawite that forms during the coating process. Accordingly, this chapter characterizes As(III) sorption on FeS and FeS-coated sand using the spectroscopic techniques of x-ray photoelectron spectroscopy (XPS) and x-ray absorption spectroscopy (XAS). This comparison of the FeS-coated sand with FeS provides an opportunity to evaluate if the coating process significantly impacts the solid phase As(III) uptake reaction products.

6.2 Methods

6.2.1 Sample preparation

X-ray photoelectron spectroscopy (XPS) and x-ray absorption spectroscopy (XAS) were used to determine the arsenic oxidation state and the relative proportion of different As species in As(III)-reacted FeS and FeS-coated sand samples. As(III)-reacted FeS samples were prepared using 300 mL of 5g/L FeS suspension in 400 mL glass reactors that allowed for the continuous measurement of pH in a closed system. The pH of a 5g/L suspension was adjusted to pH 5 or 9 using HCl, and an aliquot of a 1.33 M $NaAsO_2$ stock solution was added to achieve of concentration of 1.33×10^{-2} M As(III). The pH was monitored over a two-day equilibrium time and adjusted as necessary with acid to maintain the pH at 5 or 9. For the reaction of FeS-coated sand with As(III), 416 g/L of FeS-coated sand (equivalent to 0.5 g/L FeS based on previous work showing 1.2×10^{-3} g-FeS/g sand) was reacted with a 1.33×10^{-3} M As(III) solution in 50 mL polypropylene tubes and mixed by an end-over-end rotating mixer for two days. Since the pH measurement of this system could not be easily continuously monitored in the smaller volume reactor, multiple samples were prepared and a sample that gave a pH of 5 or 9 after two days-equilibrium time was selected for the XAS or XPS analysis. The

samples for XAS analyses were filtered using 0.22 μm nylon filters and the filtered paste of particles were transferred into airtight, crimp-sealed serum bottles without drying and then shipped to Stanford Synchrotron Radiation Laboratory (Stanford, CA) (SSRL) for XAS analysis. For XPS analysis, the sample was filtered, freeze-dried, crimp-sealed and stored in an anaerobic chamber until the analysis.

The samples for evaluating an aging effect of particulate FeS at pH 9 were prepared in a similar way. The pH of 5g/L suspension was first adjusted to pH 9 using HCl, and then an aliquot of a 1.33 M $NaAsO_2$ stock solution was added to achieve a concentration of 1.33×10^{-2} M As(III). Adding As(III) increased the pH of the suspension, so additional acid was added to titrate the suspension to pH 5. The pH was monitored over a two-day equilibration time and adjusted as necessary with acid to maintain the pH at 9. After two days of mixing with a magnetic stirring bar, one third of suspension was filtered using 0.22 μm filter and the collected solid were freeze-dried for XPS analysis. The other two portions of the suspension was reacted for 25 days and 50 days to assess the aging effect, and then filtered and collected as a solid after freeze-drying.

6.2.2 X-ray absorption spectroscopy (XAS)

XAS samples were prepared for analysis by applying wet sample pastes onto a double layer of Kapton tape inside an anaerobic glove box. XAS spectra were collected at SSRL on beamline 10-2 (3 GeV, ~100 mA of maximum current) with an unfocused beam. Arsenic K-edge XAS spectra were obtained using a Si(220) double-crystal monochromator with a 13-element solid-state Ge-array fluorescence detector or Lytle detector. The sample chamber was continuously purged with He gas to avoid potential oxidation. Based on a comparison of spectra, no oxidation was observed during the data collection. XAS spectra were also collected for model compounds such as metallic arsenic (As(0)), amorphous AsS, amorphous As_2S_3 dissolved As(III), and dissolved As(V). All arsenic reference compounds were purchased from Alfa Aesar (Lancaster, UK).

The XAS spectra were analyzed using the program package SixPACK (Webb, 2002). Individual spectra were first averaged, and the background absorbance was subsequently removed by a linear fit through the pre-edge region. X-ray absorption near-

edge structure (XANES) spectra (e.g., 11,860–11,890 eV) were obtained by normalizing the fluorescence signal to the edge jump height. The absorption edges (i.e., inflection energies) of XANES spectra were determined to compare the oxidation state of arsenic between the samples and model compounds. Extended x-ray absorption fine structure (EXAFS) spectra were also obtained by fitting a quadratic spline function above the edge. EXAFS spectra were normalized using a Victoreen polynomial function and then transformed from energy (eV) to k space ($Å^{-1}$) using E_0 = 11,885 eV. The resultant EXAFS functions ($\chi(k)$) were weighted by k^3 to amplify the higher k region, and Fourier-transformed to produce radial structural functions (RSF) in R space over k = 3.5−11.5 $Å^{-1}$.

Structural parameters were obtained by fitting k^3-weighted EXAFS functions with the phase and amplitude functions derived from FEFF 8 (Ankudinov et al., 1998). The amplitude-reduction factor (S_o^2 = 0.92) was optimized from the fitting of the model compound spectra and kept constant for all EXAFS analysis. The Debye-Waller factors (σ^2) were also fixed based on the similarity between the sample spectra and the model compound spectra or the optimization among the sample spectra to reduce the degrees of freedom during the fitting. Coordination number (N), interatomic distance (R), and energy shift (ΔE_0) were allowed to vary. The optimal fitting was obtained by minimizing the goodness of fit parameter (R_f).

6.2.3 X-ray photoelectron spectroscopy (XPS)

The model compounds used for the XPS analyses were As(0), arsenic(II) sulfide, arsenic(III) sulfide, $NaAsO_2$ and $Na_2HAsO_4 \cdot 7H_2O$, all purchased from Alfa Aesar (Lancaster, UK). The reference compounds and As(III) reacted samples were mounted on a sample bar in an anaerobic glove box and transferred, using an air-tight container filled with 95% N_2/5% H_2 gas mixture to minimize the oxygen contact with the sample surface. The Al-K_α line (1486.6 eV) was used as the radiation source. The survey spectra were obtained using analyzer pass energies of 160 eV. Narrow XPS scan peaks were obtained primarily with a pass energy 20 eV, but for the As(III)-reacted FeS-coated sand samples the higher pass energy of 160 eV was needed due to a low As loading. While a higher pass energy can be used for a qualitative comparison of peak positions to model compounds, the data cannot be used for quantitative peak analyses due to the peak

broadening that occurs when a higher pass energy is used. Energies were corrected for charging effects using the reference peaks of adventitious carbon C l*s* with a binding energy of 284.6 eV. Raw spectra were smoothed before being fitted using a Shirley base line and a Gaussian-Lorentzian peak shape. For quantitative results, to estimate the standard deviation of each of the component's contribution to the overall XPS spectrum in the fitting procedure, Monte-Carlo analysis (CasaXPS, Casa Software Ltd., UK) was applied. The program applies artificial noise to a spectrum and calculates an error matrix to give the variance of each fit based on the fitting constraints used.

6.3 Results and discussion

6.3.1 Arsenic loading

The supernatants of the samples used for spectroscopic studies were analyzed using ICP-MS to calculate the arsenic loading on the solid phase. Mackinawite removed 99% (at pH 5) and 20% (at pH 9) of the initial 1.3×10^{-2} M As(III) present in solution, and FeS-coated sand removed 63% (at pH 5) and 23% (at pH 9) of the initial 1.3×10^{-3} M As(III). These data demonstrate that substantially higher As(III) sequestration occurs at pH 5 where excess dissolved sulfide exists and the solubility of arsenic sulfide is low. It is worthwhile to note that FeS-coated sand yields more than 60% and more than 100% efficiency of the FeS system at pH 5 and pH 9, respectively, with the same Fe/As ratio based on the equivalent amount of FeS-mass similar to the results reported for pH 9 batch measurements reported in Chapter 5.

6.3.2 XANES and EXAFS analysis

XAS spectra were subjected to both XANES and EXAFS analyses. While the oxidation state of arsenic can be obtained from XANES analysis, structural parameters such as interatomic distance (*R*) and coordination number (*N*) on the near coordination environment around arsenic can be gleaned from EXAFS analysis. In XANES spectra (Figure 6.1), the absorption edges (i.e., inflection energies) of the samples are compared with those of model compounds. While a higher absorption edge energy is indicative of a higher oxidation state of arsenic, a lower absorption edge energy corresponds to a lower oxidation state. The absorption edge energies of As(0), arsenopyrite, AsS, As_2S_3,

dissolved As(III), and dissolved As(V) were 11866.7, 11867.0, 11868.1, 11869.0, 11870.9, and 11874.4 eV, respectively. At pH 5, the pure FeS system reacted with As(III) had an absorption edge energy of 11868.4 eV, only slightly higher than that of AsS, indicating that the dominant oxidation state of As in the pure FeS sample was +II. The As(III)-reacted FeS-coated sand had an absorption energy of 11869.1 eV, close to that of As_2S_3, suggesting the formation of As_2S_3. At pH 9, the pure FeS reacted with As(III) had an absorption energy of 11868.06 eV, slightly lower than that of As_2S_3 and higher than that of dissolved As(III), indicating the possible formation of species with oxidation states of As as in thioarsenite clusters. The As(III)-reacted FeS-coated sand at pH 9 had an absorption energy of 11870.87 eV, close to that of dissolved As(III), suggesting the surface complexation of arsenite species.

The EXAFS spectra and corresponding Fourier transforms of the experimental samples and model compounds are compared in Figure 6.2. For the pure FeS system at pH 5, the first coordination shell around As is characterized by the As-S interaction with the coordination number ($N_{As\text{-}S}$) of 2.1 at a distance of 2.27 Å, in good agreement with that of the AsS model compound ($N_{As\text{-}S}$ = 2.0 at 2.26 Å). Also, the second coordination shell for the pure FeS system is characterized by the As-As interaction at 3.49 Å, whose coordination number ($N_{As\text{-}As}$ = 0.95) is twice greater than that of the AsS model compound ($N_{As\text{-}As}$ = 0.41 at 3.50 Å). Compared with the AsS model compound, the pure FeS had a stronger second shell feature and a slightly higher absorption energy, indicating that another As phase, in addition to AsS, may form in the pure FeS system. Previously, a surface precipitate in the form of trimeric arsenic sulfide was proposed for As(III) sorption by PbS and ZnS (Bostick et al., 2003). The As-As bonding distance (~3.6 Å) in their study is close to the value (3.50 Å) observed here. Thus, the formation of surface precipiates as thioarsenites may explain the observed differences between the AsS model compound and the pure FeS system.

The first coordination shell of the FeS-coated sand system at pH 5 is characterized by the As-As interaction with the coordination number ($N_{As\text{-}S}$) of 2.9 at a distance of 2.26 Å, consistent with the coordination chemistry of As_2S_3 ($N_{As\text{-}S}$ = 3.0 at 2.28 Å). Unlike the pure FeS system, both the FeS-coated sand system and the As_2S_3 model compound show very weak second coordination shells ($N_{As\text{-}As}$ = 0.31 at 3.66 Å for the FeS-coated

sand system and $N_{As\text{-}As}$ = 0.37 at 3.54 Å for the As_2S_3 model compound). Taken together, the formation of a surface precipitate of thioarsenite in the FeS-coated sand system should be minimal. Instead, the formation of As_2S_3 is mainly responsible for As(III) uptake in the FeS-coated sand system.

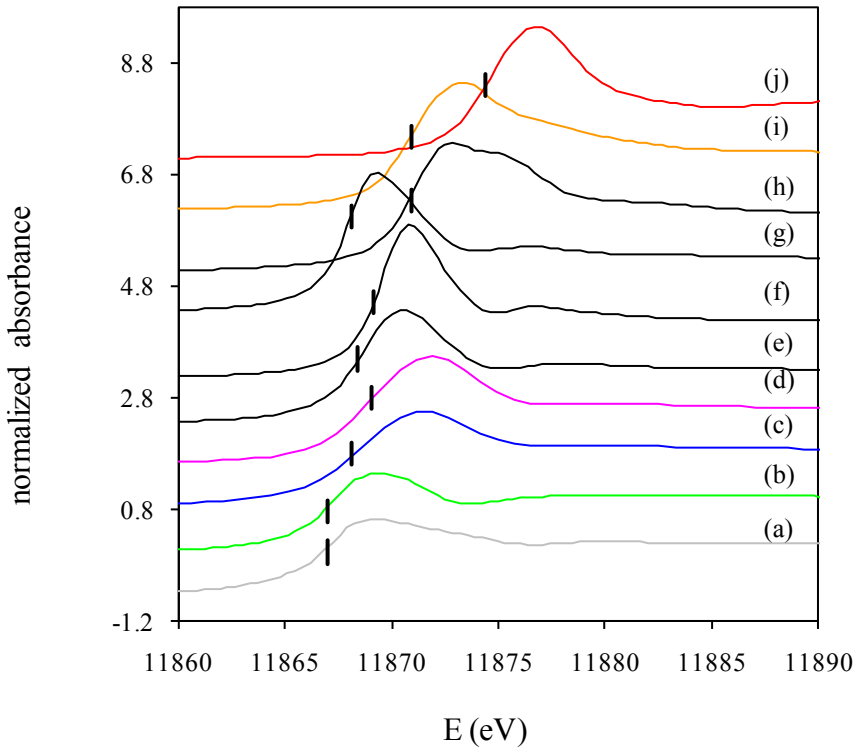

Figure 6.1 Arsenic K-edge XANES spectra of (a) As(0) (grey), (b) FeAsS (green), (c) AsS (blue), (d) As_2S_3 (pink), (e) 5g/L FeS reacted with 1.33×10^{-2} M As(III) for 2 days at pH 5, (f) 5g/L FeS reacted with 1.33×10^{-2} M As(III) for 2 days at pH 9, (g) 416 g/L FeS-coated sand reacted with 1.33×10^{-3} M As(III) for 2 days at pH 5, (h) 416 g/L FeS-coated sand reacted with 1.33×10^{-3} M As(III) for 2 days at pH 9, (i) dissolved $NaAsO_2$ (yellow) and (j) dissolved NaH_2AsO_4 (red). The absorption edges correspond to the first derivative maxima of XANES spectra.

Table 6.1 EXAFS fit results for pH 5 and 9 FeS and FeS-coated sand As(III) reacted samples and As reference model compounds

		EXAFS fit*			Crystallographic data		
	Pair	***N***	***R*(Å)**	**σ^2(Å^2)**	***N***	***R*(Å)**	**Reference**
As(0)	As-As	1.1	2.50	0.0058†	3	2.50	O`Day et al., 2004
	As-As				3	3.13	
	ΔE_0 = -6.95 eV, R_f = 0.065						
AsS	As-S	2.0	2.26	0.003†	2	2.24	Farquhar et al., 2002
	As-As				1	2.57	
	As-As	0.41	3.50	0.006†	2.5	3.44-3.51	
	As-S				1	3.41-3.52	
	ΔE_0 = -9.80 eV, R_f = 0.061						
As_2S_3	As-S	3.0	2.28	0.0045†	3	2.24-2.31	Farquhar et al., 2002
	As-As	0.37	3.54	0.006†	1	3.19	
	As-S				3	3.22-3.57	
	As-As				2.5	3.52-3.64	
	ΔE_0 = -7.75 eV, R_f = 0.047						
pH 5 FeS	As-S	2.1	2.27	0.003†			
	As-As	0.95	3.49	0.006†			
	ΔE_0 = -8.24 eV, R_f = 0.0412						
pH 9 FeS	As(III)-O	0.69	1.77	0.0045†			
	As-S	1.96	2.25	0.0045†			
	As-As(matallic)	1.10	2.55	0.008†			
	As-As(ads)	1.73	3.50	0.006†			
	ΔE_0 =-8.84 eV, R_f = 0.0205						
pH 5 coated sand	As-S	2.9	2.26	0.0045†			
	As-As	0.31	3.66	0.006†			
	ΔE_0 = -10.09 eV, R_f = 0.0974						
pH 9 coated sand	As(III)-O	2.88	1.78	0.0045†			
	ΔE_0 =-2.78 eV, R_f = 0.2119						
$As(III)_{aq}$	As(III)-O	3.0	1.76	0.0045†	3‡	1.78‡	Wolthers et al., 2005
	ΔE_0 = -7.90 eV, R_f = 0.069						
$As(V)_{aq}$	As(V)-O	4.0	1.69	0.0025†	4‡	1.69‡	Yamauchi and Fowler, 1994
ΔE_0 = -5.01 eV, R_f = 0.024							

*The amplitude-reduction factor (S_o^2) was set at 0.92.
†The Debye-Waller factors (σ^2) were fixed during the numerical fit.
‡Structural data was obtained from EXAFS analysis.

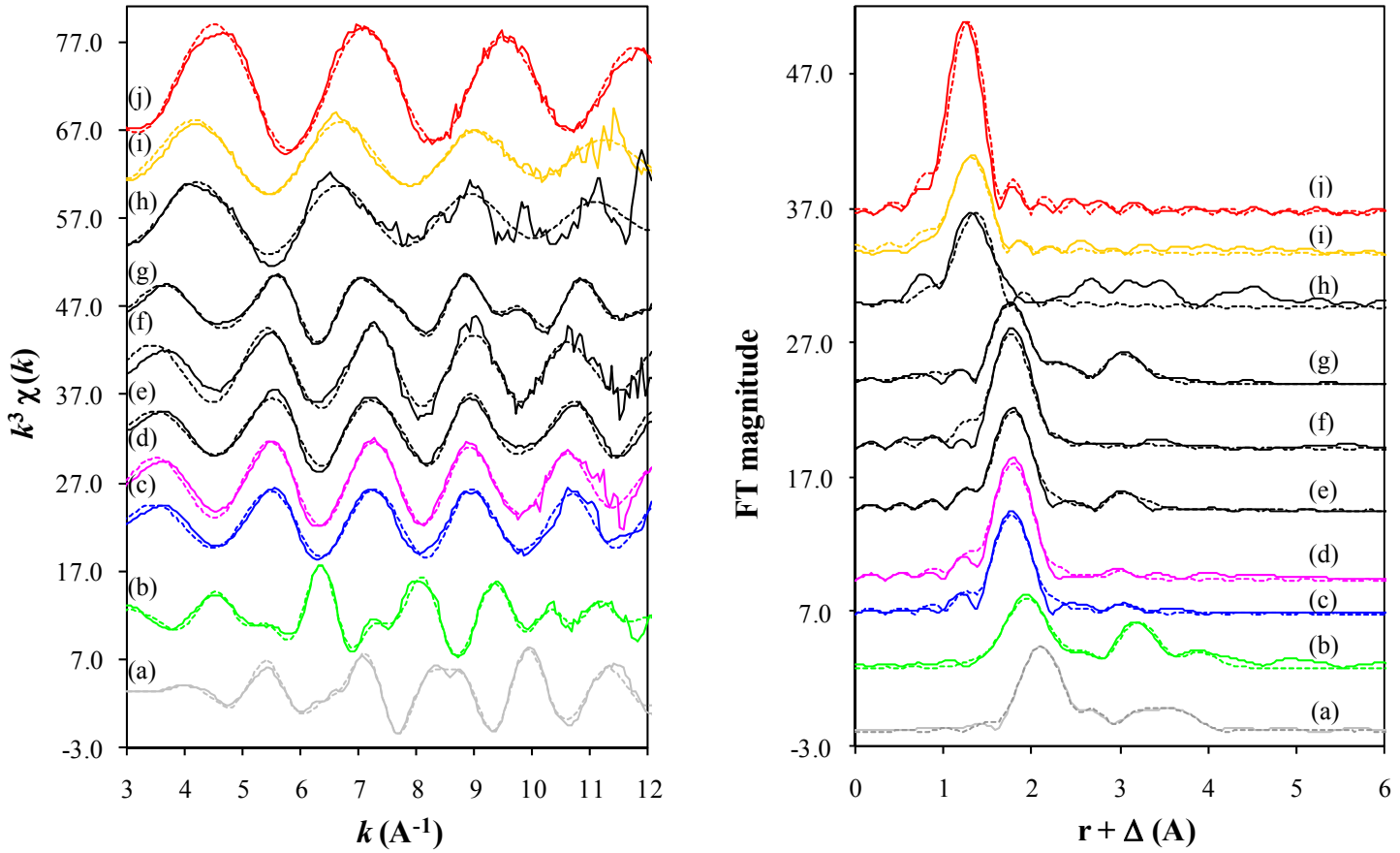

Figure 6.2 k^3-weighted arsenic K-edge EXAFS spectra ($k^3\chi(k)$) of (a) zerovalent arsenic (grey), (b) FeAsS (green), (c) AsS (blue), (d) As_2S_3 (pink), (e) 5g/L FeS reacted with 1.33×10^{-2} M As(III) for 2 days at pH 5, (f) 5g/L FeS reacted with 1.33×10^{-2} M As(III) for 2 days at pH 9, (g) 416 g/L FeS-coated sand reacted with 1.33×10^{-3} M As(III) for 2 days at pH 5, (h) 416 g/L FeS-coated sand reacted with 1.33×10^{-3} M As(III) for 2 days at pH 9, (i) dissolved $NaAsO_2$ (yellow) and (j) dissolved NaH_2AsO_4 (red). Solid lines are the experimental data; dashed lines are the numerical fits.

At pH 9, the FeS pure system displayed different characteristic in its EXAFS spectra. The radial distribution functions (RDFs) of the EXAFS data for the pH 9 FeS reacted with 1.3×10^{-2} M As(III) consist of four peaks. The fitting of the first and most prominent peak in this sample gives $N_{As\text{-}S} = 1.96$ at a distance of 2.25 Å, indicating surface complexes of thioarsenites clusters. Unexpectedly, this sample consists of As-As bonds, demonstrating the possible formation of As(0). In contrast, the FeS-coated sand sample at pH 9 reacted with 1.3×10^{-2} M As(III) displays the first coordination shell of As(III)-O interaction at 3.5 Å with a coordination number of 1.73. This result indicates there is no sulfur-coordinated environment around As in this sample, thus suggesting the surface complexation of arsenite species in the FeS-coated sand system under pH 9. The reasons for this difference in pure FeS and FeS-coated sand are discussed in Section 6.3.5.

6.3.3 XPS analysis

Figure 6.3 and Table 6.2 shows the As 3*d* spectra and the fitting parameters of arsenic reference compounds and samples reacted with As(III). Each surface species in the As(*3d*) spectrum is fitted with a doublet representing the spin-orbit splitting of the As $3d_{5/2}$ and As $3d_{3/2}$ peaks. A higher binding energy is indicative of a higher oxidation state of arsenic and a lower binding energy corresponds to a lower oxidation state. The position of As $3d_{5/2}$ peaks for (a) As(0), (b) arsenic(II) sulfide, (c) arsenic(III) sulfide, (f) $NaAsO_2$ and (g) $Na_2HAsO_4{\cdot}7H_2O$ were determined to be 41.8, 42.8, 43.1, 43.5, and 44.5eV, respectively. These model compounds revealed that each consisted of at least 83% of the expected dominant oxidation state, with minor contributions of other oxidation states of arsenic. The FWHM (full width at half maximum) values for all the model compounds were determined 1.0 eV, assuming that the reference compounds were composed of a single primary oxidation state of As. The binding energies determined by the As $3d_{5/2}$ peak positions and FWHM values were used to predict the As oxidation states of the 5g/L FeS samples reacted with 1.33×10^{-2} M As(III) and 416 g/L FeS-coated sand reacted with 1.33×10^{-3} M As(III) at pH 5 or pH 9.

At pH 5, the As $3d_{5/2}$ peaks of 5g/L FeS reacted for two days with 1.33×10^{-2} M As(III) were sharp, indicating that one prominent arsenic solid species precipitated as a result of the reaction between FeS and As(III) at pH 5 (Figure 6.3 (d)). The peaks were

well fitted with a doublet of As $3d_{5/2}$ and As $3d_{3/2}$ at binding energies of 42.8 and 43.5 eV, respectively, with FWHM = 1. These peak positions indicate that the As oxidation state is primarily As(II). This also indicates that AsS (realgar) precipitation is likely to have occurred as predicted from thermodynamic modeling of 5g/L FeS reacted for two days with 1.33×10^{-2} M As(III) presented in Gallegos et al. (2008) and shown by XAS analysis in the previous section (Section 6.3.1, Table 6.1). This precipitated AsS is likely to be amorphous AsS because no AsS peaks were observed using XRD (See Appendix A3).

Table 6.2 Fitting parameters for XPS As 3*d* for arsenic reference compounds

	As 3d $_{5/2}$ (eV)	**FWHM (pass energy 20 eV)**	**FWHM (pass energy 160 eV)**	**Component**
As(0)	41.8	1	2.2	As-As
AsS	42.8	1	2.2	As(II)-S
As_2S_3	43.2	1	2.2	As(III)-S
$NaAsO_2$	43.5	1	2.2	As(III)-O
$Na_2HAsO_47H_2O$	44.5	1	2.2	As(V)-O

*FWHM : Full-width at half maximum

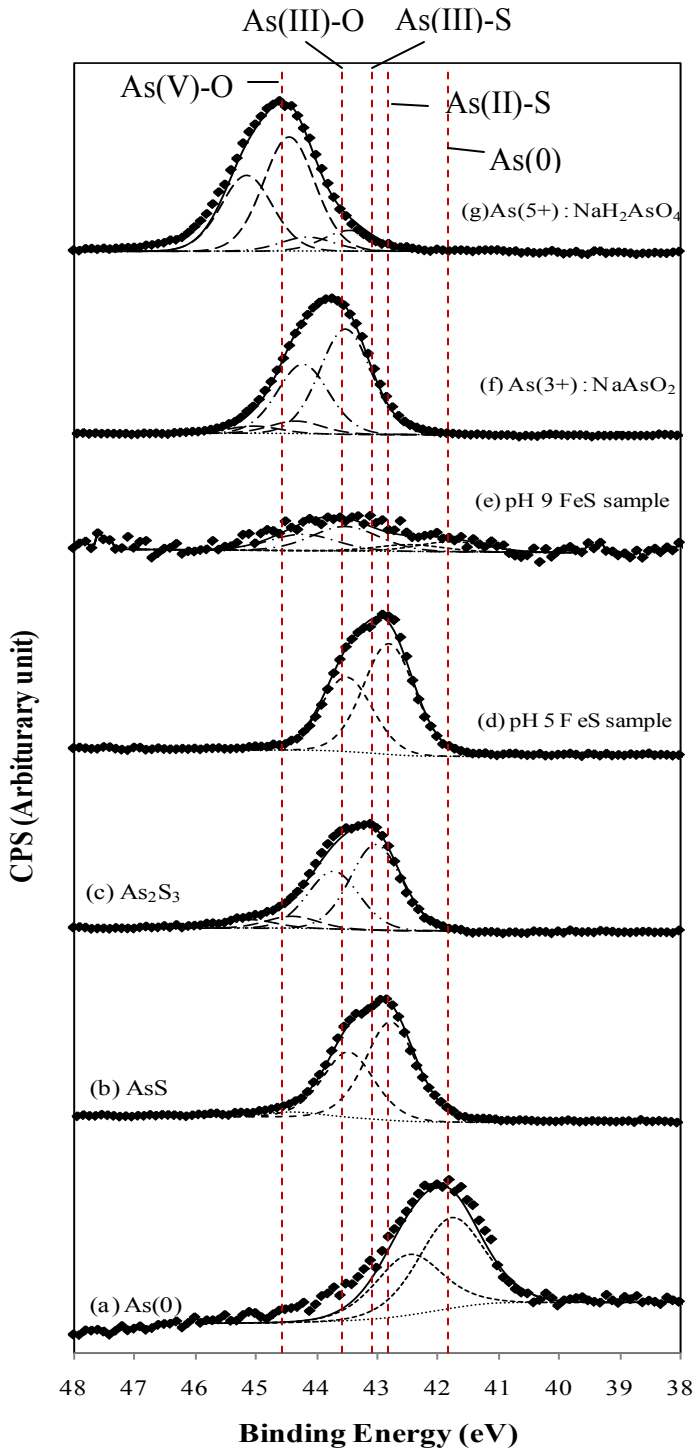

Figure 6.3 XPS spectra of As 3*d* peaks for (a) As(0), (b) AsS, (c) As_2S_3, (d) FeS reacted with 5g/L FeS reacted with 1.33×10^{-2} M As(III) for 2 days at pH 5, (e) FeS reacted with 5g/L FeS reacted with 1.33×10^{-3} M As(III) for 2 days at pH 9, (f) $NaAsO_2$ salt and (g) NaH_2AsO_4 salt using a low pass energy of 20 eV. (a, b, c, f and g are reference compounds, and d and e are samples. The spectrum of sample (e) were enlarged for better viewing.)

At pH 9, the intensity of the As $3d_{5/2}$ peaks is much smaller than that at pH 5 because only 20% out of the 1.33×10^{-2} M As(III) was immobilized compared with almost 100% at pH 5. The low arsenic loading resulted in a weak, broad-looking peak but the center of the peak is obviously shifted to a higher binding energy and the As $3d_{5/2}$ peak placed throughout the binding energy ranges of As(II)-S, As(III)-S and As(III)-O, possibly indicating the presence of a mixture of various thioarsenite species. Interpreted this way, the result is consistent with the EXAFS analysis.

The XPS spectra for As(III) reacted with FeS-coated sand at pH 5 and 9 are shown in Figures 6.4. Since the As(III) loading on FeS-coated sand after reaction with As(III) was too low to get good peak spectra, the pass energy of 160 was used instead of the more widely used pass energy of 20. A pass energy of 160 eV is sometimes used to identify an oxidation state of an element of interest (Su and Puls, 2008). In this study, the result of XPS As 3*d* spectra was used to qualitatively compare the peak position of As(III) reacted FeS-coated sand samples. Figure 6.4 shows the XPS analysis of FeS-coated sand sample reacted with As(III) at pH 5 and indicates that the solid phase reaction product is primarily As(III)-S which is consistent with the formation of orpiment. At pH 9, the results indicate the presence of primarily As(III)-O on the FeS-coated sand surface suggesting arsenite adsorption. These results support those obtained with XAS. The broadening of peak towards the low and high binding energies is likely caused by using the higher pass energy of 160. The peak broadening effect with increasing pass energy value is verified in Figure 6.5 which shows that the higher pass energy smoothed out the peak shapes, resulting in greater FWHM values. However, the highest peak positions are still displayed at the same binding energy. Consequently, the identification of the higher binding energy for the samples with weak element intensity appears to be valid when used in this qualitative way to verify the peak maximum.

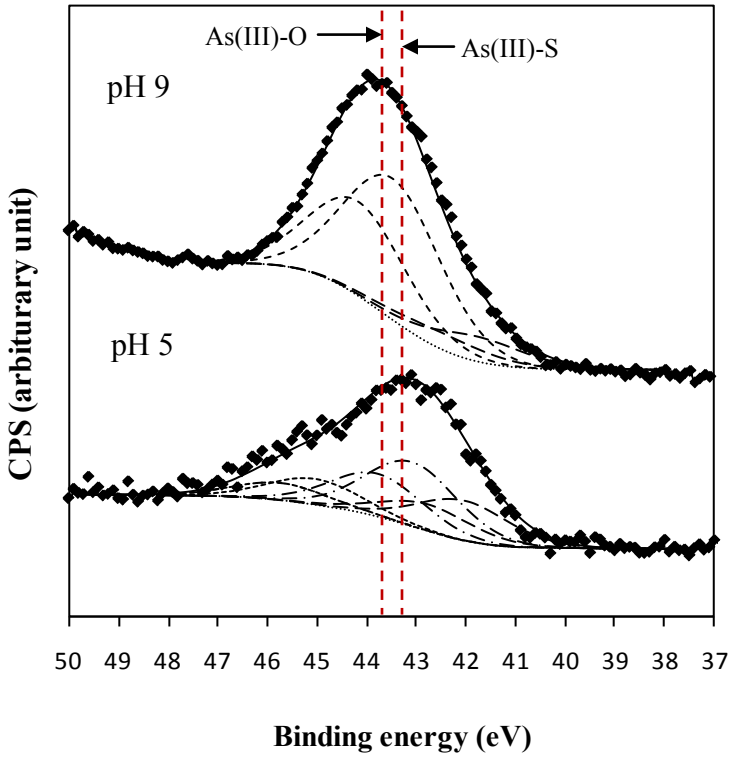

Figure 6.4 XPS As 3*d* peak spectra for As(III) reacted with FeS-coated sand at pH 5 and 9 using a high pass energy of 160 eV.

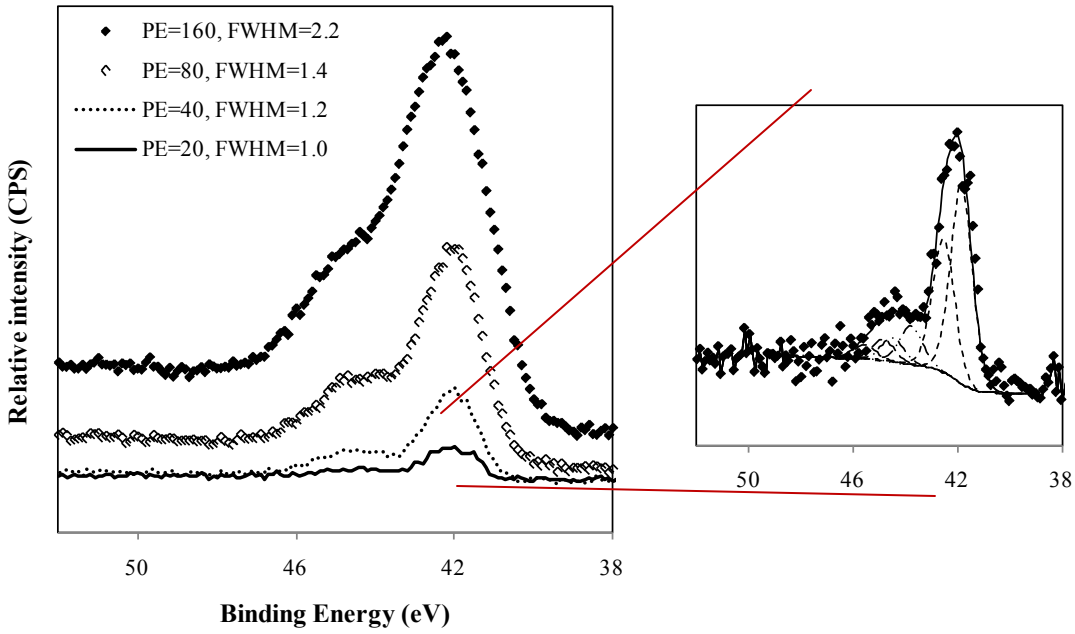

Figure 6.5 XPS As 3*d* peak spectra for As(0) reference compound as a function of pass energy (PE) ranging from PE=20 to 160. The peak intensity increases with increasing PE but with the trade-off of lower resolution spectra, as indicated by the increasing values of the full width at half maximum (FWHM). Generally the smaller FWHM represents the precise peak shape. The enlarged area shows that the peak with low pass energy of 20 eV has sharper peak shapes.

6.3.4 Comparison of FeS and FeS-coated sand systems reacted with As(III) at pH 5

Nanoparticulate FeS and FeS-coated sand reacted with a high concentration of As(III) at pH 5 resulted primarily in the precipitation of arsenic sulfides but different oxidation states were detected in each solid phase of arsenic. The XANES and EXAFS analyses suggest that the formation of AsS and a thioarsenite surface precipitate is likely responsible for As(III) uptake in the FeS system at pH 5, and the formation of As_2S_3 is likely to occur in the FeS-coated sand system at pH 5. The XPS results also support the formation of different arsenic sulfide solids in each system; in FeS, the more reduced condition of arsenic symptomatic of realgar precipitation was observed, while in FeS-coated sand, a more oxidized condition suggestive of orpiment was obtained.

These differences may be attributed to different redox conditions in those two systems. In the batch of 5g FeS /L reacted with 1.3×10^{-2} M As(III) and the batch of 416g

FeS-coated sand/L or (0.5g FeS/L) reacted with 1.3×10^{-3} M As(III), the redox potential was measured as -326 mV and -246 mV, respectively, using a platinum and an *Ag*/*AgCl* reference electrode. The calculated pe values from the measured redox potential are -2.15 for nanoparticulate FeS system and -0.91 for the FeS-coated sand system. The thermodynamic simulation by PHREEQC of the 5g FeS/L batch system predicted amorphous As_2S_3 precipitation at pe values ranging from -0.9 to -1.95, AsS precipitation at pe values ranging from -2.0 to -3.45, and As(0) precipitation at pe values under -3.45 (Figure 5.6). The different amount of total FeS in each batch may have caused the different redox conditions in the nanoparticulate FeS and FeS-coated sand systems. The thermodynamically predicted arsenic sulfide species in both systems match reasonably well the solid species of arsenic sulfide obtained from the XPS and XAS results. The formation of different arsenic sulfide species, depending on the system redox conditions, was previously simulated using MINEQL$^+$ by Gallegos et al. (2008) and similar results were reported in that orpiment precipitation was predicted at higher pe, while realgar precipitation was predicted at lower pe.

6.3.5 Comparison of FeS and FeS-coated sand systems reacted with As(III) at pH 9

Similar to the case of pH 5, the overall As(III) uptake mechanism is the same in both nanoparticulate FeS and FeS-coated sand systems at pH 9; yet at this pH, the primary removal mechanism is a surface complexation reaction. But in the FeS system, thioarsenite species were detected and in the FeS-coated sand system arsenite species were detected. These results are not consistent with the results reported by Gallegos et al. (2008) in that their nanoparticulate FeS reacted with 5×10^{-5}M As(III) showed only As-O coordination, not As-S coordination at pH 9, suggesting the arsenite surface complexation process as the As(III) uptake mechanism. Considering these two different results, it can be speculated that the exact form of arsenic surface complex might depend on the concentration of As(III) and hence, to the initially added As(III) concentration in the two systems. In the present study, the nanoparticulate FeS samples were exposed to higher As(III) concentrations than the FeS-coated sand samples or the nanoparticulate FeS samples of Gallegos et al. (2008). In the systems with a higher concentration,

arsenite may serve as an oxidizing agent. While the proton concentration controls the FeS solubility at low pH conditions, the arsenite acting as an oxidant may control the FeS solubility at higher pH. In the presence of sulfide under anoxic conditions at lower arsenic concentration, sulfide may lead to the formation of thioarsenite species. Although the dissolved iron concentration measured in the pH 9 batch of FeS-coated sand was negligible (measured as less than 10 ppb level in this study), the sulfide of FeS can still be present in the aqueous phases at appreciable concentrations, according to Rickard (2006). Consequently, arsenite is able to form thioarsenite species under basic pH conditions due to the high affinity between As(III) and sulfide. The exact forms or chemical properties of aqueous thioarsenite species are unknown but their toxicity is known to be lower than those of arsenite species (Rader et al., 2004). Therefore, changing the aqueous species of arsenic from arsenite to thioarsenite itself has some environmental benefits.

In both the XAS and XPS results of the nanoparticulate FeS at pH 9, it should be noted that As-As coordination was observed at an atomic distance 2.55 Å which represents the presence of elemental (metallic zerovalent arsenic) arsenic. The formation of As(0) by the reaction between dissolved arsenite and sulfide was identified by chromatography by Stauder et al. (2005). They proposed the disproportionation reaction to explain the simultaneous formation of thioarsenate and As(0) :

$$5H_2As(III)O_3 + 3H_2S = 2As(0) + 3H_2As(V)O_3S^- + 6H_2O + 3H^+ \qquad (6\text{-}1)$$

This equation suggests the formation of thioarsenate instead of thioarsenite which is more probable because of the high affinity between arsenate and sulfur. However, neither thioarsenate nor As(0) species were detected in the XAS study of arsenite and sulfide solutions of Beak et al. (2008). Beak et al. (2008) suggested that the rapid formation of thioarsenates is unlikely in sulfidic environments where As(III) and sulfide are initially present. In this study, long-term aged pH 9 FeS samples were, therefore, prepared to verify the slow formation of thioarsenite and As(0). Figure 6.6 shows the As 3*d* peaks of 5g/L FeS reacted with 1.3×10^{-2} M arsenite for 25 and 50 days. The As 3*d* spectra display a broad peak in both higher and lower binding energy regions, which represent As(V) and

As(0), respectively. This result verifies that the As(III) species may be undergoing disproportionation, resulting in arsenic species with As(0) and As(V) oxidation states. Here, the As(II)-S peak for the formation of realgar (AsS) and the As(III)-O peak for initially injected form of arsenite appear, suggesting the occurrence of multiple reactions in this complex system.

6.4 Summary and conclusions

The results of XAS and XPS analyses confirm the mechanism of As(III) removal by FeS and FeS coated sand, with removal at pH 5 primarily a result of the precipitation of realgar or orpiment, and at pH 9 by the adsorption of thioarsenite or arsenite, respectively. The differences between the results for FeS-coated sand and those for nanoscale FeS are thought to be due to either: (1) the higher As:Fe required in the FeS-coated sand to obtain enough signal to perform the XAS or XPS analyses, and/or (2) due to the coating process which may leave the surface partially coated with a magnetite-like iron oxide that controls As removal at pH 9 and leaves the system less reducing at pH 5 so that orpiment instead of the more reduced realgar prevails. The overall implication of these results is, however, that FeS, as a coating, still maintains the same primary removal processes (arsenic sulfide preciptation at lower pH and adsorption at higher pH).

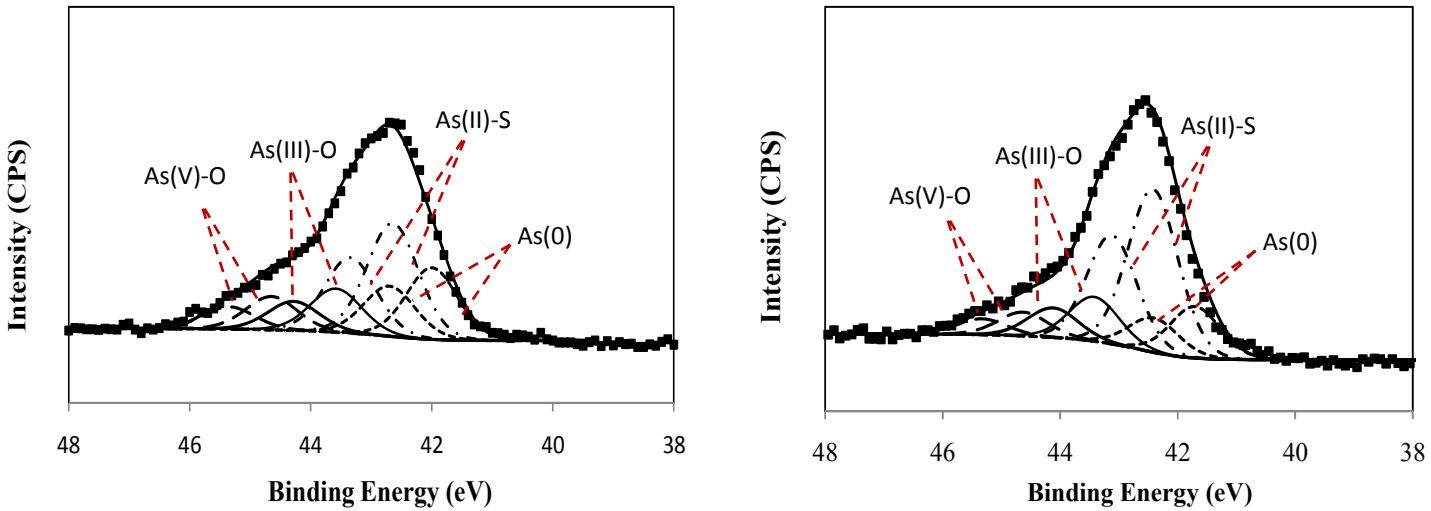

Figure 6.6 XPS As 3*d* peak spectra for 5g/L FeS reacted with 1.33×10^{-2} M As(III) at pH 9 for 25 days (a) and 50 days (b) using a low pass energy of 20 eV. The As 3*d* spectrum verifies the formation of arsenic with As(V) and As(0) oxidation states. (CPS: Count per second)

CHAPTER VII

COLUMN STUDIES OF As(III) REMOVAL BY FeS-COATED SAND

7.1 Introduction

Reactive transport in a column is more complex than a reaction in a batch reactor because it is controlled by multiple reaction phenomena such as the interaction between physical transport such as advective and/or diffusive flow and immobilization reactions such as adsorption and/or precipitation (Gabriel et al., 1998). The removal of contaminants may be controlled by the flow rate if the reaction does not reach equilibrium quickly. Furthermore, batch systems have much lower solid/solution ratios (SSR). Batch experiments can provide useful information about the removal of contaminants by sorbents such as adsorption isotherm, kinetic adsorption characteristics, etc. However, in many cases batch experimental results do not represent the reactive transport behavior in column because batch experimental conditions are fundamentally different from those in column systems (Maraqa, 2000).

The prediction of column performance using an analogous batch system generally works well if the system under consideration is physically and chemically simple: linear sorption with fast kinetics and without any co-existing ligand or competing elements. However, the FeS-coated sand and As(III) system showed highly non-linear sorption characteristics and As(III) removal involves multiple mechanisms – adsorption of As(III) on FeS-coated sand, precipitation of arsenic sulfide, the existence of oxidized phases, and transformation of FeS to more oxidized phases. Therefore, differences between batch and column removal efficiencies are expected. Moreover, the As(III) uptake is highly pH-dependent with a precipitation-dominant reaction at pH 5 and the adsorption-dominant reaction at pH 9. This difference may result in different behavior in each reactor system. This chapter presents column experiments performed at various values of

pH and a comparison of the column capacities and transport parameters with those determined in batch reactors.

7.2 Methods

7.2.1 Column experiments

The schematic diagram of column setup is displayed in Figure 7.1. FeS-coated sand was packed in a glass column (internal diameter = 4.8 cm; length = 15 cm or 4.8 cm) by successively depositing approximately 1.5 cm layers and compacting evenly with a ceramic pestle. The columns were set up vertically in an anaerobic chamber. The experimental conditions and physical parameters of column experiments are presented in Table 7.1. Acid extraction of the FeS-coated sand used in the column tests yielded 1.42×10^{-5} mol FeS/g sand, the same as the amount obtained in the batch experiments. Thus, the total amount of FeS contained in a column was calculated to be 6.75 mmol (539 mg) FeS for a 15-cm column packed with approximately 475 g sand. An influent concentration of 1 ppm As(III) was prepared with deionized and de-aerated Milli-Q water to simulate groundwater under reducing conditions and buffered at pH 5, 7 and 9. The system was buffered using the same buffer species at each different pH conditions such as 0.1M acetate buffer at pH 5, 0.1M MOPs for pH 7 and 0.1M CHEs for pH 9. The columns were conditioned with buffer solution in the absence of As(III) first until the iron concentration of the effluent stabilized. At that point, an aqueous solution containing 1 ppm As(III) was then injected at the same pore water velocity of the conditioning fluid. The solutions were pumped in an up-flow mode through the column at a constant flow rate with an HPLC pump (Varian Dynamax SD-200, Walnut Creek, CA). Then, effluent from the column was collected with an automated fraction collector (ISCO ISIS autosampler, Lincoln, NB), with about 1/10 of pore volume collected in each sampling tube. The injection of As(III) was terminated when the effluent As(III) concentration reached a plateau. Upon reaching the plateau, an As(III)-free buffer solution was pumped into the column until the effluent As(III) concentration approached 0 ppm. The collected effluent samples were taken out of the anaerobic chamber after acidification with nitric acid and then analyzed for their As(III) and Fe(II) concentration as total concentrations of As and Fe using an ICP-MS. A bromide tracer was injected

along with As(III) and the bromide concentration was measured for the first 2-3 pore volumes of effluent using an ion chromatograph (Dionex IonPac AS4A column, Perkin-Elmer 200 series LC pump, Perkin-Elmer 200 series autosampler).

The physical parameters of column porous media such as pore water velocity and dispersion coefficient were inversely obtained using the CXTFIT program (Toride et al., 1995) using a form of the advection-dispersion equation assuming that bromide acts conservatively. The dispersivity (α) was then calculated using a relationship of $D=v\,\alpha$. A retention time (R_T) of a column was calculated using the measured length of column (L) and applied flow rate (Q) using the relationship of $R_T=L\cdot A/Q$, where, A is a cross-sectional area of the column.

Table 7.1 Column experimental conditions

	pH	Column Length	Pore water velocity*	Dispersivity*	Porosity	Retention time	Bulk density
Col #	-	cm	cm/hr	cm	-	hr	g/cm^3
1	pH 5	15	4.42	0.09	0.35	3.37	1.70
2	pH 7	15	4.55	0.06	0.34	3.27	1.73
3	pH 9	15	4.55	0.08	0.34	3.31	1.72
4	pH 5	4.8	4.11	0.08	0.35	1.16	1.67
5	pH 9	4.8	4.55	0.08	0.35	1.16	1.67
6	pH 9	4.8	1.39	0.14	0.35	3.44	1.67
7	pH 5	15	varied	0.07	0.34	varied	1.75

* Values were obtained using CXTFIT fitting results of bromide breakthrough curves.

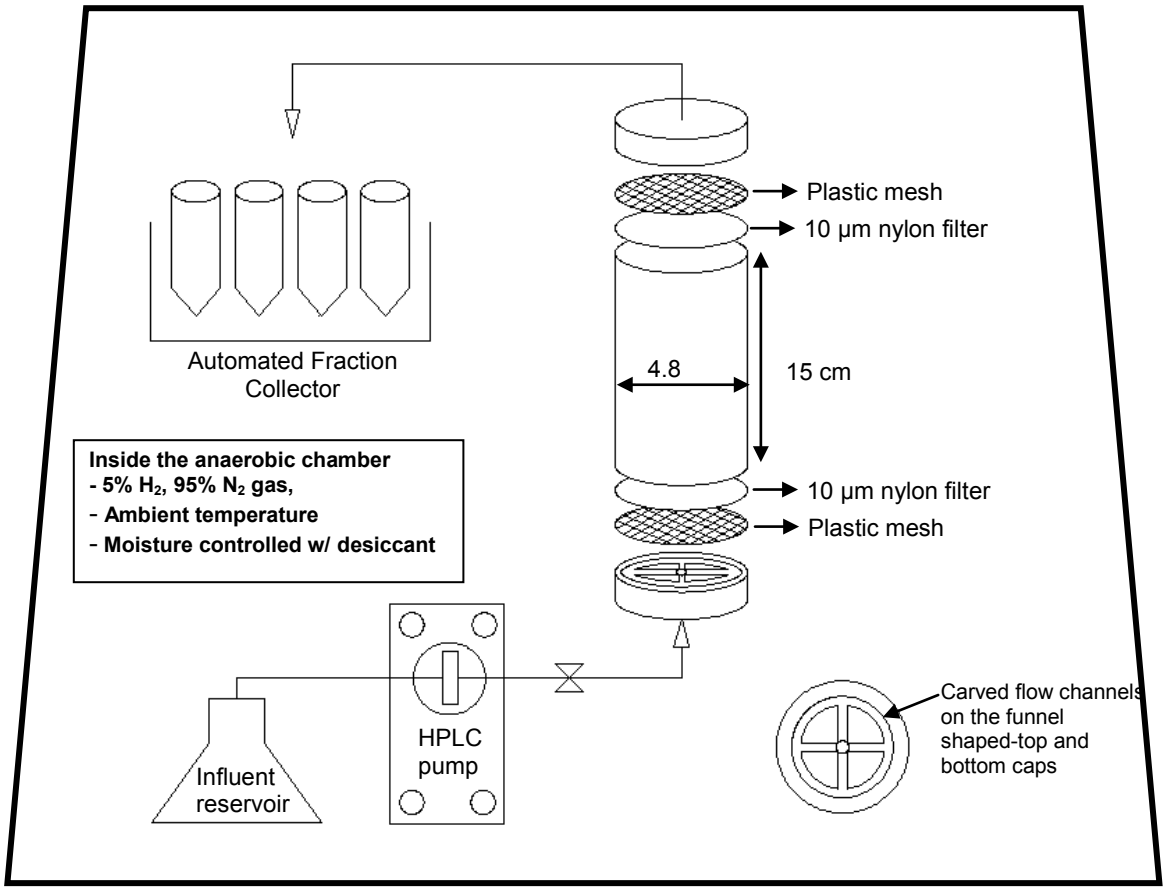

Figure 7.1 Schematic diagram of column system.

7.2.2 SSR-dependent As(III) sorption of FeS-coated sand

Solid-solution ratio (SSR)-dependent sorption isotherm tests were performed using a similar method to the sorption isotherm tests described in Chapter 5. The test tubes with 1g, 2g, and 5g of FeS-coated sand and 10 ml of buffer solutions were spiked with As(III) stock solution to achieve a concentration range of 1.3×10^{-6} M to 6.7×10^{-4} M initial As(III) concentrations for pH 5 buffered with 0.1N acetic acid, and 1.3×10^{-6} M to 2.6×10^{-4} M for pH 7 and 9 buffered with 0.1N MOPs and CHEs solution. The achieved SSRs were 100g, 200g and 500g FeS-coated sand/L solution. The reaction tubes were then mixed on an end-over-end rotator for two days. After two days, the supernatant in tubes was filtered through a 0.1 µm nylon filter, diluted, acidified with HNO_3 and then analyzed for arsenic by ICP-MS.

7.3 Results and discussion

7.3.1 As(III) transport in FeS-coated sand

Figure 7.2 shows the bromide BTCs of all the column experiments performed in this dissertation. The shapes of the BTC curves are similar among Col #1, 2, 3, and 7 which have a column length of 15 cm and among Col # 4, 5, and 6 which have a column length of 4.8 cm. Figures 7.3 – 7.5 show the breakthrough curves of FeS-coated sand columns with a retention time of about 3.3 hours at pH 5, 7, and 9 (Columns #1-#3, Table 7.2). The column that shows the highest As(III) removal is the one at pH=5, with an observed breakthrough point occurring at 213 pore volumes. The As(III) removal occurring up to the breakthrough point was 100%, so that the effluent concentration was below detection up to this point. After breakthrough, the As(III) effluent concentration increased gradually until it reached 0.2 ppm (i.e., 20% of the initial injected As(III)) and showed a more gradual increase up to 0.4 ppm over the next 85 pore volumes. This continuous high removal of As(III) at a pH 5 solution is hypothesized to be due to the continuous dissolution of FeS, providing sulfide ions for the formation of the arsenic sulfide (As_2S_3). The dissolved Fe concentration, measured as an indicator of dissolved sulfide, showed that the concentration of continuously dissolved sulfide is 0.03 mM, considerably greater than the injected concentration of 0.013 mM of As(III). This measured dissolved sulfide concentration stoichiometrically exceeds the needed sulfide concentration, but thermodynamic calculations performed by Li (2009) concluded that this amount is not enough to precipitate orpiment. Therefore, to identify whether the As(III) removal process is caused by precipitation or adsorption, further spectroscopic research using samples collected after column work should be conducted.

The long column experiment performed at pH 7 (Col #2) (Figure 7.4) resulted in the complete removal of As(III) over 10 pore volumes (effluent concentration was < 0.01 ppm). In the pH 9 long column (Col #3) (Figure 7.6), the effluent concentration of As(III) was below the detection level of 1 ppb until 2 pore volumes. Over the subsequent 4 pore volumes, more than 98% of initially injected As(III) (under 0.02 ppm As(III)) was removed until the breakthrough point which occurred at 6.4 pore volumes. At pH 5, a

considerable amount of Fe dissolved and was eluted from the column due to the high solubility of FeS at this low pH. However, the dissolved Fe concentration became stable was observed during the column tests. This was confirmed by the measured amount of FeS left in each column (Col #1, 2, and 3) after finishing the column experiments. The results of acid extraction (Figure 7.6) showed that FeS-coated sand still contain ed 90-100% of FeS on its surface after running 100 and 80 pore volumes through pH 7 and 9 columns, respectively. In contrast, at pH 5, around 60% of FeS was dissolved and eluted from the column during the injection of ~300 pore volumes in Col #1. However, this loss of FeS results in sufficient sulfide concentration to remove arsenic through arsenic sulfide precipitation, if the mole quantify of sulfide can be assumed to be equivalent to the measured Fe concentration. Based on a mass balance calculation and using the equilibrium concentration of the dissolved Fe at pH 5 (3.5×10^{-5} M Fe), the pH 5 long column can provide another 1700 more pore volumes of a similar concentration of sulfide ion assuming stoichiometric dissolution of FeS.

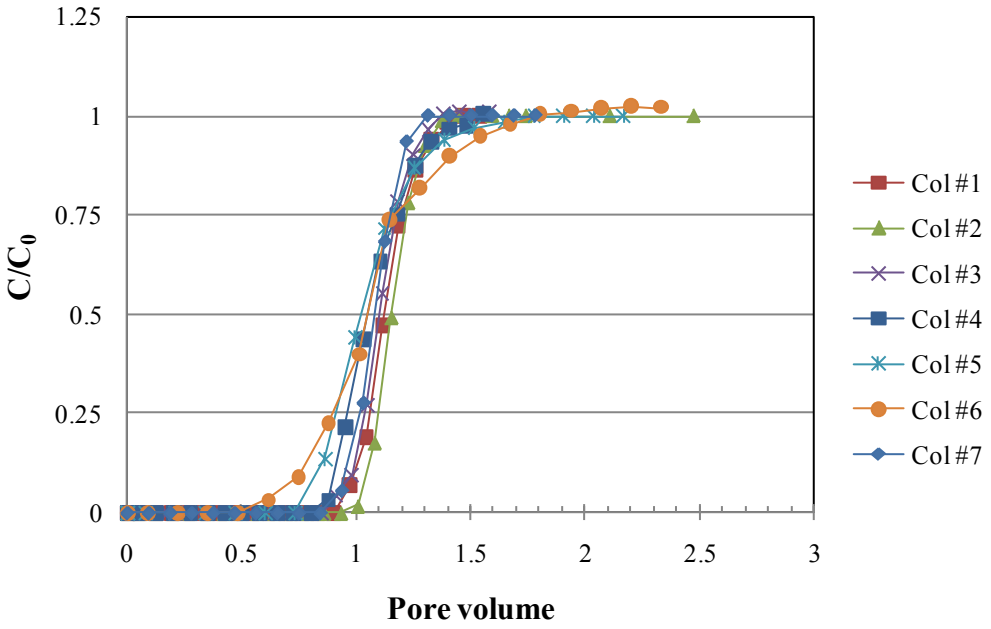

Figure 7.2 Bromide BTCs of Col #1 to Col #7. Col #1, 2, 3, and 7 and Col # 4, 5, and 6 show the different shapes of BTC which represents the different values of dispersivities in 15 cm and 4.8 cm column lengths, respectively.

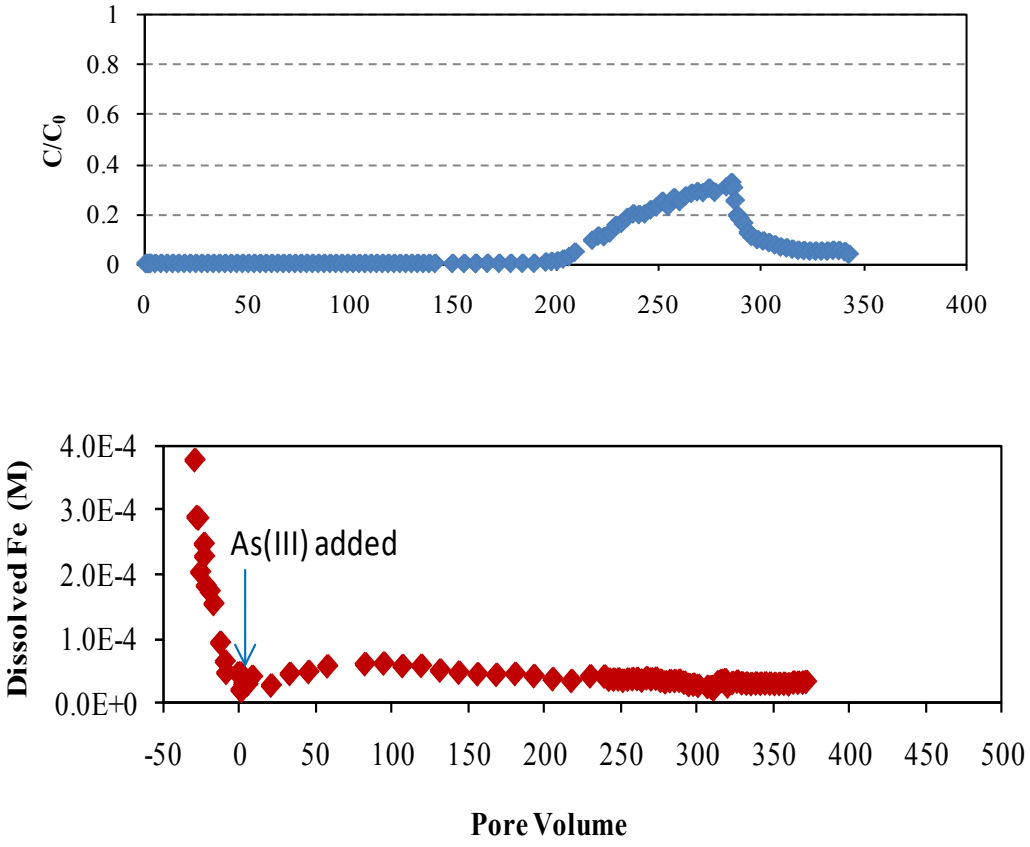

Figure 7.3 Column breakthrough curve at pH 5 (top) of FeS-coated sand column (Col #1) and concentration of dissolved Fe measured in effluent (bottom). (Influent: 0.1 M buffered solution with 0.013 mM (1 ppm) As(III) and 10 mM bromide with an average pore water velocity of 4.42 cm/hr).

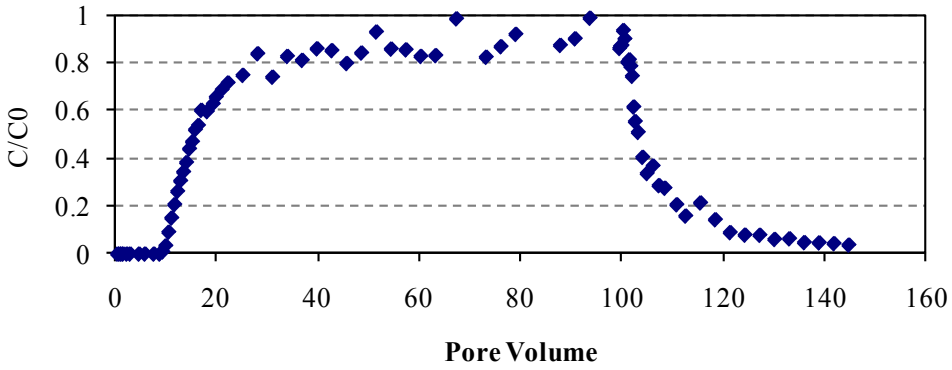

Figure 7.4 Column breakthrough curve at pH 7 of FeS-coated sand column (Col #2). (Influent: 0.1 M buffered solution with 0.013 mM (1 ppm) As(III) and 10 mM bromide with an average pore water velocity of 4.55 cm/hr).

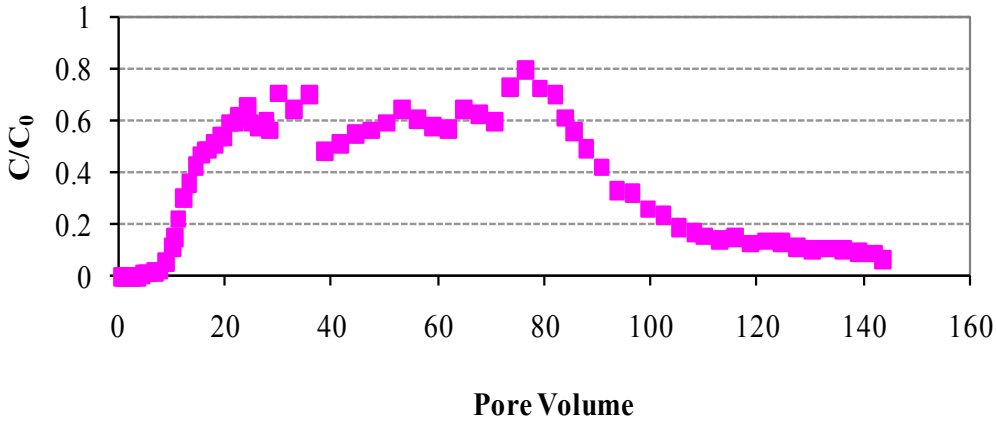

Figure 7.5 Column breakthrough curve at pH 9 of FeS-coated sand column (Col #3). (Influent: 0.1 M buffered solution with 0.013 mM (1 ppm) As(III) and 10 mM bromide with an average pore water velocity of 4.55 cm/hr).

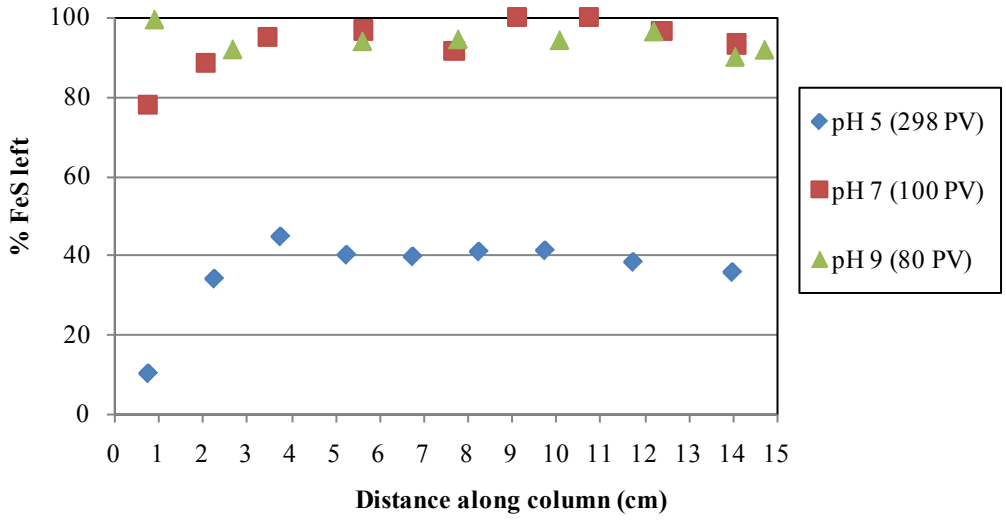

Figure 7.6 Results of acid-extraction of FeS-coated sand from Col #1 (pH 5), Col #2 (pH 7), and Col #3 (pH 9).

7.3.2 Comparison of column and batch results using capacity calculations

Table 7.2 summarizes the total immobilized As(III) per unit mass of FeS-coated sand in the batch reactor experiments based on the sorption isotherm analysis (column e, in Table 7.2) (See Section 5.3.1 for the sorption isotherm results), in the column reactor the amount up to the point of breakthrough (a), the total amount of As(III) uptake (b), and the total retained amount (c) by subtracting the amount desorbed (d) from the total. It shows that if the removals up to breakthrough are only considered, Cols #1- #3 removed 82.2%, 13.9% and 8.9% at pH 5, 7, and 9, respectively. However, if the total amount of As(III) retained at pH 5 in the long column with a retention time of 3.3 hour (Table 7.2, Column #1) after breakthrough is considered, the As(III) removal capacity of the column is greater than that obtained in the batch. In fact, the maximum capacity would be expected to be greater than the reported 105.6% since further arsenic removal would be expected as the concentration of iron (Figure 7.3), indicative of the presence of sulfide, does not show signs of declining even at 350 pore volumes. However, the maximum computed capacities of the long columns at the higher values of pH, at pH 7 and pH 9, appear to be considerably less than their respective batch capacities. Yet this comparison

may not be valid as the As concentrations in the batch systems were considerably greater (20 ppm) than those in the column systems (1 ppm).

From the desorption part of each breakthrough curve, the relative potential for the remobilization of removed As(III) from FeS-coated sand columns may be evaluated. At pH 5, only 1.8% (Col #1) of the removed As(III) was eluted, indicating very effective retention of As(III) at this pH. In contrast, at pH 7 and pH 9, much higher amounts of As(III) were eluted during the desorption step, 34.6% (Col #2) and 61.3% (Col #3), respectively. At pH 9, the desorption curve was much less steep than that at pH 7. The pH 9 column curve also showed a longer tailing feature. The differences in the desorption behavior at the various values of pH suggest the possibility of differences in the removal mechanisms. The formation of orpiment (see Chapter 6) is thought to be the primary removal mechanism at pH 5 and to a lesser extent at pH 7, resulting in more irreversible removal. The higher extent of desorption at pH 9 is thought to be caused by the slow reversibility of the adsorption.

The different desorption behavior at the various values of pH suggests a different removal mechanism under each pH condition. This incomplete reversibility at low pH is evidence that the removal mechanism responsible is likely associated with the formation of arsenic sulfide. In contrast, complete reversibility has often been assumed as evidence of a surface complexation reaction (Bostick et al., 2003) rather than precipitation. The removal reaction occurring at high pH is therefore expected to be primarily reversible adsorption. This is consistent with the formation of orpiment as the primary removal mechanism at pH 5 and to a lesser extent at pH 7, resulting in more irreversible removal.

Table 7.2 Comparison of As(III) removal capacity between column and batch reactor results

	Calculated result of As(III) removal (unit: µg As(III)/g FeS-coated sand)				Estimated parameters using Langmuir isotherm model				Using MOM
Index	a	b	c	d	e	f	g	h	i
	*BT capacity (BT point, % batch result)	Total removed (Injected PV)	Maximum capacity (% batch)	Percent desorption	q_m (g As/g sand)	K_l (L/g As)	R^2	R_B at C_{eq}=1ppm	R_C with MOM C_{eq}=1ppm (± error)
Col #1 (pH 5)	43.3 (215 PV, 82.2 %)	56.6 (298 PV)	55.6 (105.6%)	1.8	5.20×10^{-5}	1388.15	0.99	61.3	>300 (> +389%)
Col #4 (pH 5)	12.1 (60 PV, 23.2%)	17.4 (422PV)	14.3 (27.5%)	17.9					52.2 (-15%)
Col #7 (pH 5)	22.6 (112 PV, 43.4%)	62.4 (410 PV)	60.7 (116.8%)	2.6					>400 (> +552%)
Col #2 (pH 7)	1.9 (10 PV, 13.9 %)	5.6 (100 PV)	3.8 (27.7 %)	34.6	1.34×10^{-5}	781.74	0.95	16.7	14.1 (-16%)
Col #3 (pH 9)	1.3 (6.4 PV, 8.9 %)	7.4 (80PV)	2.8 (20.1%)	61.3	1.58×10^{-5}	1076.13	0.96	19.7	24.9 (+26%)
Col #5 (pH 9)	1.7 (7.4 PV, 10.5 %)	4.8 (62PV)	2.7 (16.8%)	56.7					13.8 (-30%)
Col #6 (pH 9)	4.7 (18.5 PV, 29.5%)	15.1 (83 PV)	11.9 (75.4 %)	21.1					23.6 (+20%)

- BT capacity = As(III) removal capacity of packed column until the effluent As(III) concentration meets the regulated As(III) concentration for drinking water (10 ppb)
- % batch result = mass of As(III) removed in column as percent of that removed in batch.
- PV = pore volume.
- Total removed (b) = total adsorption – total desorption.
- Maximum capacity (c) = mass removed in batch system at the given pH.
- Percent desorption (d) = mass of total As(III) removed that elutes upon injection with As(III)-free solution expressed as percent of total mass removed.
- R_B (h) = retardation factor defined by batch experiments (Eqn (2-20)).
- R_C (i) = retardation factor obtained from column experiments (Eqns (2-21)-(2-23)).
- q_m and K_l were defined in Eqn (2-8).

7.3.3 Comparison of column and batch results using retardation factors

A comparison of column and batch capacity data using the simple approach taken in the previous section may not be valid since the As(III) concentration in the batch and column experiments differ considerably, with the initial concentration in the batch equal to 20 ppm (50 ppm at pH 5) and the influent concentration in the column equal to 1 ppm. Alternatively, retardation factors may be calculated. In Table 7.2, the batch obtained-retardation coefficients, R_B (calculated from Eqn (2-20)), and column-obtained retardation coefficients, R_C (calculated using Eqns (2-21)-(2-23)), are listed. The values of R_B and R_C are more similar at pH 7 and pH 9, when adsorption dominates the As(III) removal process. Since the sorption behavior of As(III) on FeS-coated sand shows a high degree of non-linearity as evidenced by the Langmuir-shaped sorption isotherms, the retardation factors should vary with the different equilibrium As(III) concentrations. In the same manner, the column retardation factor should vary with different concentrations of injected As(III). Thus, the retardation factors were recalculated using Eqn (2-20), for various equilibrium As(III) concentrations and are shown in Figure 7.7. The retardation factor approaches R=1 as the As(III) concentration increases, while the retardation factor increases abruptly when the equilibrium As(III) concentration decreases. Based on Eqn (2-20), R_B at an aqueous As(III) concentration equal to 1 ppm was estimated to be 61.3, 16.7 and 19.7 at pH 5, 7, and 9, respectively. In contrast, the values of R_C calculated using the method of moments (MOMs) (Eqn (2-23)), are 14.9 (88% of R_B) and 24.9 (126% of R_B) at pH 7 and pH 9, respectively for the long columns at a retention time of 3.3 hr. At pH 5, the MOM cannot truly be applied to Col #1 since the effluent concentration never reaches a value greater than $0.5C_0$, due to the continuous removal of As(III) by precipitation. However, the data presented suggest that the value of R_C for this column would be greater than 300, or greater than 400% of the value of R_B. Therefore, it can be concluded that the FeS-coated sand shows reasonable performance for PRB application based on the coating stability shown in Figure 7.6 and performance under all range of pH conditions considered in this study.

7.3.4 Speculation about discrepancies between batch and column results

Two different approaches were utilized to compare As(III) removal results obtained in the batch and column reactors. The first approach used a capacity calculation based on removed amounts of As(III). If the total amounts removed are compared, greater removals occurred in the column reactor at pH = 5 where the precipitation of arsenic sulfide predominates as the As(III) removal mechanism, and lesser removals at pH 7 and pH 9, where adsorption dominates. However, the results from MOM suggested far greater removals in the column at pH 5, slightly more at pH 9, and slightly less at pH 7.

These differences may be attributable to three factors: (1) the difference in the mechanism of uptake, (2) the difference in the solid solution ratio (SSR) effect at pH 5 versus pH 9, and (3) the kinetics of removal. At pH 5, As(III) remov al occurs through the precipitation of arsenic sulfide solids (e.g., orpiment, As_2S_3). Since the flowing column system leads to a greater mass of sulfide being available for the formation of precipitates, the removals are greater in the column. At pH 7 and 9, uptake occurs mostly via a surface-limited sorption reaction (Gallegos et al., 2007). Therefore, the distribution of As(III) between the solid and solution phases is more important; if the uptake in the batch and columns systems is evaluated at similar concentrations (e.g., As(III) = 1 ppm), the uptake is comparable, as shown from the calculation based on the approach using retardation factors.

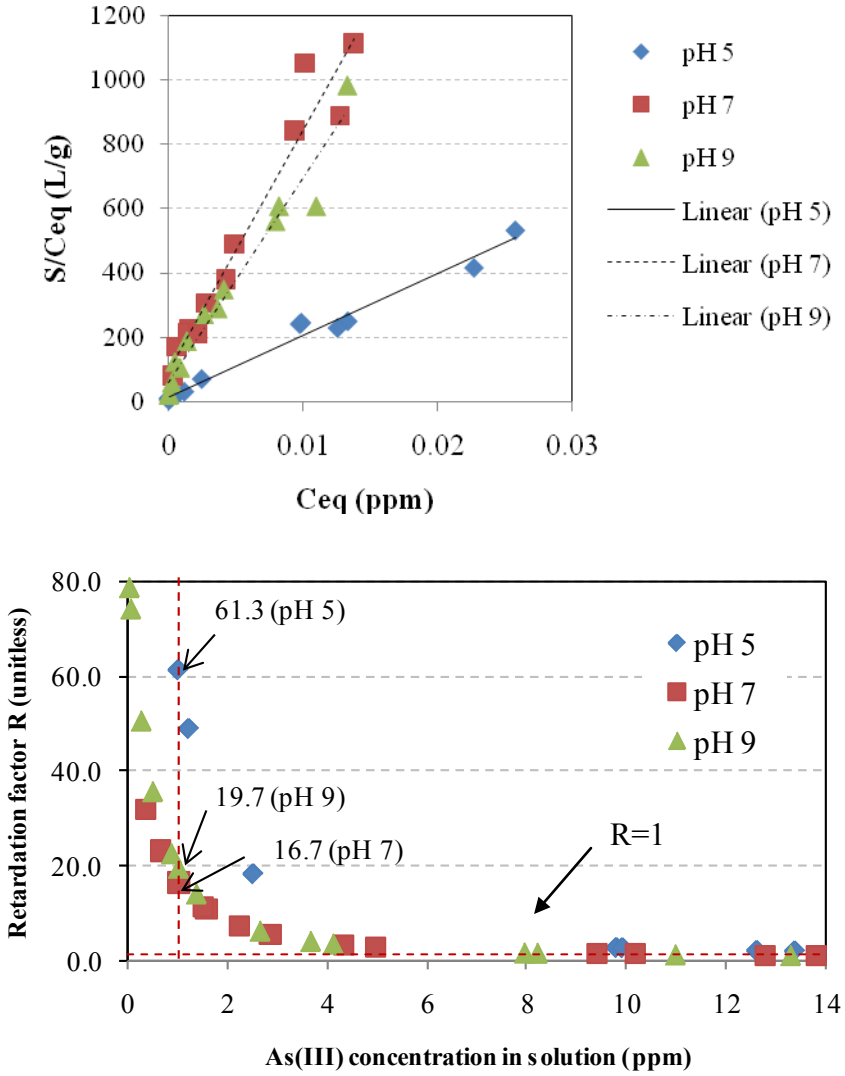

Figure 7.7 Linearized Langmuir sorption isotherm results at pH 5, 7, and 9 (top) and estimated retardation factors (bottom) with varying equilibrium arsenic concentration in solution at pH 5, 7, and 9. The vertical dotted line marks the As(III) concentration=1ppm and the horizontal dotted line shows that R approaches 1 as the As(III) concentration increases.

7.3.4.1 Solid-solution ratio (SSR) effect and redox change

The data presented in Figure 7.8 suggest the impact of the solid solution ratio (SSR) defined as mass of solid (g) to volume of solution (L). At pH 5 (Figure 7.8 a), a lower SSR results in less uptake, perhaps due to a reduction in the concentration of dissolved sulfide and an enhancement in the oxidation of FeS, resulting in the inhibition of precipitation. This is opposite to the commonly reported influence of SSR as contaminant sorption generally shows a decrease with increasing SSR (Bajracharya et al., 1996; Porro et al., 2000; Phillippi et al., 2007). The concentration of dissolved Fe (Figure 7.9 left), indicative of the concentration of dissolved sulfide ion, increases with SSR and may be the main cause of greater removals of As(III) at higher SSRs. In addition, at pH 5, the oxidation state of the FeS-coated sand suspension varies with SSR. The right side of Figure 7.8 displays measured pe values with varying SSR in FeS-coated sand suspensions. The trend of decreasing pe with increasing SSR is consistent with what was observed in the pure FeS system (Gallegos, 2007). The exact nature of the relationship between pe and As(III) uptake is unclear, but it can be speculated that a reduced condition may be more conducive to the removal of As(III) from systems where iron sulfide actively plays a role. Under highly oxidizing conditions, the FeS may be oxidized to a less soluble form of iron sulfide or iron oxide and consequently, the free sulfide ion would be present at a lower concentration. Therefore, a lower arsenic removal with a lower SSR could result partly from a more oxidized condition.

The opposite trend of SSR effect was observed at pH 9 compared to that observed at pH 5; however, the trend observed at pH 9 is the more commonly reported effect. The literature suggests that solute sorption generally decreases with SSR (Bajracharya et al., 1996; Porro et al., 2000; Phillippi et al., 2007). The reason why a higher SSR results in the inhibition of the adsorption process is not clear, but several possible explanations have been posited. At low SSRs, the amount of solute is abundant compared to the limited number of surface sites so most of the sorption sites would be utilized, regardless of favorability, while at high SSRs, the degree of sorption is far below full saturation so only the most favorable sites would be utilized (Hemming et al., 1997). The degree of favorability may be due to competitive adsorption. For example, in the study presented by Grolimund et al. (1995), prewashing the solids eliminated the SSR effect suggesting

that pre-adsorbed ions may have caused the SSR effect. In the pH 9 system here, aqueous arsenite or thioarsenite species may be present along with silicate dissolved from the natural silica sand. Moreover, the solid surface of FeS-coated sand may present a variety of sorption sites, due to the existence of FeS, oxidized magnetite or greigite of the coating and the iron oxide surface of the uncoated natural sand (Figure 4.5).

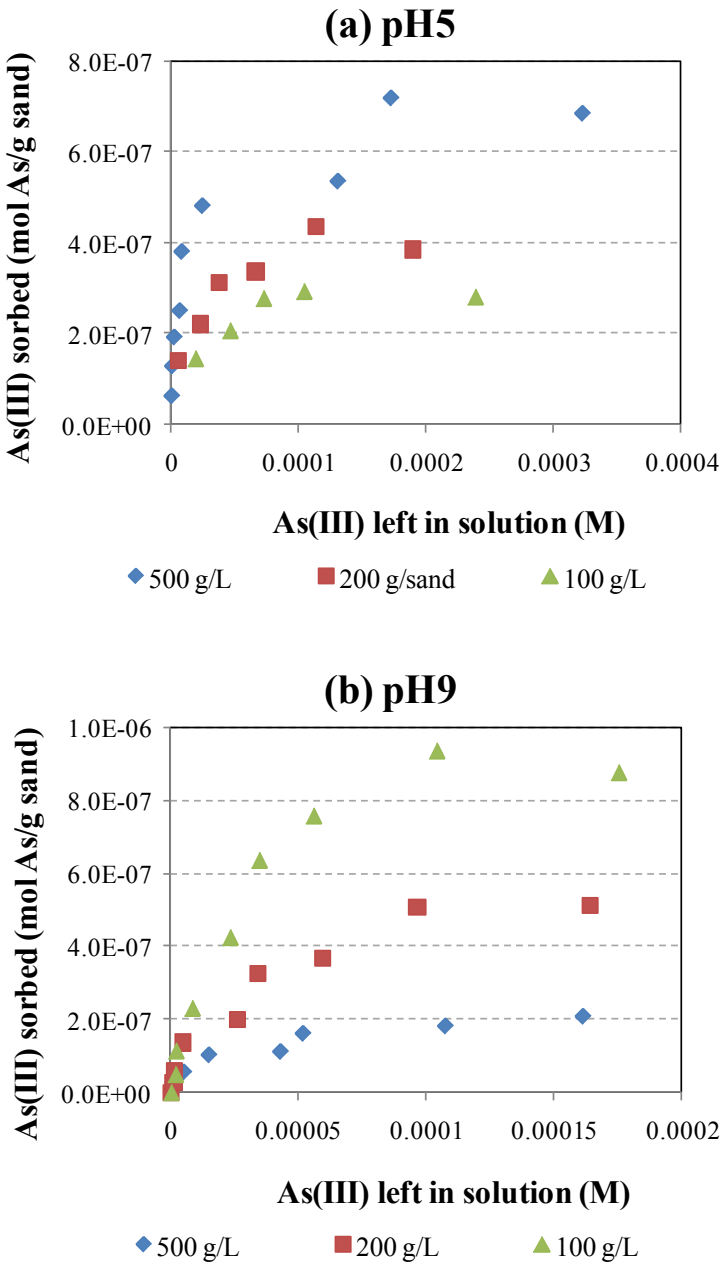

Figure 7.8 Sorption isotherms of As(III) as a function of solid/solution ratio of FeS-coated sand suspension at (a) pH 5 and (b) pH 9. The effect of SSR is more evident at pH 9.

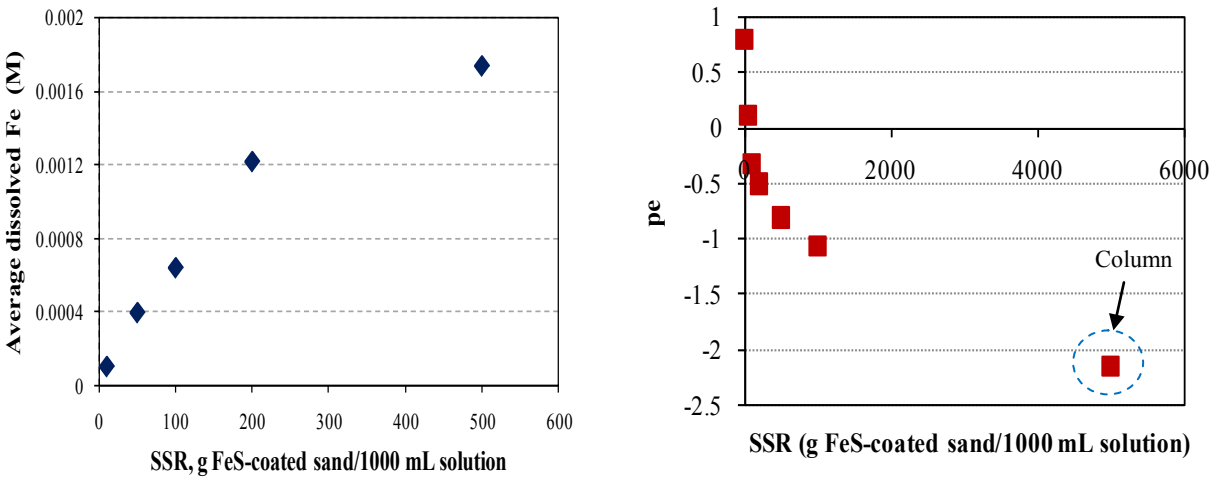

Figure 7.9 SSR-dependent Fe dissolution concentration (left) and the measured pe (right) in the pH 5 FeS-coated sand batch system. The x-axis number means the g mass of sand per 1000 mL solution. The marked point in the right plot shows the equilibrium pe value measured in a column experiment (Col #4) using a closed effluent chamber that was attached next to the column exit.

7.3.4.2 Kinetic effects (retention time-dependent BTC behavior)

Often kinetic limitations play a role in the determination of the shape of column breakthrough curves (Darland and Inskeep, 1997; Limousin et al., 2007). To examine the role of kinetics in these complex systems with different mechanisms of removal and opposite impacts of SSR, additional column experiments were carried with different retention times. This was achieved by varying the column length (Col #1 and Col #4 for pH 5, and Col #3 and Col #5 for pH 9) and by varying the flow rate (Col #5 and Col #6 for pH 9) (Table 7.2). Col #7 examined the effect of flow rates in a single column with flow rate changes.

The results are presented in Figures 7.10 and 7.11. At pH 5, the relative effluent concentration eventually reaches 1.0 in the shorter column at about 150 pore volumes, whereas when the retention time is three times, as long in the longer column, the relative effluent concentration does not reach even 0.4 after over 250 pore volumes. At pH 5, the removal of As(III) is dominated by precipitation of arsenic sulfide (Gallegos et al., 2007; also see Chapter 6). Thus, the comparative lack of removal at a shorter retention time may be due to the kinetics of the formation and deposition of the precipitate. A similar phenomenon was reported in a study investigating the deposition of goethite colloids in a column in that eventual breakthrough occurred at longer time scales as the flow velocity decreased (Jia et al., 2007). Furthermore, in a study of zerovalent iron nano-particle deposition, He et al. (2009) found that particle deposition efficiency was proportionally related to the travel distance or travel time of the particles through the porous media, resulting in the achievement of different relative concentration plateaus at different flow rates. Therefore, the different shapes of the breakthrough curve with different column lengths may be interpreted as a kinetic effect of particle-deposition due to a shorter travel time of the precipitated arsenic sulfide particles.

However, the shape of breakthrough curve of Col # 4 (short column at pH 5) is much likely to be a typical shape of a breakthrough curve which is controlled by an adsorption mechanism. Therefore, the possibility of a different removal mechanism operating in the shorter column from in the longer column cannot be ruled out. The shorter column provides only one third of contact time between FeS and the As(III)-containing influent, so that a less reduced condition may be achieved in the shorter

column. Consequently much higher oxidation condition may have accelerated the change of the mineral phase in the FeS-coated sand column to a less soluble and more oxidized condition. As a result, the As(III) removal mechanism might be mainly controlled by much more insoluble mineral phases such as greigite or Fe-oxides. This hypothesis is consistent with the 1-D transport modeling results using a equilibrium-kinetic two-site model combined with surface complexation models (SCMs) by Li (2009). The Col #4 breakthrough curve was successfully reproduced by the model without considering the precipitation of arsenic sulfide; instead, the rate-limited adsorption of As(III) on the FeS and Fe_3O_4 (magnetite) surface was used to describe the macroscopic behavior of the breakthrough curve. Even though the batch study results with high FeS and high As(III) concentration showed clear evidences of As(III)-removal mechanisms at pH 5 and pH 9 systems, no analytical or spectroscopic evidence could be collected in the column system due to the low As(III) concentration, so that the mechanism of As(III) removal in column system still remains as an open question. Further modeling and experiments need to be conducted to draw a more accurate picture of mechanisms how As(III) removal may change under different experimental conditions of pH, As(III) loading, or flow rate.

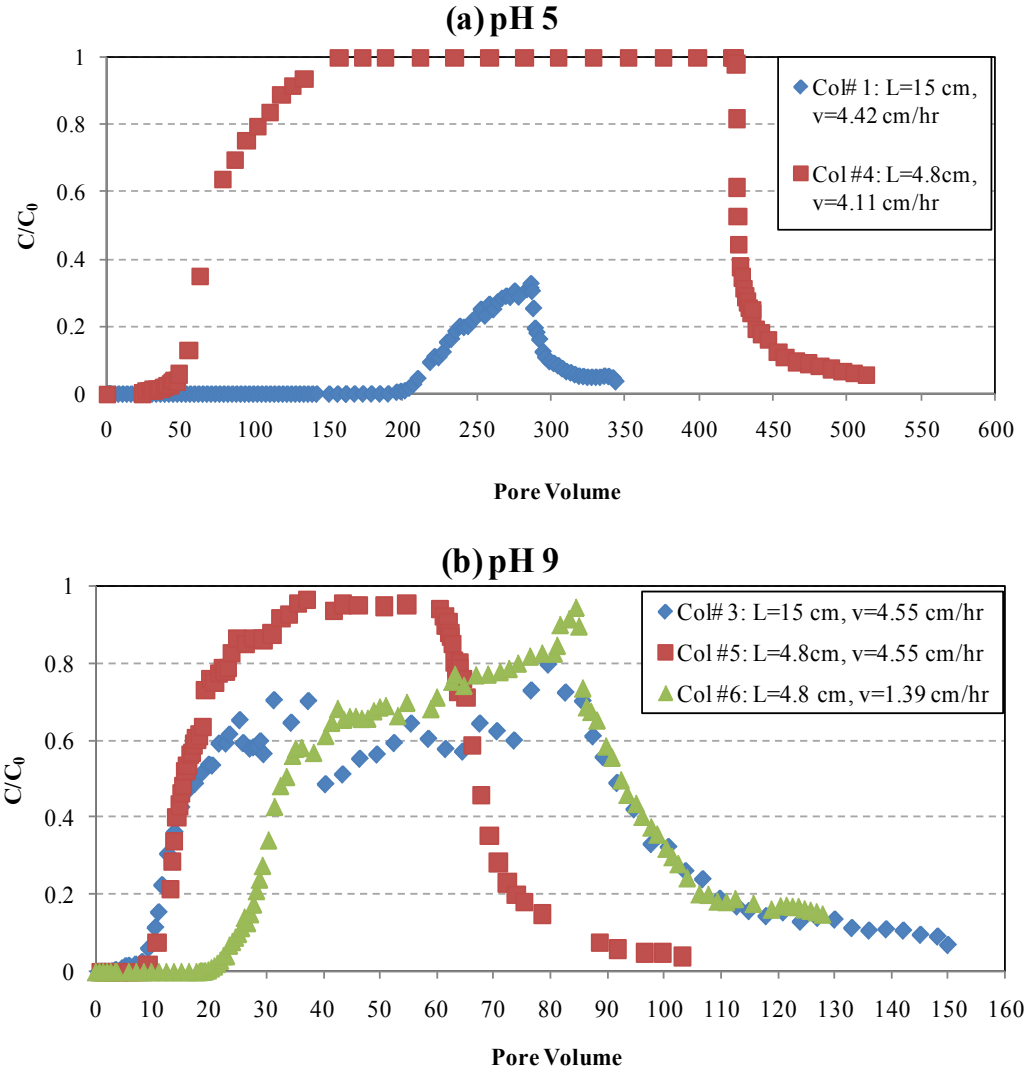

Figure 7.10 As(III) breakthrough curves with different column experimental conditions for (a) pH 5 and (b) pH 9 column influent containing 1.3×10^{-5} M (1 ppm) As(III). The solute retention (travel) time for each column is 3.37 hr (Col #1), 1.16 hr (Col #4), 3.31 hr (Col #3), 1.16 hr (Col #5) and 3.44 hr (Col #6).

At pH 9, the short column with the higher velocity (retention time = 1.16 hr) (Col #5) broke through with the fewest pore volumes of throughput and plateau at a relative concentration of 1.0. The longer column at the same velocity (Col #3), but with a longer retention time (retention time = 3.31 hr), showed initial breakthrough occurring at the same number of pore volumes as in the shorter column with the same flow rate (Col #5). However the effluent concentration plateaued at a relative concentration of about 0.7 in the longer column, followed by a subsequent increase approaching 1.0. The difference in behavior based on residence time suggests a rate-limited process in the shorter column. The short column with the slower velocity (Col #6), with a similar retention time (retention time = 3.44 hr) to the longer column (Col #3), showed a later breakthrough, but similar behavior in that the relative concentration reached an initial plateau of about 0.6, followed by an increase over another 50 pore volumes or so. The columns with the longer retention times seem to show evidence for perhaps irreversible sorption, and/or multiple types of adsorption sites. Kim et al. (2006) showed that, by incorporating irreversible sorption into the advection-dispersion equation, plateaus at relative concentrations of less than 1.0 could be simulated. In addition, simulations with two-site models showed rising relative concentrations, following an initial plateau. Certainly, the desorption results suggest some irreversible desorption. Furthermore, the spectroscopic assessment of the FeS-coated sand surface suggests the existence of a variety of sorption sites, including FeS, the oxidized magnetite or greigite of the coating and the iron oxide uncoated surface of the natural sand as described in the surface characterization of the FeS-coated sand in Chapter 4.

Figure 7.11 provides further evidence of kinetic impacts on the As(III) uptake by FeS-coated sand. Col #7 (pH 5) was run at three different flow rate starting from 1.4 cm/hr and increasing to 4.2 and then to 8.4 cm/hr. The results displays three different C/C_0 plateaus, at C/C_0=0, 0.2 (if considering the equilibrated part), and 0.4. These results suggest that the arsenic removal by FeS-coated sand is kinetically controlled. The Fe concentration remained steady despite flow increases and an interruption of the experiment (due to loss of power). Having plateaus in the effluent concentration as a function of flow rate suggests that the kinetically-controlling process is not the

dissolution of FeS but the precipitation of arsenic sulfide or the deposition of precipitated particles. Even though this explanation is postulated for the column results, more research is needed to confirm this as the basis for the observed As(III)-transport characteristics of the FeS-coated column at pH 5.

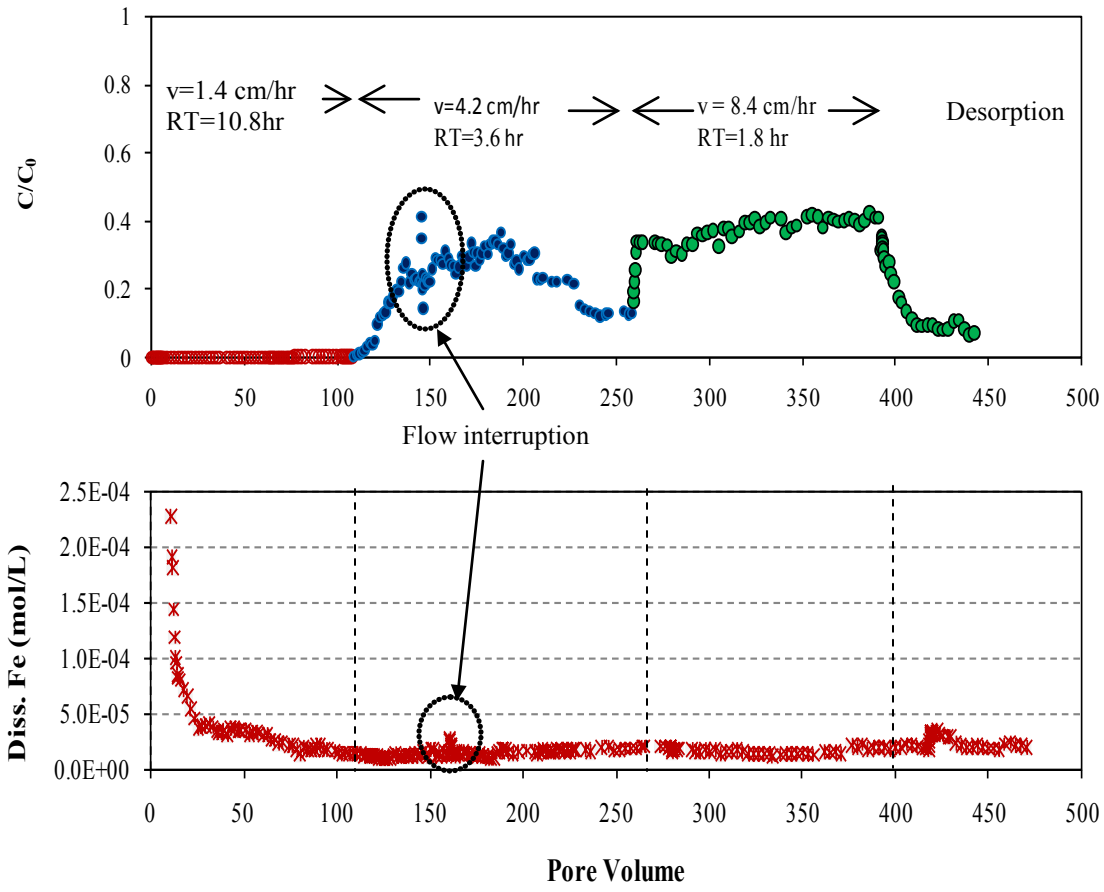

Figure 7.11 Column breakthrough curve at pH 5 (top) of FeS-coated sand column and concentration of dissolved Fe measured in effluent (bottom) with varying flow rate. (Influent: 0.1 M buffered solution with 0.013 mM (1 ppm) As(III) and 10 mM bromide with an varying pore water velocity from 1.4 to 8.4 cm/hr). The conditioning period is included in the lower graph. Thus the PV in the bottom graph includes 10 PV during which there was no As(III) in the influent. Thus PV in the top graph = PV in the bottom graph – 10.

7.3.5 Comparison with a reactive transport model

Li (2009) conducted 1-D reactive transport modeling of the As(III) uptake in the FeS-coated sand columns using the experimental transport module in PHREEQC (Parkhurst and Appelo, 1999). Of the 7 columns, Col #4 (pH 5) and #5 (pH 9) was used in 1-D reactive transport modeling. The applied model, which could successfully reproduced the breakthrough curves of two column results, combined the features of empirical two-site models commonly used in soil science and the SCMs that explicitly calculate surface speciation based on solution chemistry and surface characteristics. For modeling of the column at pH 9, the surface complexation of neutrally charged As(III) species($\equiv$S-H-H_3AsO_3) to two groups of surface sites, equal in number, was predicted similar to the suggested adsorption mechanism of arsenite in this study. Under low pH conditions, the As(III) breakthrough could still be explained by the same model with a larger rate coefficient of arsenic surface complexation on the mackinawite surface. The predicted major As(III) removal mechanism at pH 5 is different from what is suggested by the batch study results in Chapter 6 of this dissertation. Based on Li's model predictions, the concentration of HS^- released to the aqueous phase due to the slow dissolution of FeS was not high enough to form orpiment. This may be a good representation of As(III) uptake mechanism in the short column at pH 5 (Col #4), which may have a higher oxidation state and a shorter contact time with the FeS surface than in the longer column. These differences might influence the makeup of the mineral phases of iron sulfide and, if the coated iron sulfide becomes more oxidized, the dissolution of iron sulfide followed by the precipitation of arsenic sulfide may be kinetically controlled, with the net result that the adsorption process plays a main role in As(III) removal.

Alternatively, Col #4 breakthrough curve can be also interpreted assuming that particle deposition is kinetically controlled as it described in the previous section. Additional column tests, with more constrained experimental conditions, would be needed to determine which alternative explanation has more merit.

7.4 Summary and conclusions

FeS-coated sand packed columns were tested to evaluate the As(III) removal capacity under anaerobic conditions at pH 5, 7 and 9. A mechanistic understanding of

the different removal processes at different pH conditions is important to the interpretation of the column experiment results. At pH 5, where the precipitation of arsenic sulfide plays the major role in the removal of arsenic, the column shows greater removal efficiency than the batch system due to the continuous dissolution of sulfide and precipitation of arsenic sulfide. This greater removal is evident whether the comparison calculations are performed using capacity calculations or the method of moments (MOM). At pH 9, where adsorption mainly governs the arsenic removal, with a minor contribution of arsenic sulfide precipitation, capacity calculations suggest that greater removals are achieved in the batch systems than in the column systems. However, this comparison does not account for the observed nonlinearity in the sorption behavior. If sorption nonlinearity is accounted for, as in the MOM, removals are comparable in the column system. Column experiments with lower retention times, achieved either by increasing the flow rate or decreasing the column length, showed that retention time is an important factor in controlling the efficiency of As(III) removal in the FeS-coated sand columns, both at pH 5 where the removal is primarily through precipitation and at pH 9 where the removal is primarily through adsorption. Overall, the results of the column studies suggest that FeS-coated sand removes As(III) as efficiently in a column system as in a batch system, provided that an adequate retention time is provided. These results suggest that FeS-coated sand is a viable alternative for removing As(III), and is especially effective if the pH is maintained below 7. The results reported here do not consider the field complexities of, for example, spatially and temporally variable pH and pe regimes or background solutes. Further investigation should focus on developing optimum geochemical site criteria in order to maximize the efficiency of the FeS-coated sand reactive medium presented here.

CHAPTER VIII

CONCLUSIONS AND FUTURE WORK

8.1 Conclusions

In this study, the feasibility of using synthesized nanoparticulate mackinawite (FeS) as a PRB reactive medium was investigated by coating nanoparticulate FeS onto a natural sand. This FeS-coated sand appears to be a viable alternative of the more commonly used ZVI or Fe(III)-oxide coated sand for remediating As(III)-contaminated groundwater under anoxic groundwater environments. ZVI and Fe(III)-oxide have been reported to successively remove As(III) from polluted groundwater, but their effectiveness of removal is reduced under anaerobic conditions, to as low as one tenth of the capacity under aerobic conditions (Bang et al., 2005a). Furthermore, the sorbed arsenic could be released back into solution by reductive dissolution of Fe (Masscheleyn et al., 1991; McGeehan and Naylor, 1994; Tufano and Fendorf, 2008). However, the release of arsenic back to the aqueous phase is not observed in systems where the sulfide concentration is abundant, even under anaerobic conditions (Kober et al., 2005; Wilkin et al., 2009). This fact suggests that the use of a sulfide mineral such as mackinawite (FeS) could be a better choice for arsenic removal under anoxic conditions.

Synthesized mackinawite (FeS) as a nano-sized mineral, which often exists in natural reducing environments, has been verified as a suitable reactant to remove As(III) under anoxic conditions (Farquhar et al., 2002; Gallegos, 2007). To use nano-sized FeS, as a PRB reactive material necessitates the development of a methodology of formulating a particle of a reasonable size. In this study, therefore, a reproducible method for coating mackinawite (FeS) on a natural sand was developed and the synthesized FeS-coated-sand was evaluated as a sequestration agent for removing As(III) from water in batch and column experiments under anoxic conditions over a range of pH values.

In Chapter 4, the development of an optimum coating procedure of FeS on sand was presented. The greatest mass of coating occurred using an unmodified natural sand with an iron-oxide coating rather than an acid-washed sand, a coating pH of 5.5, and no rinsing following solid-liquid separation after a three-day-contact period between the FeS suspension and the sand. The surface characterization results show that FeS-coated sand surface is predominantly comprised of FeS self-aggregates along with a small fraction of an oxidized magnetite and portions of uncoated sand. Most of the coating steps were determined considering the feasibility of the procedure in a field-scale application. Using natural sand without chemical modification and drying without rinsing would make the procedure more economical and environmentally friendly. Moreover, the pH of an FeS suspension, which is initially 5.5, eventually increases to about 7 at the end of procedure by deprotonation of sand surface, so the process waste (the supernatant after coating) would be near neutral pH. This coating method can successfully deposit an appreciable amount of FeS. The obtained maximum coating was measured as 4 mg FeS/g sand but this amount perhaps can further be enhanced by a higher concentration of FeS and adjusting the pH of the suspension. Since it is speculated that the FeS coating is generated primarily by self-aggregation among FeS particles, one may obtain a better coating as long as the conditions favor the attraction among the FeS particles.

In Chapter 5, the As(III) removal capacity of FeS-coated sand was evaluated and compared with that of nanoparticulate FeS. The As(III) removal of FeS-coated sand is 30%, 70% and 300% of the maximum capacity of FeS at pH 5, 7, and 9, respectively. The As(III) uptake capacity of FeS-coated sand under anaerobic conditions is comparable to other iron or aluminum-oxide coated sand used for arsenic removal under aerobic conditions, with a maximum uptake capacity at pH 5 that decreases with pH. Under anoxic conditions, FeS-coated sand is expected to outperform other iron and aluminum oxides for As(III), given that these other sorbents are not as effective under anoxic conditions as they are under oxic conditions. Furthermore iron and aluminum oxides release arsenic when reducing conditions prevail for long time periods (Tufano and Fendorf, 2008). These results suggest that FeS, which does appear to have a similar risk of reductive dissolution, will be effective in PRB applications for the removal of arsenic.

Chapter 5 also addresses the impact of pH and silicate concentration in solution on the uptake of As(III) by FeS-coated sand and nanoparticulate FeS under similar solution conditions. For example, pH plays an important role in determining As(III) uptake in the FeS-coated sand system. For a similar amount of FeS (~0.1 g FeS/L), uptake of FeS-coated sand exhibits similar pH-dependence to that of nanoparticulate FeS at an initial As(III) concentration of 1.33 $x10^{-5}$ M (1 ppm). This suggests that the primary removal mechanism of FeS-coated sand over the range of pH values investigated is similar to that of nanoparticulate FeS. Some differences occurred at pH values higher than 11 where FeS is not effective as a As(III) scavenger but FeS-coated sand still showed some affinity for As(III) attributable to the iron hydroxide on the uncoated surface. Chapter 5 also determined the impact of silicate on the As(III) removal of nanoparticulate FeS and FeS-coated sand. No impact was observed at pH 5, 7, and 9 for nanoparticulate FeS and no impact at pH 5 and 7 for FeS-coated sand. However, a slight lowering of As(III) uptake was noted at pH 9 in the FeS-coated sand system due to the inhibition by silicate of As(III) adsorption to the iron oxyhydroxide phases. These oxyhydroxide phases are from the originally existing iron oxyhydroxide on the natural sand or formed from the oxidation of to FeS, during the coating procedure or subsequently. Since this inhibitory effect of silicate is attributable to the iron oxyhydroxide phases rather than FeS this result demonstrates another advantage of the use of iron sulfide instead of iron oxide.

In Chapter 6, the removal mechanisms for FeS-coated sand were found to be similar to those established for systems containing suspensions of nanoscale FeS and arsenic. However, the results of XAS and XPS suggest that some differences exist in the mechanisms of As(III) removal in FeS and FeS-coated sand. In the FeS-coated sand system, As(III) uptake is primarily a result of the precipitation of orpiment at pH 5, and by the adsorption of arsenite at pH 9. In contrast, precipitation of realgar at pH 5, and adsorption of thioarsenite or arsenite occurred in the FeS system, depending on the initial As(III) concentration at pH 9. These differences are thought to be due to either the different Fe or As loading and the existence of oxide phases caused by the possible partial surface oxidation and by the exposed sand surface on FeS-coated sand. However, the FeS-coated sand still maintains the same primary removal processes at each pH,

precipitation at pH 5 and adsorption at pH 9, so from a macroscopic point of view the FeS-coated sand system resembles the nanoparticulate FeS system.

Finally in Chapter 7, FeS-coated sand packed columns experiments were run to evaluate the As(III) removal capacity under anaerobic conditions at pH 5, 7, and 9 in a reactor configuration more similar to that of a field PRB. A mechanistic understanding of the different removal processes at different pH conditions is important to the interpretation of the column experiment results. At pH 5, where the precipitation of arsenic sulfide plays the major role in the removal of arsenic, the column shows a greater removal efficiency than the batch system due to the continuous dissolution of sulfide and precipitation of arsenic sulfide. This greater removal is evident whether the comparison calculations are performed using capacity calculations or the method of moments. At pH 9, where adsorption mainly governs the arsenic removal, with a minor contribution of arsenic sulfide precipitation, capacity calculations suggest that greater removals are achieved in the batch systems than in the column systems. However, this comparison does not account for the observed nonlinearity in the sorption behavior. If the nonlinearity is accounted for, as in the estimation of retardation factors using the relationship with the distribution coefficient and the Langmuir isotherm, removals are comparable in the column system. Column experiments with lower retention times, achieved either by increasing the flow rate or decreasing the column length, showed that retention time is an important factor in controlling the efficiency of As(III) removal in the FeS-coated sand columns. System complexities, such as non-linear and nonequilibrium sorption and kinetically-controlled desorption, may lead to the observed discrepancies between capacity and retardation factors estimates from the two reactor systems. Therefore, a need exists additional experiments to elucidate. Also, the importance of modeling of the experimental results might provide additional evidence of the importance of sorption irreversibility, multisite sorption and kinetically-limited reactive transport in this system.

8.2 Future work

The findings in this dissertation support the feasibility of FeS coated sand as a reactive medium for a PRB aimed at the remediation of As(III)-contaminated anoxic groundwater. From an application perspective, the performance of FeS-coated sand capacity is directly related to the amount of FeS per unit volume that is present regardless of whether FeS is injected as a colloidal suspension or coated on sand grains using the procedures developed in this work, even though some loss of efficiency may occur. In Chapter 5, the FeS-coated sand showed an appreciable amount of As(III)-removal capacity at pH 5, 7 and 9 if the performance is calculated based on the mass of FeS, but because the sand matrix is basically inert, much of the sand mass does not contribute to the removal capacity. Therefore, enhancing the amount of coating is important future work to enhance removal capacity. The possibility of producing FeS-coated sand with a higher FeS loading was demonstrated in Chapter 4 by adding more FeS in the coating reactors. Alternatively, this could also be done by either using smaller sand particles or developing forms of granular FeS. Furthermore, methods of producing bulk amounts of FeS-coated sand for field use and of reducing the number of coating steps need to be investigated. Steps that could be targeted for elimination include separating nanoparticulate FeS from suspension or drying the coated sand under anaerobic conditions. Also, it may be possible to perform the coating steps on site and produce a slurry material that can be directly pumped into a trench to create the PRB. Given these potential difficulties in field-scale application, future work should be targeted at optimizing this material for field use. If the field installation of FeS-coated sand PRB can be successfully implemented, it could improve the performance of PRBs operating under anaerobic conditions. For example, compared to currently operating ZVI PRBs, it could improve the capacity for contaminants such as As, eliminate the time needed to produce FeS by sulfate reducing bacteria, and minimize the potential for release of sorbed contaminants by reductive dissolution.

Due to the metastable characteristic of FeS, FeS-coated on sand may age to produce either greigite or magnetite, depending on the pH conditions. The data from this study indicate that aging processes are insignificant over the course of days to weeks, but it remains to be determined if longer aging periods of months to years will cause a

appreciable decrease in the reactivity of FeS-based PRB materials. Future work is needed to address the impact of these changes in the reactivity of FeS-coated sand from prolonged contact with water over time frames representative of the lifetime of a PRB. The As-FeS coated sand system is complex, and some of the discrepancies between the 1D reactive transport work performed by Li (2009) and the mechanisms elucidated experimentally hint, at additional relatively unexplored, complexities.

From the point of view of interpreting and understanding the reaction between FeS and As(III), the As(III) transport through column reactors needs to be analyzed using models including multi-site sorption, kinetic reactions and particle precipitation and deposition.

The results reported here do not consider the field complexities of, for example, spatially and temporally variable pH and pe regimes or background solutes. Further investigation should focus on developing optimum geochemical site criteria in order to maximize the efficiency of the FeS-coated sand reactive medium presented here.

APPENDICES

Appendix A1 PHREEQC simulation of FeS coating

The FeS coating procedure was simulated using PHREEQC thermodynamic modeling software. The initial condition of the coating batch was set up with 1L volume of 2g/L FeS and 1 kg of quartz sand. Wedron sand was assumed to contain the average amount of $2x10^{-6}$ mol Fe/g sand and the naturally existing iron-oxide mineral coating was assumed as goethite. The thermodynamic constant of FeS was modified using a value calculated by Li (2009) by fitting the dissolution test results of FeS-coated sand provided by this study. The modified value of K_{sp} of mackinawite was -3.6. Then, the amount of HCl added during the titration was calculated in moles and added as a reaction phase in this PHREEQC modeling. This simple thermodynamic calculation resulted in a mixture of four minerals as final products: mostly quartz sand, 97% mackinawite and some portion of greigite and magnetite. It is need to be noted that the initially added goethite was all transformed to magnetite and this predicted result of the formation of magnetite is consistent with the batch modeling result of pH-dependent dissolution (Li, 2009).

The phases added in the data base

```
PHASES
Mackinawite
      FeS + H+ = Fe+2 + HS-
      log_k              -4.8

Quartz
         SiO2 + 2H2O = H4SiO4
         log_k   -4
         delta_h22.36   kJ
```

Appendix A2-1 The added database for PHREEQC simulations of As(III) uptake by 5 g/L FeS with varying pe at pH 5

```
PHASES

Mackinawite
   FeS + H+ = Fe+2 + HS-
   log_k     -3.6

Fix_pe
   e- = e-
   log_k     0

Fix_H+
   H+ = H+
   log_k     0

Arsenopyrite    (Wagman et al., 1982)
  FeAsS + 3H2O = AsO3-3 + HS- + Fe+2 + 5H+ + 3e-
  log_k -43.40

As_native                (Garrels and Christ, 1965)
        As + 3H2O = AsO3-3 + 6H+ + 3e-
        log_k             -46.258

Realgar                   (Barton, 1969)
         AsS + 3H2O =  AsO3-3 + HS- + 5H+ + e-
        log_k  -54.281

As2S3(am)                (Eary, 1992)
        As2S3 + 6H2O = 2AsO3-3 + 3HS- +9H+
        log_k  -114.288

Scorodite
        FeAsO4:2H2O = Fe+3 + AsO4-3 + 2H2O
        log_k  -22.207

As2O5
        As2O5 + 3H2O = 2H3AsO4
        log_k   6.7061
        delta_h-22.64  kJ

Orpiment
        As2S3 + 6H2O = 2AsO3-3 + 3HS- +9H+
        log_k             -114.28
        delta_h   84.3 kcal
```

Thioarsenite species

AsO3-3 + HS- + 4H+ = As(OH)2SH + H2O

log_k 43.434

Appendix A2-2 Output results of the PHREEQC simulations of As(III) uptake with varying pe at pH 5

pH	pe	Fe(2)	Fe(3)	As(3)	As(5)	Total As	S(-2)	S(6)	Mackinawite	Greigite	Realgar	As_native	Orpiment
5	-1.0	1.85E-02	8.98E-12	1.27E-04	1.53E-12	1.33E-02	4.91E-06	4.21E-04	0.00E+00	0.009154	0.00000	0.00E+00	6.59E-03
5	-1.2	1.98E-02	5.96E-12	9.48E-05	4.56E-13	1.33E-02	5.95E-06	1.30E-05	0.00E+00	0.009243	0.00000	0.00E+00	6.60E-03
5	-1.4	1.98E-02	3.77E-12	6.73E-05	1.29E-13	1.33E-02	7.48E-06	4.10E-07	0.00E+00	0.009236	0.00000	0.00E+00	6.62E-03
5	-1.6	1.99E-02	2.38E-12	4.77E-05	3.64E-14	1.33E-02	9.40E-06	1.30E-08	0.00E+00	0.009228	0.00000	0.00E+00	6.63E-03
5	-1.8	1.99E-02	1.50E-12	3.38E-05	1.03E-14	1.33E-02	1.18E-05	4.10E-10	0.00E+00	0.009222	0.00000	0.00E+00	6.63E-03
5	-1.9	1.99E-02	1.19E-12	2.85E-05	5.46E-15	1.33E-02	1.33E-05	7.29E-11	0.00E+00	0.009220	0.00000	0.00E+00	6.64E-03
5	-1.95	1.99E-02	1.16E-12	2.78E-05	5.03E-15	1.33E-02	1.35E-05	5.82E-11	0.00E+00	0.009220	0.00000	0.00E+00	6.64E-03
5	-2.0	1.99E-02	1.07E-12	2.45E-05	3.73E-15	1.33E-02	1.41E-05	3.07E-11	0.00E+00	0.010880	0.01328	0.00E+00	0.00E+00
5	-2.05	1.99E-02	9.49E-13	2.06E-05	2.49E-15	1.33E-02	1.49E-05	1.30E-11	0.00E+00	0.010880	0.01328	0.00E+00	0.00E+00
5	-2.1	1.99E-02	7.54E-13	1.46E-05	1.11E-15	1.33E-02	1.67E-05	2.30E-12	0.00E+00	0.010870	0.01329	0.00E+00	0.00E+00
5	-2.3	1.99E-02	4.76E-13	7.32E-06	2.22E-16	1.33E-02	2.11E-05	7.28E-14	0.00E+00	0.010870	0.01329	0.00E+00	0.00E+00
5	-2.4	2.00E-02	3.78E-13	5.18E-06	9.94E-17	1.33E-02	2.37E-05	1.30E-14	0.00E+00	0.010870	0.01329	0.00E+00	0.00E+00
5	-2.5	2.00E-02	3.01E-13	3.67E-06	4.44E-17	1.33E-02	2.66E-05	2.30E-15	0.00E+00	0.010870	0.01330	0.00E+00	0.00E+00

pH	pe	Fe(2)	Fe(3)	As(3)	As(5)	Total As	S(-2)	S(6)	Mackinawite	Greigite	Realgar	As_native	Orpiment
5	-2.6	2.00E-02	2.39E-13	2.60E-06	1.98E-17	1.33E-02	2.99E-05	4.10E-16	0.00E+00	0.010870	0.01330	0.00E+00	0.00E+00
5	-2.7	2.00E-02	1.90E-13	1.84E-06	8.86E-18	1.33E-02	3.36E-05	7.28E-17	0.00E+00	0.010870	0.01330	0.00E+00	0.00E+00
5	-2.9	2.00E-02	1.20E-13	9.23E-07	1.77E-18	1.33E-02	4.25E-05	2.30E-18	0.00E+00	0.010870	0.01330	0.00E+00	0.00E+00
5	-3.0	2.00E-02	9.51E-14	6.54E-07	7.90E-19	1.33E-02	4.78E-05	4.09E-19	0.00E+00	0.010860	0.01330	0.00E+00	0.00E+00
5	-3.1	2.00E-02	7.56E-14	4.63E-07	3.53E-19	1.33E-02	5.37E-05	7.28E-20	0.00E+00	0.010860	0.01330	0.00E+00	0.00E+00
5	-3.2	2.00E-02	6.01E-14	3.28E-07	1.58E-19	1.33E-02	6.04E-05	1.29E-20	0.00E+00	0.010860	0.01330	0.00E+00	0.00E+00
5	-3.41	2.00E-02	3.71E-14	1.59E-07	2.90E-20	1.33E-02	7.75E-05	3.44E-22	0.00E+00	0.010860	0.01330	0.00E+00	0.00E+00
5	-3.43	2.00E-02	3.62E-14	1.54E-07	2.68E-20	1.33E-02	7.84E-05	2.90E-22	0.00E+00	0.010860	0.01330	0.00E+00	0.00E+00
5	-3.44	2.00E-02	3.54E-14	1.48E-07	2.47E-20	1.33E-02	7.94E-05	2.44E-22	0.00E+00	0.010860	0.01330	0.00E+00	0.00E+00
5	-3.45	2.00E-02	3.46E-14	1.43E-07	2.28E-20	1.33E-02	8.03E-05	2.05E-22	0.00E+00	0.010850	0.01330	0.00E+00	0.00E+00
5	-3.46	2.00E-02	3.43E-14	1.42E-07	2.22E-20	1.33E-02	8.07E-05	1.93E-22	0.00E+00	0.010850	0.01330	0.00E+00	0.00E+00
5	-3.47	2.00E-02	3.43E-14	1.42E-07	2.22E-20	1.33E-02	8.07E-05	1.93E-22	0.00E+00	0.010850	0.00000	1.33E-02	0.00E+00
5	-3.49	2.00E-02	3.08E-14	1.03E-07	1.30E-20	1.33E-02	8.53E-05	8.65E-23	0.00E+00	0.014180	0.00000	1.33E-02	0.00E+00
5	-3.5	2.00E-02	3.01E-14	9.59E-08	1.16E-20	1.33E-02	8.63E-05	7.28E-23	0.00E+00	0.014180	0.00000	1.33E-02	0.00E+00

pH	pe	Fe(2)	Fe(3)	As(3)	As(5)	Total As	S(-2)	S(6)	Mackinawite	Greigite	Realgar	As_native	Orpiment
5	-3.6	2.00E-02	2.39E-14	4.81E-08	3.66E-21	1.33E-02	9.08E-05	1.21E-23	5.67E-02	0.000000	0.00000	1.33E-02	0.00E+00
5	-3.7	2.00E-02	1.90E-14	2.41E-08	1.16E-21	1.33E-02	9.07E-05	1.92E-24	5.67E-02	0.000000	0.00000	1.33E-02	0.00E+00
5	-3.8	2.00E-02	1.51E-14	1.21E-08	3.66E-22	1.33E-02	9.07E-05	3.04E-25	5.67E-02	0.000000	0.00000	1.33E-02	0.00E+00
5	-3.9	2.00E-02	1.20E-14	6.05E-09	1.16E-22	1.33E-02	9.07E-05	4.82E-26	5.67E-02	0.000000	0.00000	1.33E-02	0.00E+00
5	-4.0	2.00E-02	9.53E-15	3.03E-09	3.66E-23	1.33E-02	9.07E-05	7.64E-27	5.67E-02	0.000000	0.00000	1.33E-02	0.00E+00
5	-4.2	2.00E-02	6.02E-15	7.62E-10	3.66E-24	1.33E-02	9.07E-05	1.92E-28	5.67E-02	0.000000	0.00000	1.33E-02	0.00E+00
5	-4.4	2.01E-02	3.80E-15	1.91E-10	3.66E-25	1.33E-02	9.06E-05	4.81E-30	5.67E-02	0.000000	0.00000	1.33E-02	0.00E+00
5	-4.6	2.01E-02	2.40E-15	4.81E-11	3.66E-26	1.33E-02	9.04E-05	1.21E-31	5.67E-02	0.000000	0.00000	1.33E-02	0.00E+00
5	-4.8	2.03E-02	1.52E-15	1.21E-11	3.66E-27	1.33E-02	9.00E-05	3.02E-33	5.67E-02	0.000000	0.00000	1.33E-02	0.00E+00

Appendix A3 XRD results

1. The XRD patterns of FeS-coated sand and natural Wedron sand

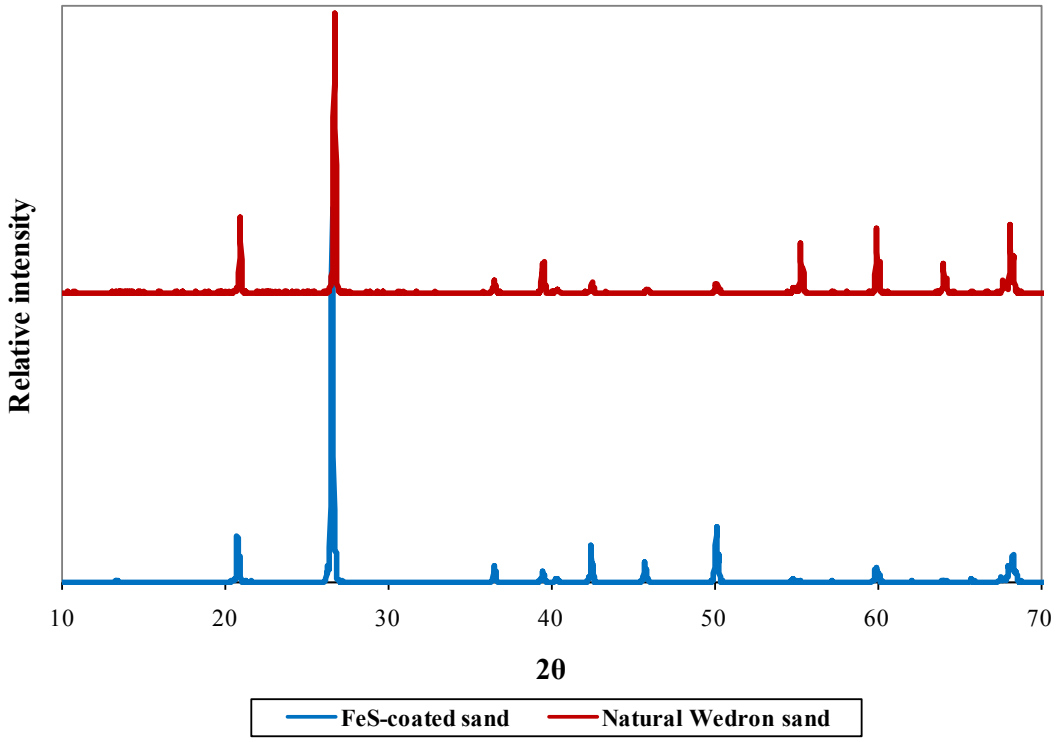

The XRD patterns for both the FeS-coated and uncoated sand are similar. Note that the FeS-coated sand does not show any peaks characteristic of FeS due to the strong absorption peaks of quartz and the disordered and low crystallinity of the FeS. To enhance the FeS patterns on the FeS-coated sand from the quartz features, two different methods were tried: crushing the sand, and detaching the FeS coating from the sand particle by scraping. However, neither method was successful in enhancing the FeS peak intensities.

2. The XRD peaks of (A) untreated-nanoscale FeS, (B) 5g/L nanoscale FeS reacted with 1000 ppm As(III) at pH 5 without buffer, and (C) 5g/L nanoscale FeS reacted with 1000 ppm As(III) at pH 5 with buffer

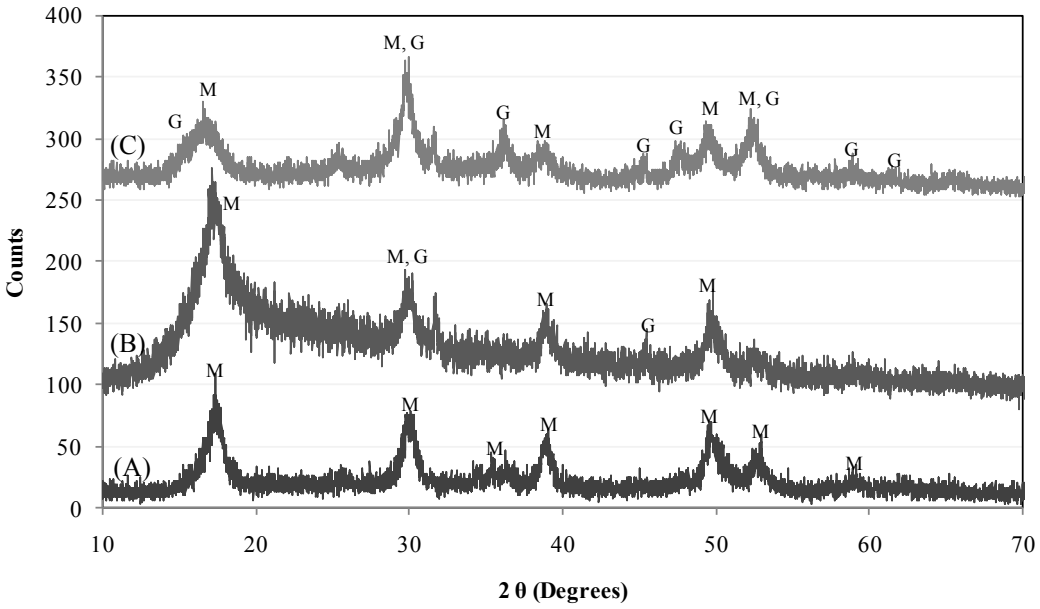

From the above XRD results, the following conclusions can be drawn: (1) the transformation of FeS at pH 5 to greigite by oxidation was greater in the 0.1N sodium acetate buffer system compared to the no buffer system; and (2) no realgar or other crystalline arsenic sulfide phases were observed, even though the precipitation of an arsenic sulfide phase (presumably not well crystalline) was determined by XAS and XPS (see Chapter 6) to be the primary product from the reaction between arsenic and FeS.

Appendix A4 Fe *2p* XPS result of the nanoscale FeS reacted with As(III)

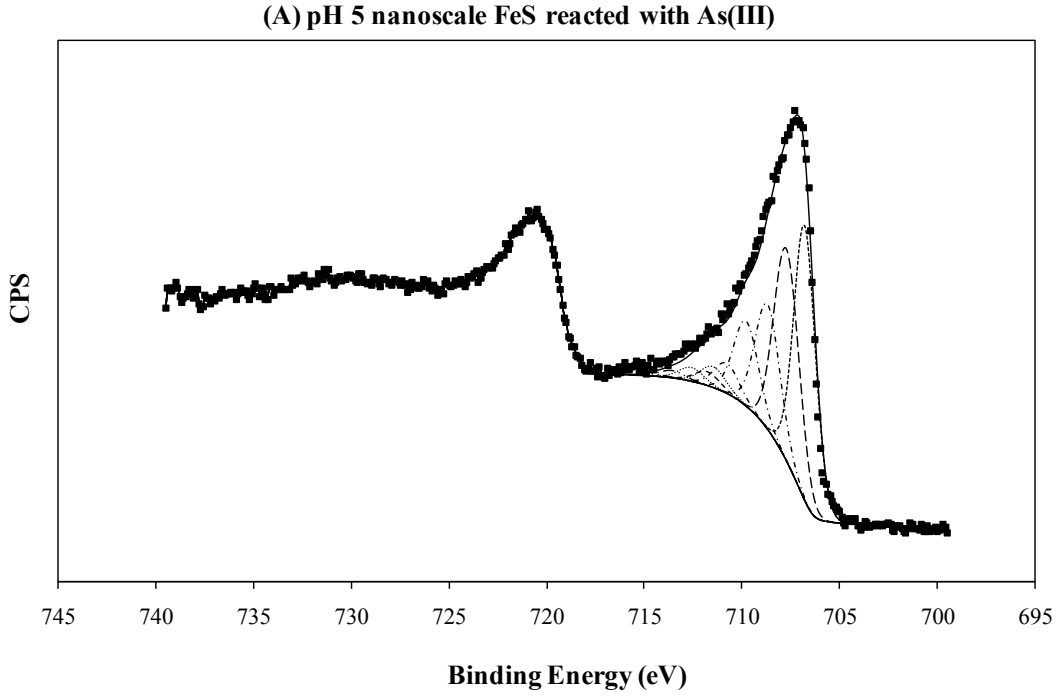

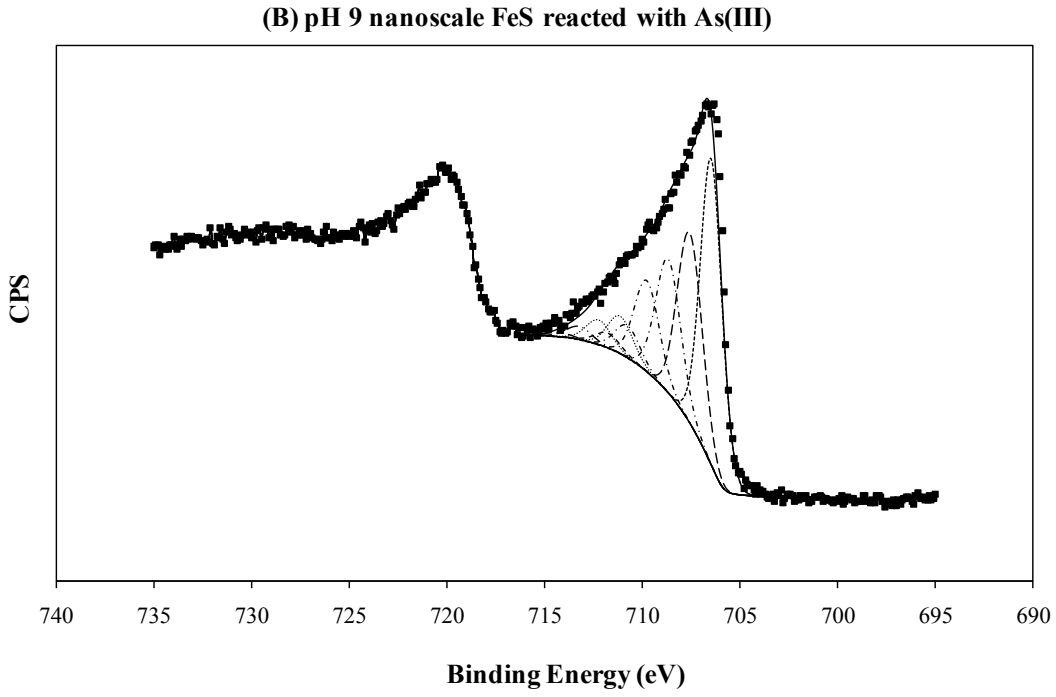

The XPS Fe *2p* spectra (A) and (B) show similar peak patterns with dominant Fe(II) peaks near the binding energy 705-708 eV. This fact demonstrates that nanoscale FeS mostly remains in its original oxidation state of Fe(II) after reacting with As(III) for 2 days at pH 5 and at pH 9. Also, given the lack of oxidation of Fe(II) noted in these XRD patterns, it can be concluded that XPS provides a good method for the analysis of surfaces of reduced samples, provided the samples are carefully handled during preparation and transfered to avoid unwanted exposure to atmospheric oxygen. Surface oxidation of iron sulfides during XPS sample preparation have been previously reported (Bostick and Fendorf, 2003b); however, in this study in which extreme care was taken to avoid exposure, no evidence of oxidation was observed.

REFERENCES

Al-Abed, S.R., Jegadeesan, G., Purandare, J. and Allen, D., 2007. Arsenic release from iron rich mineral processing waste: Influence of pH and redox potential. *Chemosphere* **66**(4), 775-782.

Anderson, P.R. and Benjamin, M.M., 1985. Effects of silicon on the crystallization and adsorption properties of ferric oxides. *Environmental Science & Technology* **19**(11), 1048-1053.

Angley, J.T., Brusseau, M.L., Miller, W.L. and Delfino, J.J., 1992. Nonequilibrium sorption and aerobic biodegradation of dissolved alkylbenzenes during transport in aquifer material - Column experiments and evaluation of a coupled-process model. *Environmental Science & Technology* **26**(7), 1404-1410.

Ankudinov, A.L., Ravel, B., Rehr, J.J. and Conradson, S.D., 1998. Real-space multiple-scattering calculation and interpretation of x-ray-absorption near-edge structure. *Physical Review B-Condensed Matter* **58**(12), 7565-7576.

Appelo, C.A.J. and Postma, D., 1999. Variable dispersivity in a column experiment containing MnO_2 and FeOOH-coated sand. *Journal of Contaminant Hydrology* **40**(2), 95-106.

Appelo, C.A.J. and Postma, D., 2005. *Geochemistry, Groundwater and Pollution*, A.A. Balkema Publishers, Leiden, Netherlands

Badruzzaman, M., Westerhoff, P. and Knappe, D.R.U., 2004. Intraparticle diffusion and adsorption of arsenate onto granular ferric hydroxide (GFH). *Water Research* **38**(18), 4002-4012.

Bailey, R.P., Bennett, T. and Benjamin, M.M., 1992 Sorption onto and recovery of Cr(VI) using iron-oxide-coated sand. *Water Science Technology*, **26**, 1239-1244,

Bajracharya, K., Tran, Y.T. and Barry, D.A., 1996. Cadmium adsorption at different pore water velocities. *Geoderma* **73**(3-4), 197-216.

Balsley, S.D., Brady, P.V., Krumhansl, J.L. and Anderson, H.L., 1996. Iodide retention by metal sulfide surfaces: Cinnabar and chalcocite. *Environmental Science & Technology* **30**(10), 3025-3027.

Bang, S., Johnson, M.D., Korfiatis, G.P. and Meng, X.G., 2005a. Chemical reactions between arsenic and zero-valent iron in water. *Water Research* **39**(5), 763-770.

Bang, S., Korfiatis, G.P. and Meng, X.G., 2005b. Removal of arsenic from water by zero-valent iron. *Journal of Hazardous Materials* **121**(1-3), 61-67.

Barnett, M.O., Jardine, P.M., Brooks, S.C. and Selim, H.M., 2000. Adsorption and transport of uranium(VI) in subsurface media. *Soil Science Society of America Journal* **64**(3), 908-917.

Barton, P.B., 1969. Thermochemical study of the system Fe-As-S. *Geochimica et Cosmochimica Acta* **33,** 841-857

Beak, D.G. and Wilkin, R.T., 2009. Performance of a zerovalent iron reactive barrier for the treatment of arsenic in groundwater: Part 2. Geochemical modeling and solid phase studies. *Journal of Contaminant Hydrology* **106**(1-2), 15-28.

Beak, D.G., Wilkin, R.T., Ford, R.G. and Kelly, S.D., 2008. Examination of arsenic speciation in sulfidic solutions using X-ray absorption spectroscopy. *Environmental Science & Technology* **42**(5), 1643-1650.

Bebie, J., Schoonen, M.A.A., Fuhrmann, M. and Strongin, D.R., 1998. Surface charge development on transition metal sulfides: An electrokinetic study. *Geochimica Et Cosmochimica Acta* **62**(4), 633-642.

Beckwith, R.S. and Reeve, R., 1964. Studies on soluble silica in soils. II. The release of monosilicic acid from soils. *Australian Journal of Soil Research* **2**(1), 33-45.

Benning, L.G., Wilkin, R.T. and Barnes, H.L., 2000. Reaction pathways in the Fe-S system below 100 degrees C. *Chemical Geology* **167**(1-2), 25-51.

Berner, R.A., 1962. Tetragonal iron sulfide. *Science* **137**(3531), 669-.

Berner, R.A., 1964. Iron sulfides formed from aqueous solution at low temperatures and atmospheric pressure. *Journal of Geology* **72**(3), 293-306.

Bilkert, J.N. and Rao, P.S.C., 1985. Sorption and leaching of three nonfumigant nematicides in soils. *Journal of Environmental Science and Health Part B-Pesticides Food Contaminants and Agricultural Wastes* **20**(1), 1-26.

Bissen M., and Frimmel, F.H., 2003. Arsenic -a review.-Part 1: Occurrence, toxicity, speciation, mobility. *Acta Hydrochimica et Hydrobiologica* **31**(1), 9-18.

Biswas, P. and Wu, C.Y., 2005. Critical Review: Nanoparticles and the environment. *Journal of the Air & Waste Management Association* **55**(6), 708-746.

Blowes, D.W., Ptacek, C.J., Benner, S.G., McRae, C.W.T., Bennett, T.A. and Puls, R.W., 2000. Treatment of inorganic contaminants using permeable reactive barriers. *Journal of Contaminant Hydrology* **45**(1-2), 123-137.

Bohart, G.S. and Adams, E.Q., 1920. Some aspects of the behavior of charcoal with respect to chlorine. *Journal of the American Chemical Society* **42**, 523-544.

Bostick, B.C. and Fendorf, S., 2003. Arsenite sorption on troilite (FeS) and pyrite (FeS2). *Geochimica et Cosmochimica Acta* **67**(5), 909-921.

Bostick, B.C., Fendorf, S. and Brown, G.E., 2005. In situ analysis of thioarsenite complexes in neutral to alkaline arsenic sulphide solutions. *Mineralogical Magazine* **69**(5), 781-795.

Bostick, B.C., Fendorf, S. and Manning, B.A., 2003. Arsenite adsorption on galena (PbS) and sphalerite (ZnS). *Geochimica et Cosmochimica Acta* **67**(5), 895-907.

Brooks, M.C. and Wise, W.R., 2005. Quantifying uncertainty due to random errors for moment analyses of breakthrough curves. *Journal of Hydrology* **303**(1-4), 165-175.

Brusseau, M.L., 1995. Transport of contaminants undergoing biodegradation. *Abstracts of Papers American Chemical Society* **209**(1-2), ENVR 72.

Brusseau, M.L., Hu, M.Q., Wang, J.M. and Maier, R.M., 1999. Biodegradation during contaminant transport in porous media. 2. The influence of physicochemical factors. *Environmental Science & Technology* **33**(1), 96-103.

Bryant, D.E., Stewart, D.I., Kee, T.P. and Barton, C.S., 2003. Development of a functionalized polymer-coated silica for the removal of uranium from groundwater. *Environmental Science & Technology* **37**(17), 4011-4016.

Burton, E.D., Bush, R.T., Sullivan, L.A. and Mitchell, D.R.G., 2008a. Schwertmannite transformation to goethite via the Fe(II) pathway: Reaction rates and implications for iron-sulfide formation. *Geochimica et Cosmochimica Acta* **72**(18), 4551-4564.

Burton, E.D., Sullivan, L.A., Bush, R.T. and Powell, B., 2008b. Iron-sulfide and trace element behaviour in sediments of Coombabah Lake, southern Moreton Bay (Australia). *Marine Pollution Bulletin* **56**(7), 1353-1358.

Butler, E.C. and Hayes, K.F., 1998. Effects of solution composition and pH on the reductive dechlorination of hexachloroethane by iron sulfide. *Environmental Science & Technology* **32**(9), 1276-1284.

Cantrell, K.J., Kaplan, D.I. and Gilmore, T.J., 1997. Injection of colloidal Fe-0 particles in sand with shear-thinning fluids. *Journal of Environmental Engineering-ASCE* **123**(8), 786-791.

Carroll, K.C., Artiola, J.F. and Brusseau, M.L., 2006. Transport of molybdenum in a biosolid-amended alkaline soil. *Chemosphere* **65**(5), 778-785.

Cheng, T., Barnett, M.O., Roden, E.E. and Zhuang, J.L., 2006. Effects of solid-to-solution ratio on uranium(VI) adsorption and its implications. *Environmental Science & Technology* **40**(10), 3243-3247.

Coles, C.A., Rao, S.R. and Yong, R.N., 2000. Lead and cadmium interactions with mackinawite: Retention mechanisms and the role of pH. *Environmental Science & Technology* **34**(6), 996-1000.

Cooper, D.C. and Morse, J.W., 1998. Extractability of metal sulfide minerals in acidic solutions: Application to environmental studies of trace metal contamination within anoxic sediments. *Environmental Science & Technology* **32**(8), 1076-1078.

Cornwell, J.C. and Morse, J.W., 1987. The characterization of iron sulfide minerals in anoxic marine-sediments. *Marine Chemistry* **22**(2-4), 193-206.

Coston, J.A., Fuller, C.C. and Davis, J.A., 1995. Pb2+ and Zn2+ adsorption by a natural aluminum-bearing and iron-bearing surface coating on an aquifer sand. *Geochimica et Cosmochimica Acta* **59**(17), 3535-3547.

Darland, J.E. and Inskeep, W.P., 1997. Effects of pore water velocity on the transport of arsenate. *Environmental Science & Technology* **31**(3), 704-709.

Davison, W., Phillips, N. and Tabner, B.J., 1999. Soluble iron sulfide species in natural waters: Reappraisal of their stoichiometry and stability constants. *Aquatic Sciences* **61**(1), 23-43.

Dixit, S. and Hering, J.G., 2003. Comparison of arsenic(V) and arsenic(III) sorption onto iron oxide minerals: Implications for arsenic mobility. *Environmental Science & Technology* **37**(18), 4182-4189.

Dufresne, A. and Hendershot, W.H., 1986. Comparison of aluminum speciation in soil solutions extracted by batch and column methods. *Canadian Journal of Soil Science* **66**(2), 367-371.

Duval, Y., Mielczarski, J.A., Pokrovsky, O.S., Mielczarski, E. and Ehrhardt, J.J., 2002. Evidence of the existence of three types of species at the quartz-aqueous solution interface at pH 0-10: XPS surface group quantification and surface complexation modeling. *Journal of Physical Chemistry B* **106**(11), 2937-2945.

Dzombak, D.A. and Morel, F.M.M. (eds), 1990. *Surface Complexation Modelling*, Wiley, New York.

Eary, L.E., 1992. The solubility of amorphous As_2S_3 from 25 to 90-degrees-C. *Geochimica et Cosmochimica Acta* **56**(6), 2267-2280.

Edwards, M. and Benjamin, M.M., 1989. Adsorptive filtration using coated sand - A new approach for treatment of metal-bearing wastes. *Research Journal of the Water Pollution Control Federation* **61**(9-10), 1523-1533.

Elgawhary and Lindsay, W.L., 1972. Solubility of silica in soils. *Soil Science Society of America Proceedings* **36**(3), 439-442.

Elliott, D.W. and Zhang, W.X., 2001. Field assessment of nanoscale biometallic particles for groundwater treatment. *Environmental Science & Technology* **35**(24), 4922-4926.

Farquhar, M.L., Charnock, J.M., Livens, F.R. and Vaughan, D.J., 2002. Mechanisms of arsenic uptake from aqueous solution by interaction with goethite, lepidocrocite, mackinawite, and pyrite: An X-ray absorption spectroscopy study. *Environmental Science & Technology* **36**(8), 1757-1762.

Furukawa, Y., Kim, J.W., Watkins, J. and Wilkin, R.T., 2002. Formation of ferrihydrite and associated iron corrosion products in permeable reactive barriers of zero-valent iron. *Environmental Science & Technology* **36**(24), 5469-5475.

Gabriel, U., Gaudet, J.P., Spadini, L. and Charlet, L., 1998. Reactive transport of uranyl in a goethite column: an experimental and modelling study. *Chemical Geology* **151**(1-4), 107-128.

Gallegos, T.J., 2007. Sequestration of As(III) by synthetic mackinawite under anoxic conditions, Ph.D. dissertation, The University of Michigan, Ann Arbor.

Gallegos, T.J., Han, Y.S. and Hayes, K.F., 2008. Model predictions of realgar precipitation by reaction of As(III) with synthetic mackinawite under anoxic conditions. *Environmental Science & Technology* **42**(24), 9338-9343.

Gallegos, T.J., Hyun, S.P. and Hayes, K.F., 2007. Spectroscopic investigation of the uptake of arsenite from solution by synthetic mackinawite. *Environmental Science & Technology* **41**, 7781-7786.

Garman, S.M., Luxton, T.P. and Eick, M.J., 2004. Kinetics of chromate adsorption on goethite in the presence of sorbed silicic acid. *Journal of Environmental Quality* **33**(5), 1703-1708.

Garrels, R.M.; Christ, C.L. *Solutions, Minerals, and Equilibria*; Haper & Row: NewYork, 1965.

Genc-Fuhrman, H. and Gencfuhrman, 2005. Arsenate removal from water using sand-red mud columns. *Water Research* **39**(13), 2944-2954.

Ghosh, M.M. and Yuan, J.R., 1987. Adsorption of inorganic arsenic and organoarsenicals on hydrous oxides. *Environmental Progress* **6**(3), 150-157.

Goel, J., Kadirvelu, K., Rajagopal, C. and Garg, V.K., 2005. Removal of lead(II) by adsorption using treated granular activated carbon: Batch and column studies. *Journal of Hazardous Materials* **125**(1-3), 211-220.

Goswami, S., Bhat, S.C. and Ghosh, U.C., 2006. Crystalline hydrous ferric oxide: An adsorbent for chromium(VI)-contaminated industrial wastewater treatment. *Water Environment Research* **78**(9), 986-993.

Gu, Z.M., Fang, J. and Deng, B.L., 2005. Preparation and evaluation of GAC-based iron-containing adsorbents for arsenic removal. *Environmental Science & Technology* **39**(10), 3833-3843.

Guha, H., Saiers, J.E., Brooks, S., Jardine, P. and Jayachandran, K., 2001. Chromium transport, oxidation, and adsorption in manganese-coated sand. *Journal of Contaminant Hydrology* **49**(3-4), 311-334.

Gupta, R.P. and Sen, S.K., 1974. Calculation of multiplet structure of core para-vacancy levels. *Physical Review B* **10**(1), 71-77.

Gupta, V.K., Saini, V.K. and Jain, N., 2005. Adsorption of As(III) from aqueous solutions by iron oxide-coated sand. *Journal of Colloid and Interface Science* **288**(1), 55-60.

He, F., Zhang, M., Qian, T.W. and Zhao, D.Y., 2009. Transport of carboxymethyl cellulose stabilized iron nanoparticles in porous media: Column experiments and modeling. *Journal of Colloid and Interface Science* **334**(1), 96-102.

Hemming, C.H., Bunde, R.L., Liszewski, M.J., Rosentreter, J.J. and Welhan, J., 1997. Effect of experimental technique on the determination of strontium distribution coefficients of a surficial sediment from the Idaho National Engineering Laboratory, Idaho. *Water Research* **31**(7), 1629-1636.

Herbel, M. and Fendorf, S., 2006. Biogeochemical processes controlling the speciation and transport of arsenic within iron coated sands. *Chemical Geology* **228**(1-3), 16-32.

Herbert, R.B., Benner, S.G. and Blowes, D.W., 2000. Solid phase iron-sulfur geochemistry of a reactive barrier for treatment of mine drainage. *Applied Geochemistry* **15**(9), 1331-1343.

Herbert, R.B., Benner, S.G., Pratt, A.R. and Blowes, D.W., 1998. Surface chemistry and morphology of poorly crystalline iron sulfides precipitated in media containing sulfate-reducing bacteria. *Chemical Geology* **144**(1-2), 87-97.

Hiemstra, T., Barnett, M.O. and van Riemsdijk, W.H., 2007. Interaction of silicic acid with goethite. *Journal of Colloid and Interface Science* **310**(1), 8-17.

Hiemstra, T. and Van Riemsdijk, W.H., 1999. Surface structural ion adsorption modeling of competitive binding of oxyanions by metal (hydr)oxides. *Journal of Colloid and Interface Science* **210**(1), 182-193.

Huertadiaz, M.A. and Morse, J.W., 1990. A quantitative method for determination of trace-metal concentrations in sedimentary pyrite. *Marine Chemistry* **29**(2-3), 119-144.

Hunger, S. and Benning, L.G., 2007. Greigite: a true intermediate on the polysulfide pathway to pyrite. *Geochemical Transactions* **8**.

Jeong, H.Y., 2005. Removal of heavy metals and reductive declorination of chlorinated organic pollutants by nanosized FeS. Ph.D. dissertation, The Univeristy of Michigan, Ann Arbor, MI.

Jeong, H.Y., Lee, J.H. and Hayes, K.F., 2008. Characterization of synthetic nanocrystalline mackinawite: Crystal structure, particle size, and specific surface area. *Geochimica et Cosmochimica Acta* **72**(2), 493-505.

Jeong, H.Y., Han, Y.-S., and Hayes, K.F., 2009. An x-ray absorption spectroscopy (XAS) study of arsenic mobilization during mackinawite (FeS) oxidation. Paper prepared for submission to *Environmental Science & Technology.*

Jerez, J. and Flury, M., 2006. Humic acid-, ferrihydrite-, and aluminosilicate-coated sands for column transport experiments. *Colloids and Surfaces A-Physicochemical and Engineering Aspects* **273**(1-3), 90-96.

Jia, Y., Breedveld, G.D. and Aagaard, P., 2007. Column studies on transport of deicing additive benzotriazole in a sandy aquifer and a zerovalent iron barrier. *Chemosphere* **69**, 1409-1418.

Kanel, S.R., Manning, B., Charlet, L. and Choi, H., 2005. Removal of arsenic(III) from groundwater by nanoscale zero-valent iron. *Environmental Science & Technology* **39**(5), 1291-1298.

Kim, S.B., Ha, H.C., Choi, N.C. and Kim, D.J., 2006. Influence of flow rate and organic carbon content on benzene transport in a sandy soil. *Hydrological Processes* **20**(20), 4307-4316.

Kober, R., Welter, E., Ebert, M. and Dahmke, A., 2005. Removal of arsenic from groundwater by zerovalent iron and the role of sulfide. *Environmental Science & Technology* **39**(20), 8038-8044.

Kretzschmar, R., Barmettler, K., Grolimund, D., Yan, Y.D., Borkovec, M. and Sticher, H., 1997. Experimental determination of colloid deposition rates and collision efficiencies in natural porous media. *Water Resources Research* **33**(5), 1129-1137.

Kuan, W.H., Lo, S.L., Wang, M.K. and Lin, C.F., 1998. Removal of Se(IV) and Se(VI) from water by aluminum-oxide-coated sand. *Water Research* **32**(3), 915-923.

Kundu, S. and Gupta, A.K., 2006. Arsenic adsorption onto iron oxide-coated cement (IOCC): Regression analysis of equilibrium data with several isotherm models and their optimization. *Chemical Engineering Journal* **122**(1-2), 93-106.

Lackovic, J.A., Nikolaidis, N.P. and Dobbs, G.M., 2000. Inorganic arsenic removal by zero-valent iron. *Environmental Engineering Science* **17**(1), 29-39.

Lai, C.H., Chen, C.Y., Shih, P.H. and Hsia, T.H., 1999. Competitive adsorption of copper and lead ions on an iron-coated sand from water, *Water Science and Technology*, **42**, 149-154.

Lakshmipathiraj, P., Narasimhan, B.R.V., Prabhakar, S. and Raju, G.B., 2006. Adsorption studies of arsenic on Mn-substituted iron oxyhydroxide. *Journal of Colloid and Interface Science* **304**(2), 317-322.

Lee, J.H., 2009. Chemical optimization of in situ emplacement of nano-particulate iron sulfide in porous media, Ph.D. dissertation, The University of Michigan, Ann Arbor, MI.

Leij, F.J. and Dane, J.H., 1991. Solute transport in a 2-layer medium investigated with time moments. *Soil Science Society of America Journal* **55**(6), 1529-1535.

Lennie, A.R., Redfern, S.A.T., Schofield, P.F. and Vaughan, D.J., 1995. Synthesis and Rietveld crystal structure refinement of mackinawite, tetragonal FeS. *Mineralogical Magazine* **59**(397), 677-683.

Li, W., 2009. Performance evaluation of FeS-coated sand based permeable reactive barriers for remediation of arsenic contaminated groundwater using geochemical modeling and reactive transport modeling. Ph.D. dissertation, Tufts University.

Somerville, MA.Li, Z.B. and Shuman, L.M., 1997. Estimation of retardation factor of dissolved organic carbon in sandy soils using batch experiments. *Geoderma* **78**(3-4), 197-206.

Lien, H.L. and Wilkin, R.T., 2005. High-level arsenite removal from groundwater by zero-valent iron. *Chemosphere* **59**(3), 377-386.

Limousin, G., Gaudet, J.P., Charlet, L., Szenknect, S., Barthes, V. and Krimissa, M., 2007. Sorption isotherms: A review on physical bases, modeling and measurement. *Applied Geochemistry* **22**(2), 249-275.

Lo, S.L. and Chen, T.Y., 1997. Adsorption of Se(IV) and Se(VI) on an iron-coated sand from water. *Chemosphere* **35**(5), 919-930.

Lo, S.L., Jeng, H.T. and Lai, C.H., 1997. Characteristics and adsorption properties of iron-coated sand. *Water Science and Technology* **35**(7), 63-70.

Luo, J., Cirpka, O.A. and Kitanidis, P.K., 2006. Temporal-moment matching for truncated breakthrough curves for step or step-pulse injection. *Advances in Water Resources* **29**(9), 1306-1313.

Luxton, T.P., Eick, M.J. and Rimstidt, D.J., 2008. The role of silicate in the adsorption/desorption of arsenite on goethite. *Chemical Geology* **252**(3-4), 125-135.

Macintyre, W.G., Stauffer, T.B. and Antworth, C.P., 1991. A comparison of sorption coefficients determined by batch, column, and box methods on a low organic-carbon aquifer material. *Ground Water* **29**(6), 908-913.

Manna, B.R., Dey, S., Debnath, S. and Ghosh, U.C., 2003. Removal of arsenic from groundwater using crystalline hydrous ferric oxide (CHFO). *Water Quality Research Journal of Canada* **38**(1), 193-210.

Manning, B.A., Hunt, M.L., Amrhein, C. and Yarmoff, J.A., 2002. Arsenic(III) and arsenic(V) reactions with zerovalent iron corrosion products. *Environmental Science & Technology* **36**(24), 5455-5461.

Maraqa, M.A., 2000. Sorption distribution coefficients: Discrepancy between batch and column techniques. *Geoengineering in Arid Lands* **1**, 403-409.

Maraqa, M.A., Zhao, X., Wallace, R.B. and Voice, T.C., 1998. Retardation coefficients of nonionic organic compounds determined by batch and column techniques. *Soil Science Society of America Journal* **62**(1), 142-152.

Masscheleyn, P.H., Delaune, R.D. and Patrick, W.H., 1991. Arsenic and Selenium Chemistry as Affected by Sediment Redox Potential and Ph. *Journal of Environmental Quality* **20**(3), 522-527.

Mayer, T.D. and Jarrell, W.M., 2000. Phosphorus sorption during iron(II) oxidation in the presence of dissolved silica. *Water Research* **34**(16), 3949-3956.

McGeehan, S.L. and Naylor, D.V., 1994. Sorption and redox transformation of arsenite and arsenate in 2 flooded soils. *Soil Science Society of America Journal* **58**(2), 337-342.

Meng, X.G., Jing, C.Y. and Korfiatis, G.P., 2003. A review of redox transformation of arsenic in aquatic environments. *Biogeochemistry of Environmentally Important Trace Elements* **835**, 70-83.

Mihaljevic, M., Sisr, L., Ettler, V., Sebek, O. and Prusa, J., 2004. Oxidation of As-bearing gold ore - a comparison of batch and column experiments. *Journal of Geochemical Exploration* **81**(1-3), 59-70.

Miller, D.M., Sumner, M.E. and Miller, W.P., 1989. A comparison of batch-generated and flow-generated anion adsorption-isotherms. *Soil Science Society of America Journal* **53**(2), 373-380.

Moore, J.N., Ficklin, W.H. and Johns, C., 1988. Partitioning of arsenic and metals in reducing sulfidic sediments. *Environmental Science & Technology* **22**(4), 432-437.

Morse, J.W. and Arakaki, T., 1993. Adsorption and coprecipitation of divalent metals with mackinawite (Fes). *Geochimica et Cosmochimica Acta* **57**(15), 3635-3640.

Morse, J.W. and Luther, G.W., 1999. Chemical influences on trace metal-sulfide interactions in anoxic sediments. *Geochimica et Cosmochimica Acta* **63**(19-20), 3373-3378.

Mullet, M., Boursiquot, S., Abdelmoula, M., Genin, J.M. and Ehrhardt, J.J., 2002. Surface chemistry and structural properties of mackinawite prepared by reaction of sulfide ions with metallic iron. *Geochimica et Cosmochimica Acta* **66**(5), 829-836.

Mullet, M., Boursiquot, S. and Ehrhardt, J.J., 2004. Removal of hexavalent chromium from solutions by mackinawite, tetragonal FeS. *Colloids and Surfaces A-Physicochemical and Engineering Aspects* **244**(1-3), 77-85.

O'Day, P.A., Vlassopoulos, D., Root, R. and Rivera, N., 2004. The influence of sulfur and iron on dissolved arsenic concentrations in the shallow subsurface under changing redox conditions. *Proceedings of the National Academy of Sciences of the United States of America* **101**(38), 13703-13708.

Ohfuji, H. and Rickard, D., 2006. High resolution transmission electron microscopic study of synthetic nanocrystalline mackinawite. *Earth and Planetary Science Letters* **241**(1-2), 227-233.

Onyango, M.S., Kojima, Y., Matsuda, H. and Ochieng, A., 2003. Adsorption kinetics of arsenic removal from groundwater by iron-modified zeolite. *Journal of Chemical Engineering of Japan* **36**(12), 1516-1522.

Pang, L.P., Close, M., Schneider, D. and Stanton, G., 2002. Effect of pore-water velocity on chemical nonequilibrium transport of Cd, Zn, and Pb in alluvial gravel columns. *Journal of Contaminant Hydrology* **57**(3-4), 241-258.

Pang, L.P. and Close, M.E., 1999. Non-equilibrium transport of Cd in alluvial gravels. *Journal of Contaminant Hydrology* **36**(1-2), 185-206.

Parkhurst, D.L. and Appelo, C.A.J., 1999. User's guide to PHREEQC (Version 2): A computer program for speciation, batch reactions, one-dimensional transport, and inverse geochemical calculations. U.S. Geological Survey, Water-Resources Investigations.

Phillippi, J.M., Loganathan, V.A., McIndoe, M.J., Barnett, M.O., Clement, T.P. and Roden, E.E., 2007. Theoretical solid/solution ratio effects on adsorption and transport: Uranium(VI) and carbonate. *Soil Science Society of America Journal* **71**(2), 329-335.

Pokrovski, G.S., Schott, J., Garges, F. and Hazemann, J.L., 2003. Iron (III)-silica interactions in aqueous solution: Insights from X-ray absorption fine structure spectroscopy. *Geochimica et Cosmochimica Acta* **67**(19), 3559-3573.

Porro, I., Newman, M.E. and Dunnivant, F.M., 2000. Comparison of latch and column methods for determining strontium distribution coefficients for unsaturated transport in basalt. *Environmental Science & Technology* **34**(9), 1679-1686.

Pratt, A.R., McIntyre, N.S. and Splinter, S.J., 1998. Deconvolution of pyrite marcasite and arsenopyrite XPS spectra using the maximum entropy method. *Surface Science* **396**(1-3), 266-272.

Prima, S., Evangelou, V.P. and McDonald, L.M., 2002. Surface exchange phase composition and nonionic surfactant effects on the nonequilibrium transport of atrazine. *Soil Science* **167**(4), 260-268.

Puls, R., 1999. Long-term performance monitoring for a permeable reactive barrier at the US Coast Guard Support Center, Elizabeth City, North Carolina. *Journal of Hazardous Materials* **68**(1-2), 109-124.

Rader, K.J., Dombrowski, P.M., Farley, K.J., Mahony, J.D. and Di Toro, D.M., 2004. Effect of thioarsenite formation on arsenic(III) toxicity. *Environmental Toxicology and Chemistry* **23**(7), 1649-1654.

Rainwater, K.A., Wise, W.R. and Charbeneau, R.J., 1987. Parameter-estimation through groundwater tracer tests. *Water Resources Research* **23**(10), 1901-1910.

Ramos, M.C., 2006. Metals in vineyard soils of the Penedes area (NE Spain) after compost application. *Journal of Environmental Management* **78**(3), 209-215.

Rickard, D., 1969. The chemistry of iron sulphide formation at low temperatures. *Stockholm Contriutions in Geology.* **26**, 67-95.

Rickard, D., 1995. Kinetics of FeS precipitation. 1. Competing reaction-mechanisms. *Geochimica et Cosmochimica Acta* **59**(21), 4367-4379.

Rickard, D., 2006. The solubility of FeS. *Geochimica et Cosmochimica Acta* **70**(23), 5779-5789.

Rickard, D. and Morse, J.W., 2005. Acid volatile sulfide (AVS). *Marine Chemistry* **97**(3-4), 141-197.

Roberts, L.C., Hug, S.J., Ruettimann, T., Billah, M., Khan, A.W. and Rahman, M.T., 2004. Arsenic removal with iron(II) and iron(III) waters with high silicate and phosphate concentrations. *Environmental Science & Technology* **38**(1), 307-315.

Rueda, E.H., Ballesteros, M.C., Grassi, R.L. and Blesa, M.A., 1992. Dithionite as a dissolving reagent for goethite in the presence of EDTA and citrate - application to soil analysis. *Clays and Clay Minerals* **40**(5), 575-585.

Saleh, N., Sirk, K., Liu, Y.Q., Phenrat, T., Dufour, B., Matyjaszewski, K., Tilton, R.D. and Lowry, G.V., 2007. Surface modifications enhance nanoiron transport and NAPL targeting in saturated porous media. *Environmental Engineering Science* **24**(1), 45-57.

Savage, K.S., Tingle, T.N., O'Day, P.A., Waychunas, G.A. and Bird, D.K., 2000. Arsenic speciation in pyrite and secondary weathering phases, Mother Lode Gold District, Tuolumne County, California. *Applied Geochemistry* **15**(8), 1219-1244.

Scheidegger, A., Borkovec, M. and Sticher, H., 1993. Coating of silica sand with goethite - preparation and analytical identification. *Geoderma* **58**(1-2), 43-65.

Schoonen, M.A.A. and Barnes, H.L., 1991. Reactions forming pyrite and marcasite from solution .2. Via FeS precursors below 100-degrees-C. *Geochimica et Cosmochimica Acta* **55**(6), 1505-1514.

Schrick, B., Hydutsky, B.W., Blough, J.L. and Mallouk, T.E., 2004. Delivery vehicles for zerovalent metal nanoparticles in soil and groundwater. *Chemistry of Materials* **16**(11), 2187-2193.

Seo, D.C., Yu, K. and DeLaune, R.D., 2008. Comparison of monometal and multimetal adsorption in Mississippi River alluvial wetland sediment: Batch and column experiments. *Chemosphere* **73**(11), 1757-1764.

Singh, T.S. and Pant, K.K., 2004. Equilibrium, kinetics and thermodynamic studies for adsorption of As(III) on activated alumina. *Separation and Purification Technology* **36**(2), 139-147.

Singh, T.S. and Pant, K.K., 2006. Experimental and modelling studies on fixed bed adsorption of As(III) ions from aqueous solution. *Separation and Purification Technology* **48**(3), 288-296.

Smedley, P.L. and Kinniburgh, D.G., 2002. A review of the source, behaviour and distribution of arsenic in natural waters. *Applied Geochemistry* **17**(5), 517-568.

Smyth, D.J.A., Blowes, D.W., Benner, S.G. and Ptacek, C.J., 2001. In situ treatment of metals-contaminated groundwater using permeable reactive barriers. *Bioremediation of Inorganic Compounds* **6**(9), 71-78.

Spycher, N.F. and Reed, M.H., 1989. As(III) and Sb(III) sulfide complexes - an evaluation of stoichiometry and stability from existing experimental-data. *Geochimica et Cosmochimica Acta* **53**(9), 2185-2194.

Srivastava, V.C., Prasad, B., Mishra, I.M., Mall, I.D. and Swamy, M.M., 2008. Prediction of breakthrough curves for sorptive removal of phenol by bagasse fly ash packed bed. *Industrial & Engineering Chemistry Research* **47**(5), 1603-1613.

Stahl, R.S. and James, B.R., 1991. Zinc sorption by iron-oxide-coated sand as a function of pH. *Soil Science Society of America Journal* **55**(5), 1287-1290.

Stauder, S., Raue, B. and Sacher, F., 2005. Thioarsenates in sulfidic waters. *Environmental Science & Technology* **39**(16), 5933-5939.

Stumm, W. and Morgan, J.J., 1981. *Aquatic Chemistry, Chemical Equilibria and Rates in Natural Waters*, Wiley, New Youk.

Stumm, W. and Morgan, J.J., 1996. *Aquatic Chemistry*, Wiley, New York.

Su, C.M. and Puls, R.W., 2001. Arsenate and arsenite removal by zerovalent iron: Effects of phosphate, silicate, carbonate, borate, sulfate, chromate, molybdate, and nitrate, relative to chloride. *Environmental Science & Technology* **35**(22), 4562-4568.

Su, C.M. and Puls, R.W., 2003. In situ remediation of arsenic in simulated groundwater using zerovalent iron: Laboratory column tests on combined effects of phosphate and silicate. *Environmental Science & Technology* **37**(11), 2582-2587.

Su, C.M. and Puls, R.W., 2008. Arsenate and arsenite sorption on magnetite: Relations to groundwater arsenic treatment using zerovalent iron and natural attenuation. *Water Air and Soil Pollution* **193**(1-4), 65-78.

Swedlund, P.J. and Webster, J.G., 1999. Adsorption and polymerisation of silicic acid on ferrihydrite, and its effect on arsenic adsorption. *Water Research* **33**(16), 3413-3422.

Szenknect, S., Ardois, C., Gaudet, J.P. and Barthes, V., 2005. Reactive transport of Sr-85 in a Chernobyl sand column: Static and dynamic experiments and modeling. *Journal of Contaminant Hydrology* **76**(1-2), 139-165.

Thirunavukkarasu, O.S., Viraraghavan, T. and Subramanian, K.S., 2003. Arsenic removal from drinking water using iron oxide-coated sand. *Water Air and Soil Pollution* **142**(1-4), 95-111.

Thomas, H.C., 1944. Heterogeneous ion exchange in a flowing system. *Journal of the American Chemical Society* **66**, 1664-1666.

Thomas, J.E., Jones, C.F., Skinner, W.M. and Smart, R.S., 1998. The role of surface sulfur species in the inhibition of pyrrhotite dissolution in acid conditions. *Geochimica et Cosmochimica Acta* **62**(9), 1555-1565.

Toride, N., Leij, F.J. and van Genuchten, M.T., 1995. The CXTFIT code for estimating transport parameters from laboratory or field tracer experiments. U.S. Salinity Laboratory, USDA, ARS, Riverside, CA.

Tsang, D.C.W., Zhang, W. and Lo, I.M.C., 2007. Modeling cadmium transport in soils using sequential extraction, batch, and miscible displacement experiments. *Soil Science Society of America Journal* **71**(3), 674-681.

Tufano, K.J. and Fendorf, S., 2008. Confounding impacts of iron reduction on arsenic retention. *Environmental Science & Technology* **42**(13), 4777-4783.

Tume, P., Bech, J., Longan, L., Tume, L., Reverter, F. and Sepulveda, B., 2006. Trace elements in natural surface soils in Sant Climent (Catalonia, Spain). *Ecological Engineering* **27**(2), 145-152.

Vaishya, R.C. and Gupta, S.K., 2004. Modeling arsenic(V) removal from water by sulfate modified iron-oxide coated sand (SMIOCS). *Separation Science and Technology* **39**(3), 645-666.

van Oorschot, I.H.M. and Dekkers, M.J., 2001. Selective dissolution of magnetic iron oxides in the acid-ammonium oxalate/ferrous iron extraction method - I. Synthetic samples. *Geophysical Journal International* **145**(3), 740-748.

Wagman, D.D., Evans, W.H., Parker, V.B., Schumm, R.H., Halow, I., Bailey, S.M., Churney, K.L. and Nuttall, R.L., 1982. The NBS tables of chemical thermodynamic properties: selected values for inorganic and C1 and C2 organic substances in SI units. *J. Phys. Chem. Ref. Data*, ***11*****,** 392.

Waltham, C.A. and Eick, M.J., 2002. Kinetics of arsenic adsorption on goethite in the presence of sorbed silicic acid. *Soil Science Society of America Journal* **66**(3), 818-825.

Wang, T.H., Li, M.H. and Teng, S.P., 2009. Bridging the gap between batch and column experiments: A case study of Cs adsorption on granite. *Journal of Hazardous Materials* **161**(1), 409-415.

Webb, S.M., 2002. *Sam's Interface for XAS Package (SixPACK)*, Stanford Synchrotron Radiation Laboratory, Menlo Park, CA.

Webster, J.G., 1990. The solubility of As_2S_3 and speciation of As in dilute and sulfide-bearing fluids at 25-degrees-C and 90-degrees-C. *Geochimica et Cosmochimica Acta* **54**(4), 1009-1017.

Weisener, C.G., Sale, K.S., Smyth, D.J.A. and Blowes, D.W., 2005. Field column study using zerovalent iron for mercury removal from contaminated groundwater. *Environmental Science & Technology* **39**(16), 6306-6312.

Wibulswas, R., 2004. Batch and fixed bed sorption of methylene blue on precursor and QACs modified montmorillonite. *Separation and Purification Technology* **39**(1-2), 3-12.

Widler, A.M. and Seward, T.M., 2002. The adsorption of gold(I) hydrosulphide complexes by iron sulphide surfaces. *Geochimica et Cosmochimica Acta* **66**(3), 383-402.

Wilkin, R.T., Acree, S.D., Ross, R.R., Beak, D.G. and Lee, T.R., 2009. Performance of a zerovalent iron reactive barrier for the treatment of arsenic in groundwater: Part 1. Hydrogeochemical studies. *Journal of Contaminant Hydrology* **106**(1-2), 1-14.

Wilkin, R.T. and Barnes, H.L., 1996. Pyrite formation by reactions of iron monosulfides with dissolved inorganic and organic sulfur species. *Geochimica et Cosmochimica Acta* **60**(21), 4167-4179.

Wilkin, R.T. and Ford, R.G., 2006. Arsenic solid-phase partitioning in reducing sediments of a contaminated wetland. *Chemical Geology* **228**(1-3), 156-174.

Wilkin, R.T., Wallschlager, D. and Ford, R.G., 2003. Speciation of arsenic in sulfidic waters. *Geochemical Transactions* **4**, 1-7.

Wise, W.R., 1993. Effects of laboratory-scale variability upon batch and column determinations of nonlinearly sorptive behavior in porous media. *Water Resources Research* **29**(9), 2983-2992.

Wolthers, M., Charlet, L., Van der Weijden, C.H., Van der Linde, P.R. and Rickard, D., 2005. Arsenic mobility in the ambient sulfidic environment: Sorption of arsenic(V) and arsenic(III) onto disordered mackinawite. *Geochimica et Cosmochimica Acta* **69**(14), 3483-3492.

Wolthers, M., Van der Gaast, S.J. and Rickard, D., 2003. The structure of disordered mackinawite. *American Mineralogist* **88**(11-12), 2007-2015.

World Health Organization, 1997. Environmental Health Criteria; Aluminium.

Wood, S.A., Tait, C.D. and Janecky, D.R., 2002. A Raman spectroscopic study of arsenite and thioarsenite species in aqueous solution at 25 degrees C. *Geochemical Transactions* **3**, 31-39.

Xu, Y. and Axe, L., 2005. Synthesis and characterization of iron oxide-coated silica and its effect on metal adsorption. *Journal of Colloid and Interface Science* **282**(1), 11-19.

Yamauchi, H. and Fowler, B.A., 1994. Toxicity and metabolism of inorganic and methylated arsenicals. *Advances in Environmental Science and Technology; Arsenic in the environment, Part II: Human health and ecosystem effects*, Wiley, New York, 35-53.

Zhu, B.J. and Tabatabai, M.A., 1995. An alkaline oxidation method for determining total arsenic and selenium in soils. *Soil Science Society of America Journal* **59**(6), 1564-1569.